Master Thesis
TVVR 15/5006

Coastal Evolution at Nha Trang Bay, Vietnam

Susanna Böös
Anna Dahlström

Division of Water Resources Engineering
Department of Building and Environmental Technology
Lund University

Coastal Evolution at Nha Trang Bay, Vietnam

By:
Susanna Böös
Anna Dahlström

Master Thesis

Division of Water Resources Engineering
Department of Building & Environmental Technology
Lund University
Box 118
221 00 Lund, Sweden

Water Resources Engineering
TVVR-15/5006
ISSN 1101-9824

Lund 2015
www.tvrl.lth.se

Master Thesis
Division of Water Resources Engineering
Department of Building & Environmental Technology
Lund University

English title:	Coastal Evolution at Nha Trang Bay, Vietnam
Authors:	Susanna Böös Anna Dahlström
Supervisors:	Magnus Larson Nguyen Manh Hung Le Dinh Mau
Examiner:	Hans Hanson
Language	English
Year:	2015
Keywords:	Nha Trang; coastal evolution; longshore sediment transport; EBED; GENESIS

LUNDS TEKNISKA HÖGSKOLA
Lunds universitet

Lund University
Faculty of Engineering, LTH
Departments of Earth and Water Engineering

This study has been carried out within the framework of the Minor Field Studies (MFS) Scholarship Programme, which is funded by the Swedish International Development Cooperation Agency, Sida.

The MFS Scholarship Programme offers Swedish university students an opportunity to carry out two months' field work in a developing country resulting in a graduation thesis work, a Master's dissertation or a similar in-depth study. These studies are primarily conducted within subject areas that are important from an international development perspective and in a country supported by Swedish international development assistance.

The main purpose of the MFS Programme is to enhance Swedish university students' knowledge and understanding of developing countries and their problems. An MFS should provide the student with initial experience of conditions in such a country. A further purpose is to widen the human resource base for recruitment into international co-operation. Further information can be reached at the following internet address: http://www.tg.lth.se/mfs

The responsibility for the accuracy of the information presented in this MFS report rests entirely with the authors and their supervisors.

Gerhard Barmen
Local MFS Programme Officer

Postadress Box 118, 221 00 Lund *Besöksadress* John Ericssons väg 1*Telefon dir* 046-222 9657, *växel* 046-222 00 00 *Telefax* 046-2229127 *E-post* Gerhard.Barmen@tg.lth.se

Acknowledgements

First of all we would like to thank our supervisor Professor Magnus Larson at Division of Water Resource Engineering, Faculty of Engineering, Lund University, for all help and support with our master thesis and journey. We would also like to thank Professor Hans Hanson at Division of Water Resource Engineering, Faculty of Engineering, Lund University, for the guidance with the model GENESIS. Our supervisor Doctor Nguyen Manh Hung at Institute of Mechanics in Hanoi gave us a warm welcome in Vietnam and helped us a great deal with practical arrangement as well as contributed with interesting discussions for our thesis. We appreciate all the help with collection of data and the model EBED that Doctor Pham Thanh Nam and Mr. Duong Cong Dien from Institute of Mechanics in Hanoi gave us. At University of Water Resources in Hanoi, Doctor Nguyen Trung Viet and Doctor Nguyen Xuan Tinh with fellow workers have kindly helped us with collection of previous data and useful discussions.

At the Institute of Oceanography in Nha Trang we would like to thank our supervisor Doctor Le Dinh Mau and Mr Nguyen Chi Cong for support in both practical arrangement and discussion about our thesis. We also wish to express our deep gratitude to the Department of Marine Physics and Department of Marine Geology for their kind and warm welcome and for their help during our fieldwork and thesis.

This master thesis would not have been possible without the funding from the Swedish International Development Cooperation Agency, Sida, and The ÅForsk Foundation, which made it possible to fulfil this master thesis.

Last but not least, we wish to thank our families and friends who have supported us throughout our master thesis and entire education; thank you!

Abstract

Over the past years the southern beach of Nha Trang, located in the south central of Vietnam, has started to indicate signs of erosion in the northern part. As the beach plays an important role for this touristic hotspot, the fear that the erosion will become severe has been raised. The limited knowledge and previous performed studies of the general coastal processes affecting the shoreline evolution has motivated this master thesis and abovementioned were investigated through field trips, data collection and simulations. Data and samples of sediment, beach profiles, shoreline position, wave and current properties and longshore sediment transport were collected. The model EBED was used to simulate the nearshore wave climate from deep water wave data for the previous 25 years. The resulting wave climate was further used as input data to the shoreline evolution model GENESIS, which calculated the net transport rate and the shoreline evolution. The field measurements and data analysis indicated a relatively stable shoreline, except for in the northern part where the retreat of the shoreline was visible. Beach nourishment would improve the condition of the northern part of the beach but required renourishment every second year. The wave climate in the bay is highly affected by the northeast monsoon, which generates a longshore sediment transport to the south, and the sheltering surroundings with the many islands and mountains.

Keywords
Nha Trang, coastal evolution, longshore sediment transport, EBED and GENESIS.

Table of Contents

1. Introduction

1.1 Background

The city of Nha Trang is located on the southeast coast of Vietnam. In former years the income in the region was mostly made up from agriculture and fishing activities. Nowadays the city experiences new possibilities to earn capital as tourists are drawn to the area. Many people come for the appealing weather, but the long and central located sandy beach is also making it an attractive place for leisure. Many constructions such as hotels and services are built in the direct precinct of the beach. The year following the hardening around Yersin Park and an adjacent restaurant, located on the south of the Cai river mouth, observations of beach changes were made. A sand spit at the river mouth disappeared and shoreline changes of the southern beach started to be more pronounced in the most northern part. As the beach located north of Cai river mouth eroded and left a less attractive area behind with only seawalls, concern about the evolution of the south beach was raised.

1.2 Objectives

Few former studies regarding the coastal evolution and hydrodynamic processes in the area of Nha Trang bay has been performed. Therefore, the study was performed to achieve a greater understanding of the governing processes of the shoreline evolution at Nha Trang bay. The main objectives of this study were to investigate and quantify the nearshore processes governing sediment transport and coastal evolution on the southern beach in Nha Trang bay, Vietnam. To see the evolution of the shoreline a model was to be used to calculate the longshore sediment transport occurring along it. The transport rates could be used to see changes of the position of the beach in Nha Trang bay.

Planning of the experimental set up, executing fieldwork and processing data, both in the laboratory and the raw data, were some of the goals with the thesis. Field measurements were seen as an important tool to get a deeper understanding of the theory and the processes that take place on the beach and in the nearshore zone.

To practise the role of project leaders and write a paper of the process and its

results were other objectives when doing this master thesis. Performing two months of the master thesis in Vietnam was seen as an instructive and developing way of dealing with challenges and problem that might occur in such a project. The knowledge of working in an international environment with a different culture and habits was seen as a strength in this master thesis, giving us experience for future work at an international arena.

1.3 Procedure

The project started in January 2015 with concretisation of the aim and acquiring a general understanding of the project, planning of the field measurements, achieving knowledge of the governing coastal processes by doing a literature study, gathering of information about the studied area, establishing contacts with collaborating institutes and other preparations of the journey. Also, a course at Sida Partnership Forum in Härnösand was undertaken to prepare for the coming trip. Practical information for field work in an international environment as well as knowledge about Swedish aid strategy were discussed.

Nine weeks of the master thesis, the 23rd of February until the 24th of April 2015, were spent in Vietnam. The majority of the time was spent in Nha Trang, where field work on the project site of Nha Trang beach was practised. The shoreline was measured as well as the beach profile at several locations along the shoreline, when comparing this with old data from the same location, the evolution of the shoreline and profile could be seen. Grain sizes along the shoreline as well as in cores were taken to see how the river influences the flow of sediment to the beach. By studying grain sizes, the relationship between the distance and the grain sizes can be obtained. The current climate in the bay was measured and sampling with a sediment trap was performed to get a validation of the currents in the area and to achieve a greater understanding of the current reign in the area. Laboratory work was performed and data were processed at the Department of Marine Geology and the Department of Marine Physics, respectively, at the Institute of Oceanography in Nha Trang. Previous studies and measurements done in Nha Trang bay were collected and studied. Having measurements at different times gives the possibility to see the beach evolution and the trends of the area to a greater extent than to only have a snapshot of the status of the beach.

The wave climate in the South China Sea was used to estimate the nearshore wave climate in Nha Trang bay with the help of the modelling program EBED.

Cooperation was also made with the Institute of Mechanics in Hanoi, where the program EBED was discussed as well as the results from the field trip from Nha Trang bay. Visits were also made to Water Resource University in Hanoi for gathering data from previous project in Nha Trang and discussions with researchers were kept.

After returning to Sweden, the remaining weeks of the project were spent on the Department of Water Resource Engineering at LTH, Lund. The nearshore wave climate was used to simulate the longshore sediment transport along the bay with the shoreline change model GENESIS. The magnitude of the transport gives an estimation of the direction of the beach evolution.

1.4 Outline

In Chapter 2 a general presentation about wave theory is presented to introduce the topic and give the reader useful background to understand the mechanisms involved in beach evolution. It is followed by general information about the area of interest, Vietnam, in Chapter 3. There the area is presented with information about the climate in the region so that the focus area can be put into a greater context. More specific information about Nha Trang bay is described in Chapter 4. Mechanisms affecting the climate in the bay are explained as well as background about the development and processes of the coastal area.

Furthermore, the fieldwork and the results are visualized and described in Chapter 5. Information regarding the wave transformation model EBED and a validation of the model are presented in Chapter 6. The longshore sediment transport rates computed by the model GENESIS are stated in Chapter 7. The results are discussed in Chapter 8 followed by Chapter 9 where future work is suggested. Finally, Chapter 10 consists of the conclusion that could be drawn in this master thesis.

2. Coastal Processes

All the coastal processes affecting the geomorphology and coastal shape are initiated by the wave movements (Pethick, 1984), hence it is of great importance to acquire the knowledge of wave mechanisms to be able to evaluate its effect on the shore.

As the wind blows over the water surface the shear stress will create a higher resistance for the streamlines close to the water surface than the one furthest away. Eventually the parallel streamlines will try to balance the force field and shift into circular streamlines, forcing the water to start oscillate. During this process, wind energy is transferred to the wave, which carries the energy by iterating energy form between kinetic to potential as the wave propagates (Pethick, 1984). So it continues until it reaches shallow water where it eventually breaks and dissipates the energy along the shoreline. The motion of the waves induces the water particles beneath the wave to move in an orbital path with a positive net movement forward causing a slight transportation force. This transportation force creates a crosshore transport of sediment. At deep water the oscillation path obtains a circular movement all the way down to the bottom, while at transitional and shallow water the oscillation path becomes elliptical and almost completely horizontal at the sea bed, see Figure 1.

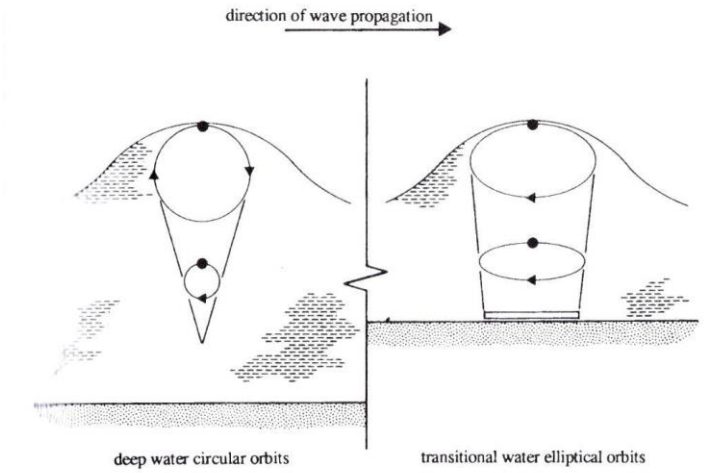

Figure 1. The water particle of a wave propagating at deep water moves in a circular orbit (left-hand side), while a wave propagating at transitional water moves in an elliptical orbit (right-hand side) (Reeve et al., 2012).

In ideal conditions, a wave would oscillate as a perfect sinusoidal curve. This is usually not the case though, since the wind might fluctuate in strength and direction and create a chaotic and complex mixture of waves of various shape and direction (Pethick, 1984). This complexibility is hard to describe mathematically because of the nonlinearities, three-dimensional characteristics and random behaviour. Therefore, waves are assumed to act as simple waves, i.e. a sinusoidal wave, when calculations are performed (U.S. Army Corps of Engineers, 1984). There are three different theories that combine and calculate the four wave properties; Airy wave theory, Stokes' wave theory and solitary wave theory. The most commonly used linear wave theory is the one derived by Airy in 1845 which is applicable for waves with a small wave height in relation to the wavelength and the water depth (Reeve et al., 2012). In this project all calculations were based on Airy's linear wave theory.

2.1 Wave Characteristics

A simple sinusoidal wave is described by the properties wavelength (L), wave height (H), wave period (T) and water depth (d), see Figure 2. The wavelength is the horizontal distance between corresponding points in two consecutive waves. The height of the wave represents the vertical height between the crest and the trough of the wave. The wave period is the time it takes for corresponding points in two consecutive waves to pass a fix point. And finally, the water depth is the vertical distance from the still water level to the sea bed (U.S. Army Corps of Engineers, 1984).

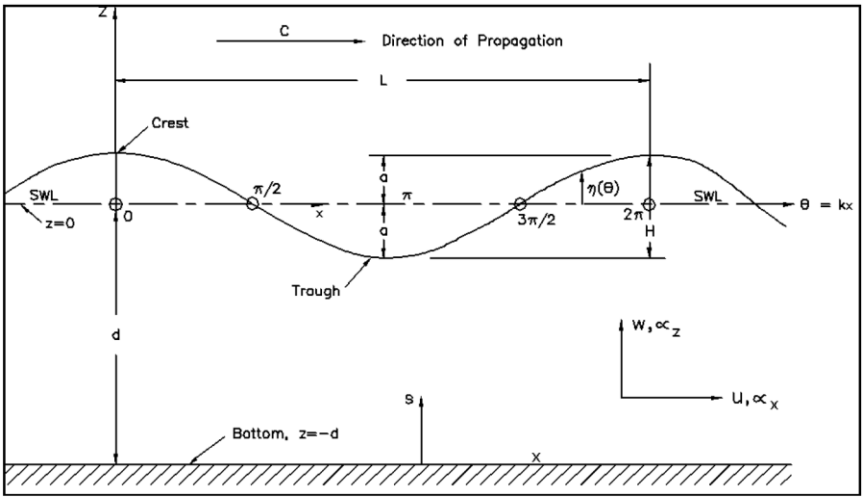

Figure 2. An ideal sinusoidal wave can be defined by its properties wave height (*H*), wavelength (*L*) and wave period (*T*) at a certain water depth *d* (U.S. Army Corps of Engineers, 2012).

The wave celerity (*C*) is related to the wavelength and wave period, since the travelled distance by the wave during one wave period is equal to the wave length. A relationship between the three parameters, seen in Equation 1, makes it easy to calculate between the wave's different wave properties. The wave height on the other hand, is not related to the other wave properties and has to be found through measurements. The wave period also initially needs to be found through measurements. The wave celerity can also be calculated with the dispersion relationship, seen in Equation 2, which relates the wave celerity to the wavelength and the water depth. The two expressions can be combined and indicates that waves with different periods travel at different speeds.

$$C = \frac{L}{T} \tag{1}$$

$$C = \sqrt{\frac{gL}{2\pi}\tanh\left(\frac{2\pi d}{L}\right)} \tag{2}$$

where g is the gravitational acceleration 9.81 m/s^2 and d is the water depth in metres.

The profile of the sinusoidal wave (η), i.e. the elevation of the free water surface over the still water level (SWL), can be estimated with Equation 3 (U.S. Army Corps of Engineers, 2012).

$$\eta = \frac{H}{2}\cos\left(\frac{2\pi x}{L} - \frac{2\pi t}{T}\right) \quad (3)$$

where *x* is the horizontal direction in metres and *t* is the time in seconds.

2.2 Wave Classifications

There are many different perspectives to consider when classifying a wave. Some of the classifications which waves might be divided into consider the movement of the water particle beneath the wave, the water depth, the spectrum or how they are generated. Waves with a motion in relation to a fix point is classified as a progressive wave and waves which only moves up and down in relation to a fix point is classified as a standing wave. While considering how the wave is generated, a wave might be classified as an impulse wave, like a tsunami caused by an earthquake, or as a constant forcing wave induced by wind or tidal force (U.S. Army Corps of Engineers, 1984).

2.2.1 Shallow Water Wave and Deep Water Wave

Computation of wave characteristics with the linear wave theory is dependent on the classification of deep water, transitional water and shallow water. As the bathymetry throughout the ocean can vary suddenly and drastically, it is of importance to have a clear definition of the difference between a deep water wave and a shallow water wave, as different rules applies for them. A wave is said to be a deep water wave when the depth is higher than half the wavelength, i.e. that the depth to wavelength relationship is 0.5, see Table 1. A shallow water wave is defined as such when the depth divided by the wave length is lower than 1/25. The waves that do not fit into those categories are called transitional waves, which also have specific rules and equation which applies to them (U.S. Army Corps of Engineers, 1984).

Table 1. Classification of water depth is defined by the relationship between the water depth (*d*) and the wavelength (*L*).

Classification	***d/L***
Deep water	> 1/2
Transitional water	1/25 to 1/2
Shallow water	< 1/25

2.2.2 Classifications of Breaking Waves

As the waves progress towards shallower parts of the ocean the energy is redistributed so the wave height increases and wavelength decreases. Waves at deep water theoretically break when the wave height divided by the wavelength is equal to 1/7, but normally the breaking of the wave occurs in an earlier stage. On the other hand, waves at shallow water depths theoretically break before the wave height divided by the water depth becomes 0.78. At the breaking point, the wave crest is usually so steep that the water particles in the crest have a higher velocity, as the particle orbit increases, than the water particles in the waveform. This causes the wave to break (Komar, 1998).

A wave that breaks is classified in different categories depending on its features. The different types are spilling, plunging, surging and collapsing waves, see Figure 3. A spilling wave usually occurs on beaches with little slope and happens when the crest little by little reaches its peak and then fall down as foam and bubbles. A plunging wave approaches the beach, which usually is steep, with a vertical crest that rolls over with a big fountain of water. A surging wave is almost like a plunging wave but differs in the sense that the wave base reaches the beach before the crest and thus makes the wave collapse and disappears. Surging waves most often occur on very steep beaches and where the waves have a quite small wave height. The collapsing wave is a mix of a surging and a plunging wave. Many ocean waves are a mixture of the explained categories of breaking waves, which makes it difficult to distinguish between them (Komar, 1998).

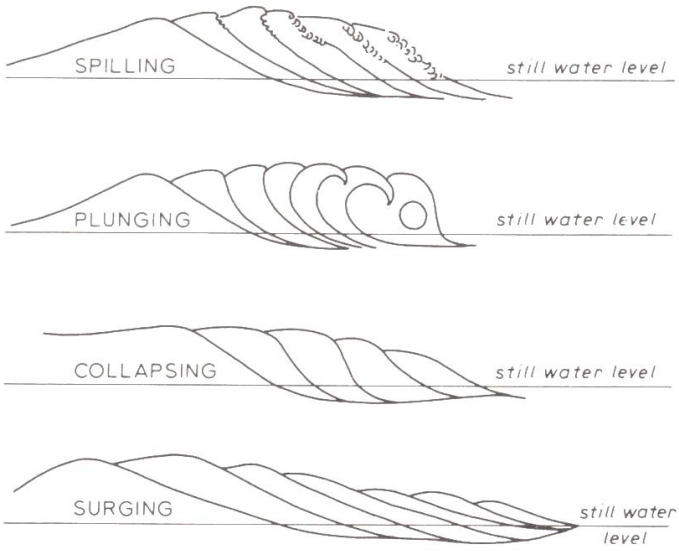

Figure 3. Illustrative sketches of the four different categories of breaking waves; spilling wave, plunging wave, collapsing wave and surging wave (Pethick, 1984).

2.3 Coastal Area Zones

The beach profile and the shoreline can look very different at various locations and seasons, which make it hard to have precise definitions of the different areas in the coastal zone. The water closest to the shoreline and the immediate land next to it is referred to as the littoral zone, while the water area closest to the shoreline is called the nearshore zone, i.e. a section of the littoral zone, see Figure 4.

The nearshore zone can further be divided into three zones; the breaker zone, the surf zone and the swash zone. In the breaking zone the first possibility comes for a wave to break, but it can also break in the next coming section; the surf zone. The surf zone is usually wide where the beach consists of fine sediments and less wide in areas with coarser sediment. This is a result of the wave energy in the zone, because waves with higher energy manage to transport coarser and consequently heavier sediment. In the swash zone, the waves subject the beach for run-up and backwash as the waves hit the beach face (Komar, 1998, Mau, 2014).

The foreshore in the littoral zone has almost the same definition as the beach face, but is the area between the berm and the lowest point at the low tide swash. The berm is a flat area on the beach and is part of the backshore, located next to the foreshore in the onshore direction. It can exist more than one berm on a beach and it can be hard to identify them as the appearance of beaches can be very different. The backshore stretches all the way out to a change in the physical setting, which can be a cliff, a sand dune or a construction etc. (Komar, 1998, Mau, 2014).

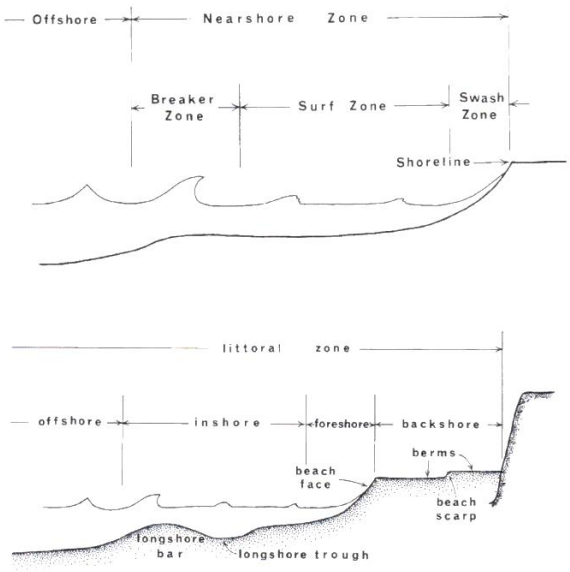

Figure 4. The different zones and definitions of the nearshore zone (upper illustration) and littoral zone (lower illustration) (Komar, 1998).

2.4 Wave Transformation

A deep water wave propagating shoreward into shallower water will be exposed to the wave transformation processes wave shoaling and wave refraction. Wave shoaling affects the wave height while wave refraction affects the wave celerity and wavelength and thus also the direction of the wave. The wave transformation processes wave reflection and wave diffraction occur when the wave encounters a barrier which influence the pattern of the wave crests.

2.4.1 Wave Shoaling

The law of conservation of energy states that energy cannot be created nor lost but it can change form. This means that the energy of a deepwater wave crest must be equal to the energy of the same wave crest in shallow water. To maintain the energy as the wave enters shallower waters and the celerity and the wavelength decrease, the wave height will typically increase, i.e. the kinetic energy of the wave is converted into potential energy. The wave period will remain unchanged during the process, which is called shoaling. Eventually the wave crest becomes too steep and unstable and thus transforms into a breaking wave. The wave shoaling process distributes the energy along the profile of the wave train (Hanson, 2014a).

2.4.2 Wave Refraction

The wave celerity is related to the water depth and wave period and as the wave propagates shoreward, towards shallower water depths, the wave crest will turn and eventually become parallel to the contour of the shore. This wave transformation process is called wave refraction and it will, together with shoaling, affect the direction, velocity, height and length of the wave. As the wave crest moves shoreward with a certain angle to the shore, the wave crest will be curved with one part of the crest closer to shore and one part of the crest more seaward. Due to the relationship between the wave celerity and the water depth, the more seaward part of the crest will move with a higher velocity and eventually catch up to form a straight parallel crest to the shoreline (Pethick, 1984).

The same wave refraction process occurs in situations where waves approach headlands, embayments and islands, but considering the land contours and the bathymetry there will be a spreading out or a contraction of the wave rays. The wave rays will be contracted and the energy will be concentrated at headlands, while the wave rays will spread out and the energy will be dispersed at embayments, which is shown in Figure 5. With this follows that the wave height will increase in headlands and decrease in bays, due the conservation of energy (Pethick, 1984). This results in that the wave refraction process distributes the energy along the coast (Hanson, 2014a).

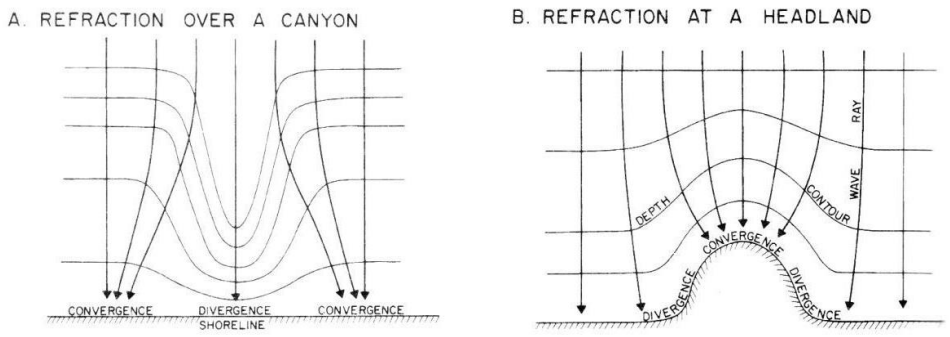

Figure 5. Land contours and bathymetry affects the wave refraction at canyons/embayments (left-hand side) and headlands (right-hand side) by spreading out or concentrating the wave rays and the wave energy (Komar, 1998).

2.4.3 Wave Reflection

Natural or man-made vertical barriers, e.g. harbour walls or seawalls, might have a great influence locally on wave processes and vice versa. As the incoming wave hits the barrier the energy of the wave is reflected instead of being dissipated along the shore. Depending on the material of the barrier waves can be partially or fully reflected. An impermeable wall which fully reflects the wave corresponds to a reflection coefficient equal to 1.0 and the total energy of the wave is reflected. This means that the reflected wave will have an equal wave height as the incident wave (U.S. Army Corps of Engineers, 1984). A permeable barrier, e.g. rouble mound breakwater, will partly let through the wave energy and less energy will be maintained in the reflected wave.

An incoming wave crest perpendicular to a vertical, impermeable barrier is reflected in the opposite direction and receives the same frequency, period and amplitude as the incident wave. The resulting wave becomes a so called standing wave and the water surface profile can easily be estimated by superposing the two identical waves with opposite propagation direction (U.S. Army Corps of Engineers, 1984). On the other hand, if the incoming wave angle to the normal from the vertical barrier is equal to α, then the angle of the reflected wave will be equal to α on the opposite side of the normal (Reeve et al., 2012).

This kind of reflection phenomenon induced by man-made constructions has a great impact on not only the construction itself but also on the sediment

transport. For example, in a harbour multiple reflections can build-up energy which can result in disturbance and surging within the harbour area, which in turn affects the harbour construction and anchored ships (U.S. Army Corps of Engineers, 1984).

2.4.4 Wave Diffraction

Propagating water waves are also transformed when encountering obstructions, for example breakwaters or islands, by transferring the wave energy sidewise along the wave crest (U.S. Army Corps of Engineers, 1984). As the waves approach the obstruction, three regions will be formed; a shadow region, a short-crested region and an undisturbed region, see Figure 6. The region in front of the obstruction will be affected by both the incident waves and the waves that are reflected against the barrier creating a region with short-crested waves. When the wave passes the barrier, the lateral dispersion of the wave energy will force the wave to bend around the tip of the barrier and form a circular wave crest with centre at the tip of the barrier. In reality though, this wave transformation process is much more complicated since the waves that are reflected by the barrier in the short-crested region will diffract into the undisturbed region. Hence, the short-crested region will be extended into the undisturbed region (Reeve et al., 2012).

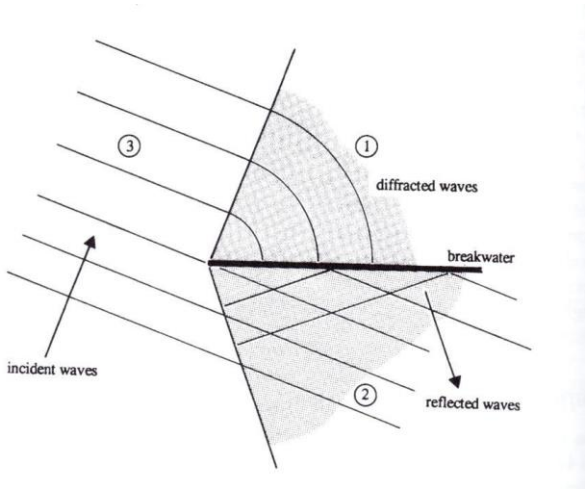

Figure 6. As a wave hits an obstruction and diffracts, three different regions appear; a shadow region (1), a short-crested region (2) and an undisturbed region (3) (Reeve et al., 2012).

2.4.5 Nearshore Currents

There are several different types of currents in the nearshore zone that plays an important role on the nearshore coastal environment. Most commonly one talks about the two categories crosshore and longshore currents, which make up of different kinds of currents that act in the shoreward-seaward direction and the direction parallel to the shoreline, respectively.

As waves propagate shoreward into shallower waters, a current is generated below the wave in the same direction and after the wave has broken a current is driven seaward by the backwash flow. These currents are referred to crosshore, or onshore-offshore, currents as the currents move in a direction perpendicular to the shoreline. A current along the lower water column in the seaward direction is also generated to compensate the flow balance as the wave breaks. This so called undertow current also contributes to the crosshore currents.

Longshore currents are formed in the surf zone as the incoming waves break and generate currents parallel to the shoreline. The strength and direction of the longshore currents depend on the angle between the crest of the incoming breaking wave and the shoreline. For a maximal current strength the incoming wave crest should be 45 degrees to the shoreline. Longshore currents can sometimes turn into rip currents. As the incoming, normally incident, wave hits the shoreline, longshore currents in opposite directions are formed. Eventually the longshore current will collide with a current in the opposite direction and create a rip current, i.e. the current turns seaward. This creates a cell circulation of the currents in the nearshore zone (Hanson, 2014b).

2.5 Littoral Transport

Most of the beach morphological change occurs in the littoral zone because of the dissipation of energy along the shoreline as waves break. If it were not for the waves there would be no littoral processes. Sediment transported by waves and currents in the littoral zone, i.e. the zone between the backshore and the most seaward breaking waves, is defined as littoral transport. The sediment may be transported by three different transport modes, bed load, suspended load and sheet flow. Bed load is when the grains are moving along the bottom caused by the shear stress induced by the moving water above the sediment bed, while during suspended load are the grains lifted upward from the bottom by turbulent fluid motion. Sheet flow transport occurs when the grains move

collectively as a layer along the bottom surface. Further, the littoral transport can be divided into two categories depending on the direction of the sediment movement in relation to the shore. Transport of sediment parallel to the shore is referred to as longshore transport, while transport of sediment perpendicular to the shore is called crosshore transport (U.S. Army Corps of Engineers, 1984). The crosshore transport is the significant transport process in the offshore zone, while both crosshore transport and longshore transport are significant in the surf zone (U.S. Army Corps of Engineers, 1977).

2.5.1 Sedimentary Sources

A beach can consist of material in a wide range of sizes, from boulders, gravel to sand, and the highest amount of sediment is transported by rivers. The transported material can come from for example glaciers, biogenious sources or weathered rocks (Pethick, 1984) and depending on the bedrock in the area sediments will have different compositions. The most commonly existing materials are the minerals quartz and feldspar that are generally used as building blocks in bedrock. Heavy minerals can also be found on beaches around the world and since they are usually of a darker colour they can form a distinct darker stretch on the shore, which easily can be visualized. Organic material can also be of great quantities on some beaches where the turnover of calcium carbonate organism is high, i.e. corals and shells that are deposited on the beach (Komar, 1998).

The present size of the beach sediment is determined by the energy of the waves, the resource of the sediment and the offshore slope where the beach is constructed. A resource which could provide the right grain size is needed if a beach is to exist. Waves with high energy will have the capacity to transport more sediment, which results in a higher span of grain sizes that can be transported offshore as well as longshore. The greater the slope of the nearshore zone is, the coarser the beach sediment will be. Because there is usually a relationship between high wave energy levels and steep nearshore slopes. There are deviations from this, e.g. sheltered bays with coarse grains, but mostly a relationship can be seen between the three variables (Komar, 1998).

2.5.2 Grain Size Distribution along a Beach Profile

In general, the grain sizes decrease in the offshore direction and the finest material is found furthest from the shoreline. The coarse sediment at the beach

profile is found in the breaking zone, where the waves break and continue propagating towards the surf and swash zone. Below a broken wave a bar is formed and here the grain sizes of the sediment tend to be slightly bigger than in the rest of the breaking zone. This is due to that the wave loses energy as it breaks and thus coarser sediment is lost from the propagation of the wave and settled at the sea bottom. The highest grain sizes are found just before the swash zone as the final breaking of the incoming wave occurs. The backwash from the swash is only driven by gravity force, hence smaller sediment tends to be left on the beach slope, meanwhile coarser material is left at the start of the swash zone (Komar, 1998).

2.5.3 Sediment Budget

The method called budget of sediments is a useful tool for determining the sediment transport within a specified control volume and time span. All processes adding or removing sediment to the control volume can then be estimated and quantified. Both natural flow of sediment and manmade paths can be mapped (Komar, 1998). If looking at the absolute longshore transport of sediment, i.e. adding both what goes in and what goes out of the control volume without concerning about the direction of the transport, the gross sediment transport is investigated. On the other hand, if looking at the net longshore sediment transport, the direction of the transport is accounted for and it and can be either positive or negative depending on the reference of choice (Hanson, 2014c). When talking about sediment budgets it is important that it is clearly stated which of the transports one is referring to so no misunderstandings occur. Net transportation is an important tool when investigating if a beach remains stable, is eroding or, to the contrary, is accreting. Different processes that affects the budget is discussed further in *2.6 Causes of Shoreline Erosion.*

2.5.4 Crosshore Sediment Transport

Ideal deepwater waves generate a circular movement of the water particles perpendicular to the wave crest. The strength and scale of this circulation decrease with depth and is non-existing at the sea bottom. Thereby, the movement will not reach as deep to have an impact on the sediment at the bottom. As the wave propagates onshore, the water depth becomes shallower and the circular movement becomes elliptical. The elliptical movement also here decreases with depth, but has a greater impact on the bottom sediment, and the water at the bottom begins to move. At shallow waters the elliptical

movement stretches and becomes almost a horizontally straight line. These horizontal water movements transport sediments shoreward and seaward, which is referred to crosshore sediment transport (U.S. Army Corps of Engineers, 1977). Crosshore sediment transport is mainly affected by the steepness of the wave, the sediment grain size and the beach slope. High and steep waves tend to move more and coarser material offshore, while lower waves of long period move finer material onshore (U.S. Army Corps of Engineers, 1984). If the amount of sediment transported with the swash up on the beach slope equals the amount being transported with the backwash out to the sea again, the slope is said to be in dynamic equilibrium (Komar, 1998). Undertow and rip currents also contributes to the seaward crosshore sediment transport.

2.5.5 Longshore Sediment Transport

As the waves break in the breaking zone or the surf zone, energy is supplied to the sediment, which stirs up from the sea bottom. The longshore current generated parallel to the shore, catches the free drifting sediment and transport it along the shoreline. This transport of sediment may only be local rearrangement, or it may be transported for several kilometres (U.S. Army Corps of Engineers, 2012). As large amounts of sediments get trapped by coastal structures, such as groins and jetties, the knowledge about the proportion of littoral sediments that is being transported is now well known. The longshore transport rates may vary from nearly nothing up to several million cubic meters per year (Inman, 1966). Hence, this process is the most essential process concerning the change of the beach morphology (U.S. Army Corps of Engineers, 2012).

Sediment can also be transported in the longshore direction by the swash. The broken waves transport sediment up on the beach with the swash, but at the same time the longshore current makes the wave run down with the backwash in an angle different to the incoming angle of the swash. This creates a positive net transport of the sediment in the longshore current direction.

The longshore transport rate (Q_l), i.e. the rate at which the sediment moves parallel to the shore, can be predicted with several different methods and is usually measured in units of volume per time. In this study, the wave energy flux method was adapted to estimate the longshore transport rate at Nha Trang bay and the so called CERC formula was used. The wave energy flux method assumes that the longshore transport rate depends on the longshore component

of energy flux in the surf zone, which is estimated by using the linear wave theory to calculate the conservation of energy in shoaling waves (U.S. Army Corps of Engineers, 1977). The energy flux per unit length of wave crest is estimated with Equation 4.

$$P = (EC_g)_b \tag{4}$$

where the wave energy at the breaker line is calculated with Equation 5

$$E_b = \frac{\rho g {H_b}^2}{8} \tag{5}$$

and the wave group speed at the breaker line C_{gb} is calculated with Equation 6

$$C_{gb} = \sqrt{g d_b} = (g \frac{H_b}{\kappa})^{1/2} \tag{6}$$

where d_b is the depth at the breaker line, H_b is the wave height at the breaker line and κ is the breaker index H_b/d_b (U.S. Army Corps of Engineers, 2012).

The longshore component of the energy flux (P_l) is given by Equation 7

$$P_l = (EC_g)_b sin\alpha_b cos\alpha_b \tag{7}$$

where $(EC_g)_b$ is the energy flux in the breaker zone and α_b is the angle of the incoming wave to the shore (Komar, 1998).

Finally, the longshore transport rate (Q_l) can the predicted with the CERC formula presented in Equation 8

$$Q_l = \frac{K}{(\rho_s - \rho) g (1-n)} P_l \tag{8}$$

where ρ_s and ρ are the density of the sediment and of the sea water, respectively, g is gravitational acceleration force, K is a dimensionless transport coefficient affected by the grain size and n is the porosity of the sediment (U.S. Army Corps of Engineers, 2012).

2.6 Causes of Shoreline Erosion

A beach and its shoreline are not a fixed state, but nature has a tendency to change and adapt to new features and conditions. Some shores are subjected to growth and expand while other might be subjected to erosion and contract. Both of these shoreline changes could be caused by natural processes, but anthropogenic impact is not to forget.

2.6.1 Natural Variation

When a beach is exposed to higher waves than normal, sediment from the beach will be transported out into deeper parts of the sea with the crosshore currents. Often bars are formed in the ocean this way. When a calmer period comes, sediments are transported back to the beach again by the waves. Higher waves often occur in relationship with storms and hard weather and calm period comes in between. This makes it a seasonal loop that alters the beach appearance from season to season. Such system can be in balance and do not have to imply that erosion is taking place. But it could be that some sediment are lost to deeper parts of the ocean where it is lost from the crosshore system, resulting in a negative net transport of sediment and hence erosion. The seasons of the year also have a clear relationship to the condition of the beach, as the rough weather during the winter implies that the beach retreats while the beach accretes during the gentle summer weather (U.S. Army Corps of Engineers, 1984).

Longshore currents can also influence the natural variation of the complete shoreline orientation. Depending on the angle and strength of the incoming wave, which vary with the seasons, the shoreline alternates. With waves coming from a north direction, the shoreline might retreat in the southern part and accrete in the northern part. If waves instead come from a south direction, the reverse will occur. This makes the shoreline to naturally shift in gradient from a plan view.

Strong winds can also carry sediment from the beach and thus change the sediment budget. Other changes in the weather condition can also decrease the transport of sediment to the beaches. For example if an area is experiencing a drought, the rivers will have less flowing water and thus the amount of sediment that is transported is less (U.S. Army Corps of Engineers, 1984).

The beaches are also affected by the climate change. If the sea level rises, the beach will try to adjust to get the same profile once more, as it was in a stable state. This will make the beach retreat and sediment will be lost (U.S. Army Corps of Engineers, 1984). Sea level rise occurs naturally around the world, but there is also a fear of higher speed of such a rise due to global warming that might melt glaciers and thus adding big volumes of water to the sea.

2.6.2 Human Impact on Erosion

Humans can interrupt the stability of beaches around the world; one example of this is the mining of sand. Since sand is an ingredient in building material it is coveted in today's society when population growth is increasing and thereby also more properties are built. Often the sand comes from rivers, floodplain and terrace deposits and removal of sand from these places will set the system in unbalance as the sediment budget is altered and the hydraulics of the channel is changed (Padmalal and Maya, 2014). If less sand is transported in the rivers, it will be harder for the beach to renourish.

Constructions of dams in river systems are also changing sediment budget for many rivers. The dams could be built to act as, for example, water source for hydropower or irrigation and fresh water source. The sediment is trapped inside the dams and thus it is hindered from its transport further down in the river and eventually to the coast.

In harbours or channels, sediment will often get stuck and hinder the flow of water. Therefore dredging of material in harbours and channel is often done. The sediment is then removed and relocated at some other place in the sea, thus the material is lost from the sediment balance of the coast (U.S. Army Corps of Engineers, 1984). When dredging bars outside the beaches, the wave pattern will be changed and if waves are not breaking at the bar any longer they will continue their way towards the beach with higher energy and thus the risk for erosion at the beach will increase.

The beach can also be subjected to change by man for example by removing vegetation that binds sediment with its roots. Also flattening of the beach to make it more attractive for sunbathers will affect the sediment transport processes. Building pavements and hardening the surface are also working in favour for erosion. Other constructions along the coastline, like sea groins and seawalls, can also increase the risk of erosion by changing the wave climate in front of them (U.S. Army Corps of Engineers, 1984). Sometimes these

measures protect the nearby shores but will change the sediment budget for areas downstream, resulting in a movement of the erosion problem.

3. General Background about Vietnam

Vietnam is located in the Southeast Asia with the neighbouring countries China, Laos and Cambodia, which can be seen in Figure 7. The country is oblong with some parts as narrow as approximately 50 kilometres wide (Google Inc, 2015), but in total the land area covers an area of 170,000 square kilometres (Inman, 1966) with a population of 90.7 million people (Mårtensson and von Konow, 2015). A great part of the land border, more precisely 3,260 kilometres, is located along the coast and adjacent to the South China Sea in the east and to the Gulf of Thailand in the south. The coastline got an irregular profile with a lot of headlands and embayments (Inman, 1966).

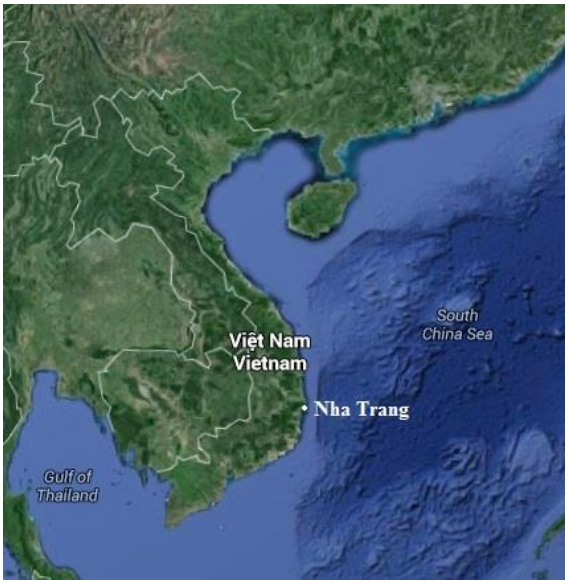

Figure 7. Vietnam is located in Southeast Asia with the adjacent countries China, Laos and Cambodia and oceans South China Sea and Gulf of Thailand (Google Inc, 2015).

3.1 Climatology

The location of Vietnam by the Southeast Asian waters is in the region where semi-permanent high-pressure areas occur alternately with the winter hemisphere over the landmasses of Asia and Australia. This creates the ideal conditions for monsoon climate. The tropical monsoon climate of Vietnam affects the temperature, precipitation and wind direction seasonally. Also the northeast and southwest monsoons influence the climatic conditions

differently throughout the country. The northeast monsoon has the strongest impact on the northern parts of Vietnam due its relation to the South China Sea, while the southwest monsoon tends to be more pronounced in the southern parts of the country. In this way, precipitation, wind and duration of season vary throughout the country. In October to March (winter time) the winds of the northeast monsoon blows in a clockwise direction from southwest to northeast, and then in May/June (summer time) the winds change direction to southeast/south. The southeast monsoon begins in June/July and is fully developed and reaches the highest wind velocities during the latter part of July/August (Inman, 1966). The wind atlas, developed by Duong Cong Dien from Institute of Mechanics, Hanoi, presented in Figure 8 show the mean wind velocity during winter and summer time, respectively. It is clearly shown that during winter time the winds reach higher amplitude and winds blowing from northeast dominate, while during summer time the wind is more gentle and dominates from the south.

Figure 8. The seasonal mean wind velocity over Vietnam and the Southest Asian

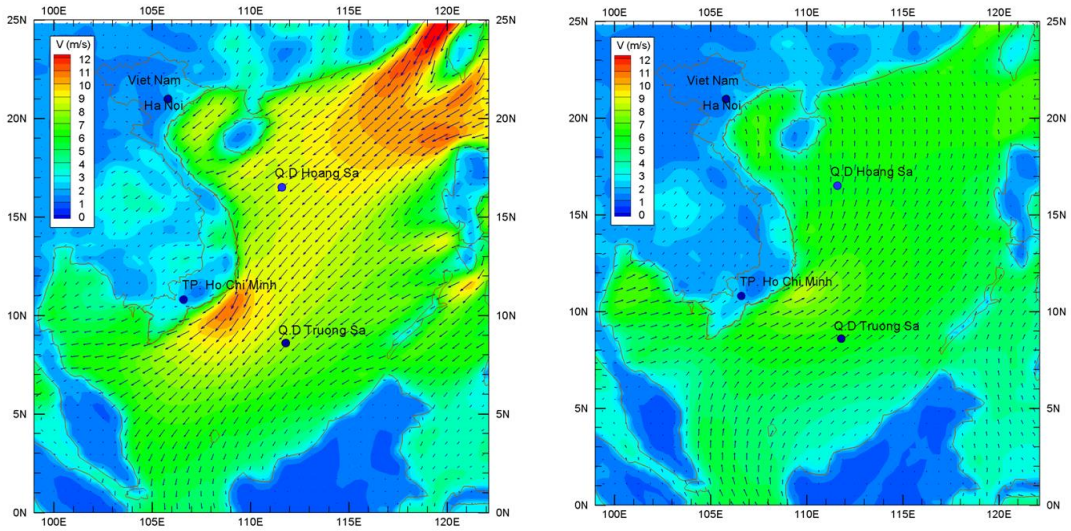

waters during winter time (left-hand side) and summer time (rigth-hand side), when the northeast and the southwest monsoons, respectively, occur (Courtesy of Duong Cong Dien, Institute of Mechanics, Hanoi).

The average temperature in Vietnam ranges from 24 to 30 degree Celsius while the annual precipitation ranges from 1,000 mm to over 3,000 mm. The amount of precipitation is also related to the topography of the country. The occurrence of rainfall is more frequent in areas with higher elevation, like the plateaus and

mountainous areas in the north, which can receive an annual precipitation of up to 4,000 mm. The greatest coastal rainfall appears in Hue, located coastline in central of Vietnam, and then the rainfall intensity decreases in southerly direction (Inman, 1966).

3.2 Marine Phenomena

The South China Sea adjacent to the Vietnamese coastline results in a complex system with waves, tides and typhoons. Direction and height of the waves in the sea are related to the direction and strength of the winds, which in turn is in direct relationship with the monsoons and seasonal variations. The waves generally follow the direction of the wind, which means that during the northeast and southwest monsoons the waves come from northeast and southwest, respectively. The weather tends to be rough during the northeast monsoon, with stronger winds and higher amount of precipitation, and with that follows a rough wave climate with higher waves.

The tidal processes are very complex due to the many different types of tides present along the coastline, such as diurnal, semi-diurnal, mixed diurnal, mixed semi-diurnal and tideless zones (Nguyen and Larson, 2014). A location with diurnal tide experience a high tide and a low tide each day, while a location with semi-diurnal tide experience two high tides and two low tides each day. At some places along the coastline even a mixture of these kinds of tides occur, e.g. the mixed diurnal tide and mixed semi-diurnal tide.

Tropical cyclones and typhoons are common occurring natural phenomena in the area of the North West Pacific and may cause great devastation with its forceful winds and torrential rainfall. In average, 4-5 tropical cyclones and typhoons affect Vietnam every year and normally the typhoon season lasts from August to November with start in the northern Vietnam and proceeds southward. With the ongoing climate changes the typhoon season will be moved to a later time of the year and the typhoons will decrease in intensity but occur much more frequent (Ministry of Natural Resources and Environment, 2003).

3.3 Topography

The northern two thirds of Vietnam are covered by semi-mountainous areas, while the inland consists of high plateaus with elevations up to 2,000 meters. Between the inland and the coastline, the environment consists of

intermountain and alluvial plains transported by sea streams and oceanic waves and currents. The southern one third of Vietnam is a low-lying area with dominating alluvial deltas, which often is exposed to floodings. The continental shelf along Vietnam slopes gently from the shoreline out to the edge of the shelf down to 200 meters then continues more steeply down to depths of 3,000 meters and more in the South China Sea (Inman, 1966).

3.4 Geology and Geomorphology

The geologic setting of Vietnam is dominated by hard rocks of the Annamite Range, which is an extended mountain chain from the Himalayan Mountains. The hard rocks contain coarse-grained, intrusive rocks (granite), older sedimentary formations (largely metamorphosed to limestones, quartzites and schists) and volcanic rocks (basalt and rhyolite). The south part of the Annamite Range has eroded and which has led to the formation of the high plateaus in the northern and central Vietnam (Inman, 1966).

Many of the headlands along the irregular coastal areas of the north and central Vietnam are composed by former islands in a Holocene sea and were created by littoral deposition. There are many sandy beaches along the coast stretch that do not exceed the length of ten kilometres, with the exception for the 128 kilometres long beach at Hue. Old barriers of beach ridges, dated up to between 2,500 and 4,000 years, indicate the former coastlines. Due to this long-lasting remaining of the sea water level, an extensive amount of littoral deposits appear along the Vietnamese coast. In some places the deposits have blown inland and created great sand dunes (Inman, 1966).

The sediments of the deltas in the southern areas consists of the fine-grained fluvial deposits muds and sands, which are transported by rivers like the Mekong river, and covers the hard Annamite rock with at least a 400 m thick layer (Inman, 1966).

3.5 Geomorphological Change along the Vietnamese Coastline

A great part of the Vietnamese land-frontier is located by the coast and is exposed to the interactions between land and sea, and natural and human processes. Hence, Vietnam is facing the issue of coastal erosion, which results in morphological changes and may have a strong and negative impact on not only nature itself but also on facilities. Between the years of 1990 and 2003,

263 sites spread along the Vietnamese coastline exposed to erosion were recorded with a total eroded area of 8,839 ha. Some of the stretches experience only local and short-section erosion problems, while other stretches are exposed to severe erosion (Cat et al., 2006).

4. Nha Trang Bay

Nha Trang bay is located in the province of Khanh Hoa, which is situated in the south central part of Vietnam, approximately 500 kilometres northeast from Ho Chi Minh City, see Figure 7 and Figure 9. Nha Trang bay covers 507 square kilometres and diving is a popular attraction as the bay provides an ecosystem with coral reefs, especially along the islands where the conditions are favourable (Nguyen et al., 2013). Two rivers enter the bay, Cai in the middle and Tac in the south. There are nineteen islands located in the bay, the biggest among them being the island of Hon Tre (Mau, 2014). The bathymetry in Nha Trang bay is quite complex and varies due to the presence of the islands. The islands provide sheltered areas which have made anchoring here easy and were probably the reason why Nha Trang has functioned as an important harbour for many years. There is a fishing harbour located in the Cai river entrance (Inman, 1966) but also an international and bigger harbour in the south of the bay (Nguyen et al., 2013).

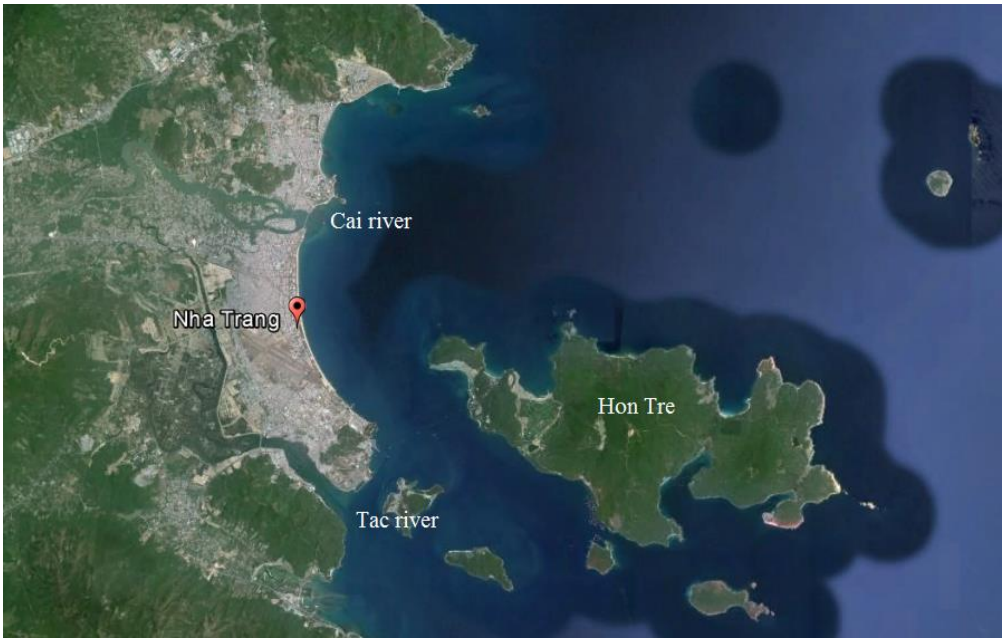

Figure 9. Satellite image of Nha Trang bay where the location of Nha Trang city is marked (Google Inc, 2015).

4.1 Nha Trang City

The city of Nha Trang is located in the bay and the population was in the year of 2010 estimated to be 304,200 people (Mårtensson, 2015). The city stretches along the 16 kilometres long beach located in the bay, see Figure 9. The beach is divided into the north and south beach which are separated by the river mouth of Cai river. The main attraction of the city is the southern sandy beach, see Figure 10, running along the Tran Puh street, which covers a length of 7 kilometres (Mau, 2014). While the northern beach has suffered from severe erosion and is at the present lacking beach on large stretches only leaving the groins visible, see Figure 11.

Figure 10. The sandy beach south of Cai river mouth in Nha Trang.

Figure 11. The beach of Cai river mouth has suffered from severe erosion and today the beach is absent and only the seawall is visible

Before the year of 2000, the region got most of their income from fishery, agricultural and forestry activities. Today the tourist brings capital to the area and plays an important role in the local economy of the region. To meet the increasing demand, new facilities and services must be built to deliver the need of the growing interest in the region. The building industry increases and generates work when new roads and hotel complex etc. are built. Most of the new constructions are located along the southern beach and Tran Phu street. Today the tourism and industrial construction is making 80% of the total gross domestic in the region of Khanh Hoa (Nguyen et al., 2013).

4.2 Climatology

In Nha Trang the year is divided into two seasons, the dry season and the wet season. The precipitation is around 1,500 millimetres per year. The dry season usually occurs in the months of January until August. Between the years of 1995-2004 the mean precipitation was 8.40 millimetres in February, which makes it the driest month of the year, see Figure 12. The months September to December is the wet season, with the most precipitation appearing in November, which has a mean value of 386 millimetres of rain during the time period 1995-2004 (Mau, 2014).

The large amount of rainfall coincides well with the time of year when the northeast monsoon is taking place, i.e. in the months of October to March (Lefebvre et al., 2014). The large amount of rainfall also leads to a higher river

discharge through Cai river, which is visualized in Figure 12. A larger volume of water being transported in the river generates a larger force, which in turn manage to transport a greater amount of grains through the river and out to the sea (Mau, 2014).

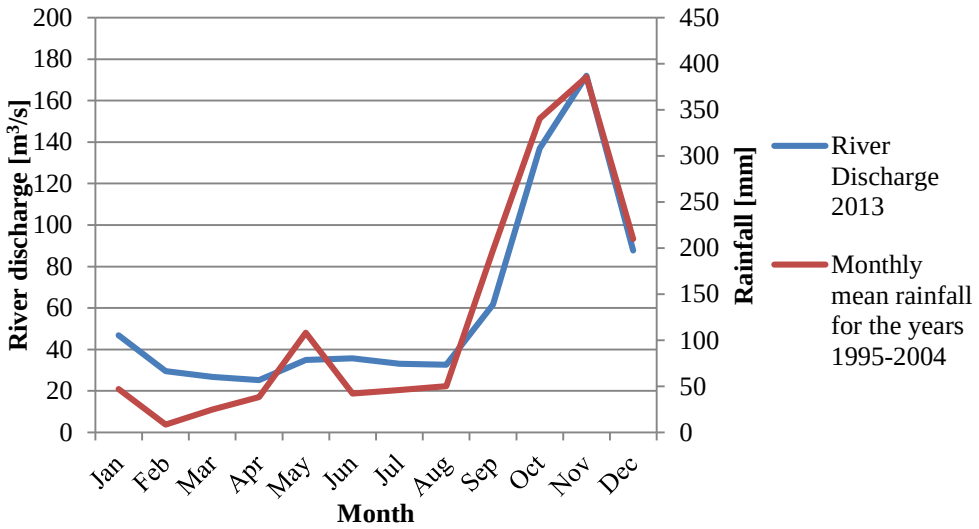

Figure 12. The discharge from Cai river in the year of 2013 as well as the mean rainfall in Nha Trang in the years 1995-2004.

Nha Trang is affected by two monsoons, the northeast monsoon and the southwest monsoon. The northeast monsoon is the strongest one and is most dominant in the months November and January. In the years 1988 to 2007 the maximum recorded wind velocity was measured to be 28 m/s in November 1988. The southwest monsoon is most dominant in the month of June to September. The maximum recorded wind velocity between the years of 1988 to 2007 was recorded to be 16 m/s and occurred in September 1992 (Mau, 2014). Figure 13 and Figure 14 show the amplitude and direction of the winds in the months September and November, which represents the months of the southwest and northeast monsoons, respectively, during the years 2002-2011. The weather data, i.e. the precipitation and the wind data, have been measured at the meteorology station in Nha Trang at the latitude 12°13' and longitude 109°12'.

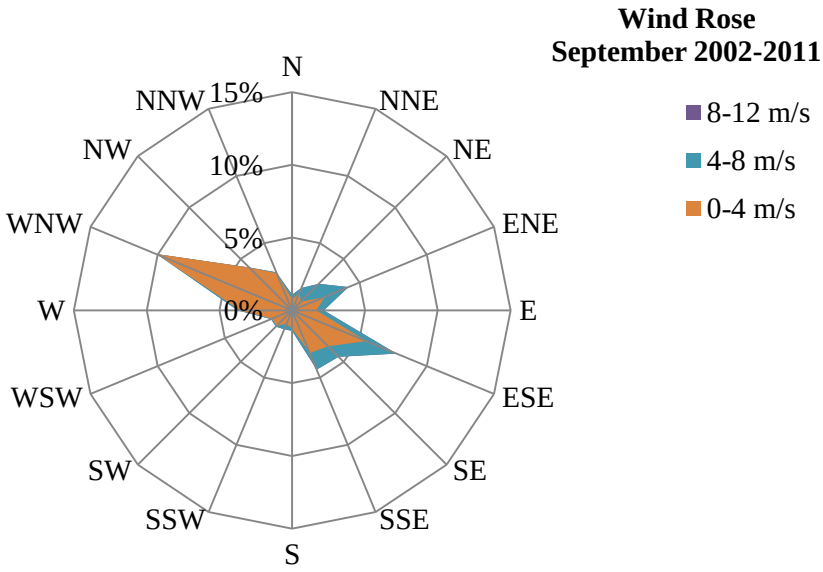

Figure 13. The variation of the wind amplitude and direction for September during the years of 2002-2011, i.e. during the southwest monsoon.

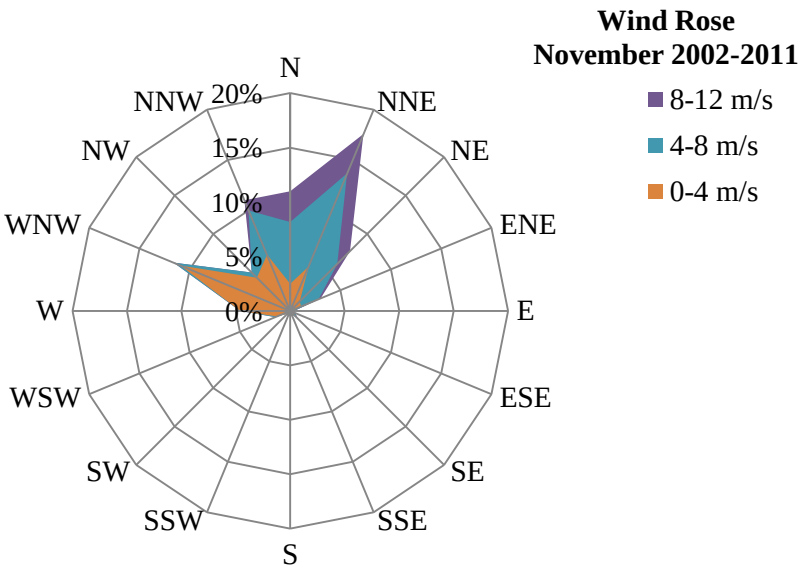

Figure 14. The variation of the wind amplitude and direction for November during the years of 2002-2011, i.e. during the northeast monsoon.

The temperature in Nha Trang is fairly constant throughout the years. It only varies slightly between the higher temperature of 29 degrees Celsius during the summer months of June, July and August and the mean temperature of 24 degrees Celsius occurring during the winter months of December and January (Mau, 2014).

4.3 Hydrodynamics

The wave climate at Nha Trang coincide with the wind patterns and monsoons. During the northeast monsoon, strong waves are entering from the northeast, while during the southwest monsoon, weaker waves enters from the southeast. Water bodies can also be affected by the gravitation force that the earth experience from the sun and moon. Depending on the location, the difference in water level could range from almost none to several meters (U.S. Army Corps of Engineers, 1984). Diurnal tide means that the water body experience one high and one low tide every day. Semi-diurnal tides on the other hand have two high and two low tides per day. As the lunar day is not equal to a sun day, each tide is occurring in a delay of approximately 50 minutes per day. The largest tide is called the spring tide and occurs when the sun and moon is linear and thus exert its force in the same direction. When being perpendicular to each other the tide is at its lowest point, called neap tide (Pinet, 1998). Nha Trang experiences a mix of the diurnal tide and the semi-diurnal tide. In Nha Trang the spring tide can reach 2.5 metres and the neap tide can be as low as 0.4 metres (Bui et al., 2014). The tidal level for the year of 2013 can be seen in Figure 15.

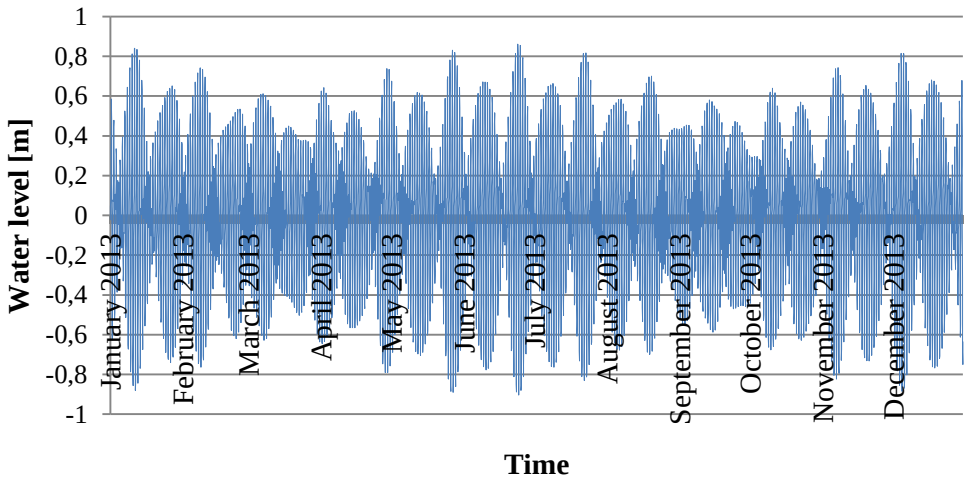

Figure 15. The tidal level variation in the south of Nha Trang bay in the year of 2013 measured at Institute of Oceanography Tide Station in Nha Trang

4.4 Geology and Geomorphology

At the city of Nha Trang the geology is made up from granitic rock but in some areas the bedrock also consists of volcanic rock. The geology in Nha Trang and the surrounding islands in the bay differ to some extent (Inman, 1966).

The main contributor to sediment in the Nha Trang bay is the river Cai. It deposits sediment in the bay and forms ridges there and thus the sediment is said to have terrigenous background. Only 2% of the material on the beach at Nha Trang is made up from biogenous material, that contains a lot of calcium carbonate like shells, corals etc. The situation is different when looking in small bays that are sheltered on the island in the bay, where the calcium carbonate content in the sediment reaches a much higher level, due to the higher distance to the river mouth (Inman, 1966).

The sand in the bay has some differences in the appearance. Most of the sediment discharge from the river Cai is made up of sand (Mau, 2014) and this sand is light in colour and have irregular surfaces (Inman, 1966). Only a minor part if the sand is made up from darker and slightly more reddish sand. Inman (1966) suggest that this is remains from previous sedimentation cycle and thereby it differs in the appearance.

The city of Nha Trang is built on old beach ridges which have coarse sand. Below this layer of approximately 10 metres, another layer of more silty sand is located. It is believed to be the remains of the beach existing prior to the modern beach of Nha Trang (Inman, 1966).

4.5 General Processes

There are two rivers entering Nha Trang bay, the rivers Cai and Tac, see Figure 9. Cai is entering the bay in the centre of the bay, while Tac's river mouth is situated in the south of the bay and thereby only contributes minor to the freshwater flow into the bay. The catchment area for the river Tac is 72 square kilometres while Cai has a catchment area of 1,880 square kilometres (Inman, 1966). The catchment areas originate from an altitude of approximately 500 metres above sea level and from there the water have a relatively short distance to the outlet in Nha Trang bay (Nguyen et al., 2013). The flow varies much depending on the season. Between the months of October to December to flow is highest in Cai and can reach up to 173 cubic metres per second. When the flow is at its lowest in Cai in April, when it drops to 25.7 cubic metres per

second (Mau, 2014). During the low flow months in the Cai river the saltwater intrusion is significant and can extend all the way up to 8 kilometres in the river (Inman, 1966). The total amount of water transported from Cai is roughly 916 cubic kilometres of water per year. Since Tac is being a smaller river the contribution of flow to the bay is less, only 0.09 cubic kilometres per year is entering the bay.

Sediments follow with the water flow and Cai yearly transport 80.38 million tonnes of sediment into the bay, most of it entering the bay when the flow is high in the winter months. On the other hand, Tac only transport 0.26 million tonnes of sediment per year to the bay (Nguyen et al., 2013). According to Inman (1966), Cai brings 195,000 cubic metres of sediment per year to the outlet of which sand is estimated to be approximately 63% of that load (Inman, 1966).

In the outflow from the rivers to the bay there are also contaminants from anthropological activities such as farming and industries located upstream of the outlet (Peresypkin et al., 2011). This will affect the quality of the water in the bay. A study by A.D. Nguyen et al. (2013) showed that trace metals in the bay has increased since the year of 2000 and that the coral reefs in the bay has deteriorated.

4.6 Sediment Transport Mechanism in Nha Trang Bay

The flow, and thereby also the transport of sediment, is mostly dependent the wave and current climates inside the bay. The wave and current climates are in turn affected by the local winds, the monsoons and the bathymetry of the bay (Mau, 2014).

The flow from Cai varies to a great extent due to the uneven occurrence of precipitation, large amount of rainfall leads to larger flow and little precipitation leads to lower flow. As the sediment is transported by the water, the amount of sediment reaching the bay varies with the precipitation. The sediments reaching the bay are to some extent settled inside the bay while some, normally finer particles, are transported seaward or sediments are transported further south down the coast and are deposited in for example Cam Ranh, a city about 40 kilometres from Nha Trang. When there is little or low wind speed, the freshwater from the river floats on top of the seawater due to the difference in density. Thus the sediment have lower tendency to settle and the beach will have less nourishing of sand. (Inman, 1966).

Waves contain energy and can thus transport sediment. As the waves are higher in the northeast monsoon the tendency to transport sediment, and also heavier sediment, is thus higher then. The waves create stronger currents which create stronger longshore currents and the sediment transport increases. The islands in the area also play a role in how the transportation is affected. By being an obstacle to the South China Sea, the sediment is not affected by offshore drift to the full extent. The islands also affect the wave climate by causing the wave to diffract along its contours and waves are reflected against the islands. Thereby, the islands create a more complex wave climate (Inman, 1966).

The tide present in the bay can also transport sediment in the crosshore direction as the sea level alters and a tidal current is generated. But as the current is relatively small compared to the currents created by the wave motion, it has only a little impact of the transport of the bay. The small current can mostly transport very fine material and thus the low transport has little impact on the evolution of the beach.

Between the islands and the mainland the wind affects the water by creating a strong current with a high velocity that prevents the particles from settling easily, especially the fine particles coming from the river. That would likely be one of the factors explaining the relatively deep passage of 24 metres between the Hon Tre island and the mainland (Inman, 1966).

4.7 Coastal Engineering Measures

Along the shoreline of Nha Trang city there has been built many constructions, such as seawalls, piers and harbours etc., built during the last two decades, some of which can be seen in Figure 16. The wave climate and the sediment transport in the bay are affected by the constructions along the shore as well as the constructions built upstream the river Cai, which is described in *4.8 River Flow Regulations.*

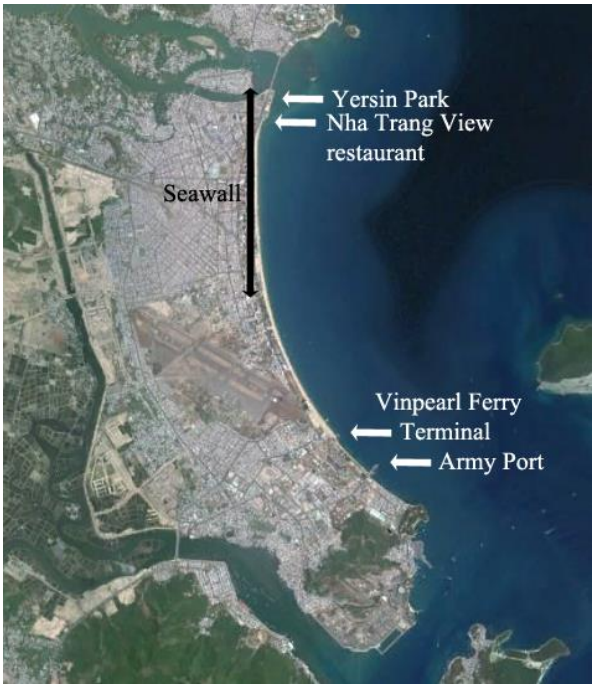

Figure 16. Location of some of the constructions along the shoreline of Nha Trang beach (Google Inc, 2015).

At the bridge abutment of Cau Tran Phu bridge, built in 1999 to 2002, approximately 450 metres of hard concrete surfaces surrounds the Alexandre Yersin Park and continues around the restaurant Nha Trang View cafe, see Figure 17, Figure 18 and Figure 19. The concrete surfaces are estimated to be built after the year of 2009 after the sand spit at the river mouth started to erode. South of the cafe there are also two jetties made of tetrapods, constructed approximately in the years 1990-1992, protecting the structure, see Figure 20 (Vu and Nguyen, 2015).

Figure 17. Concrete constructions around the northern section of Yersin Park at the river mouth of Cai river.

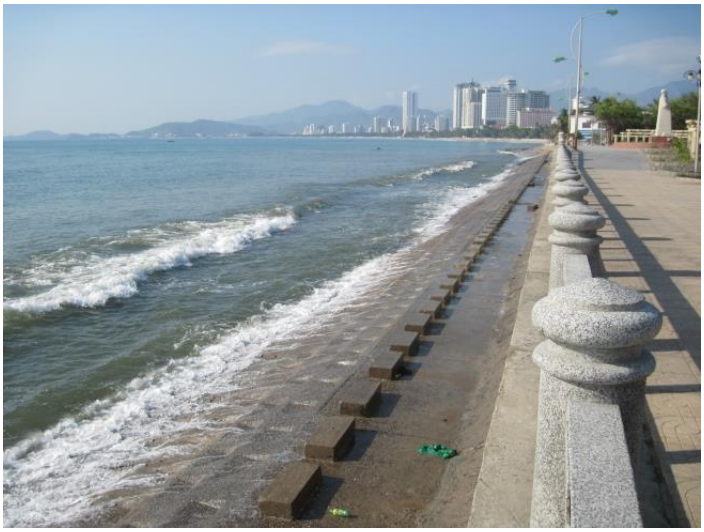

Figure 18. The groins are visible on the east stretch of Yersin Park. The picture is taken towards the south of Nha Trang.

Figure 19. The seawall and the groins at the beach south of Nha Trang View restaurant.

Figure 20. Two jetties made from tetrapods at the south of Nha Trang View restaurant.

A vertical seawall stretches for approximately 2,000 metres along the beach from the Nha Trang View restaurant to the structure Hoa Bien, see Figure 21. Since somewhere between the years 1996 to 1999 the seawall has been constructed in concrete, but formerly it was made of steel. In front of the vertical seawall nearby Nha Trang View restaurant a lower concrete seawall

sloping seawards has been constructed in the around the year of 1999 (Vu and Nguyen, 2015).

Figure 21. A part of the vertical and sloping seawall along the stretch between Nha Trang View restaurant and the structure Hoa Bien.

The Vinpearl ferry terminal was built in 2003 and served as a ferry terminal to transport people to the island Hon Tre. It is a L-shaped groin, with a 60 metres long pier placed crosshore and a 50 metres wide arm attached to it, see Figure 22. It only served as a terminal for a few years, until the cable car to Vinpearl Island was built north of Tac river mouth and was taken into use at the year of 2007 (Vu and Nguyen, 2015).

Figure 22. Vinpearl ferry terminal.

Approximately 600 metres further down the coastline of the Vinpearl ferry terminal lies the Army port. It was built by the US Army in 1965-1966 and was further extended in later years. It was originally 80 metres crosshore, but then extended with 100 metres further out into the sea. Nowadays, the pier is used by the Naval Academy (Vu and Nguyen, 2015).

Dredging has been done in Nha Trang bay. Both in the channel of the Army port and in the Tac river mouth, but also when building hotel complex on the islands in the bay. Since the year of 2000 approximately 2 million cubic metres of dredging material has been removed and dumped outside the bay at the sea (Nguyen et al., 2013).

4.8 River Flow Regulation

The flow to the bay is affected by the presence of both hydropower plants and dams built upstream the rivers, the locations can be seen in Figure 23. The constructions hinder the water flow in the river and consequently also the sediment transport in the river. The lowered volume of transported sediment, which eventually reaches the river mouth and the bay, will affect the shoreline evolution in the bay as the sediment budget gets disturbed.

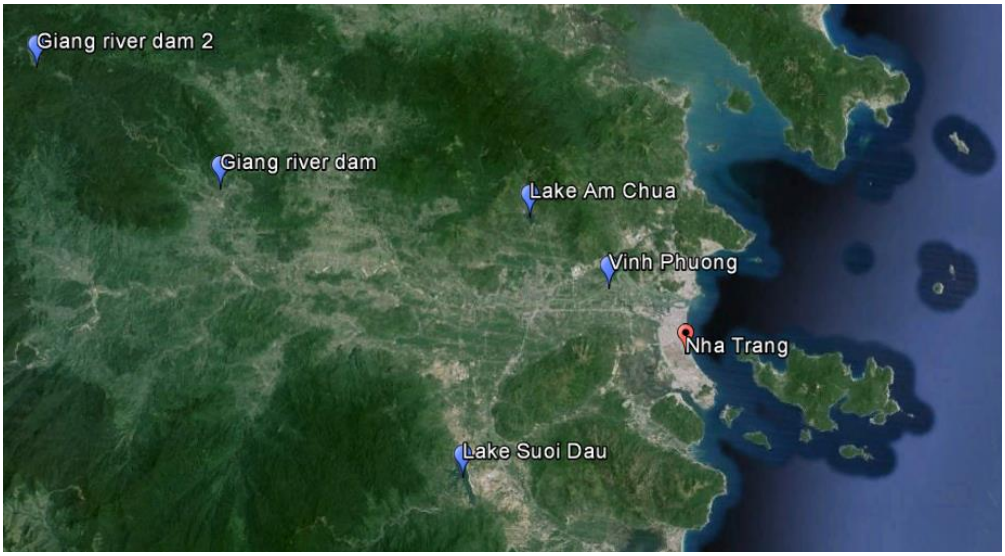

Figure 23. The locations of hydropower plants and dams affecting the flow to Nha Trang bay.

Upstream the Cai river, two hydropower plants, the Giang river dam and the Giang river dam 2, were constructed and opened in the year of 2014. They have a catchment area of 123 square kilometres each and produce 37 MW each (Nguyen, 2015).

Another dam was built by the Vinh Phuong Bridge, approximately 8 kilometres upstream the river mouth, in the year of 2002 to ensure no salt water intrusion upstream of the Cai river. In the rainy season the same year as constructed, the dam was swept away due to the high water flow in the river. A new dam was built the following year only to be swept away in the rainy season once again. In the year of 2004, a new dam was built that has hindered the intrusion, and reduced sediment transport, since then (Anonymous, 2006).

There are also two lakes, Am Chua lake and Suoi Dau lake, in the area that are dammed and thus have their flow regulated. In the Am Chua lake the water is used for irrigation and cultivation, with a yearly outtake of 45 million cubic metres per year (Nguyen, 2015). The Suoi Dau lake functions as a freshwater source for drinking water to the neighbouring city of Cam Ranh and Dien Khanh and contains 30 million cubic metres of water (Anonymous, 2006).

5. Field Measurements

Data of present shoreline and beach profile positioning, wave and current speed and direction, sediment samples and sediment transport rates were gathered during the stay in Nha Trang, Vietnam, in the Spring of 2015. The objective of all compiled data was to achieve a greater understanding for the essential nearshore processes acting in the bay of Nha Trang. Some of the data would also be comparable to previous researches done on the area of the south beach in Nha Trang. Also observation of the beach and its environment was performed during the field investigations.

The dedicated efforts of fieldwork were undertaken during the stay in Nha Trang, the 7th of March and the 11th of April 2015, for collecting all necessary data.

5.1 Conditions of Field Trips and Locations for Measurements

On the 7th of March 2015 a field trip to the beach south of Cai river mouth was carried out. The weather was calm with indiscernible winds during the day and no precipitation had occurred the days before. The data was collected between 8:30 am and 4 pm. According to a tidal prediction table (Center of Oceanography, 2015), the tide fluctuated between 1.2 m and 1.4 m above minimum tide level during the time of the measurements, with the lowest sea level at the start of the data collection and the peak sea level at 1 pm. The tide level was predicted to sink during the afternoon and reached 1.3 m at the end of the measurement day. The maximum tidal level during the day was at 12 am when the tidal level reached 1.5 metres. The minimum tidal level during the same day was 1.0 meter which occurred from 6 to 7 am (Center of Oceanography, 2015).

Samples were carried out at four different sections along the south beach at the first field trip occasion. During the field trip following samples were taken; one sediment core sample at the mean seawater level and one sediment core sample at the upper berm at Section 2, three Nagata sediment trap samples at Section 2, Section 3 and Section 4 and wave and current data at Section 2. Also, the beach profiles at the Section 1-4 and the shoreline were measured. For locations of the sections, see Figure 24

On the 11th of April 2015 another field trip was carried out to the beach south of Cai river mouth. During the field trip and the days before the weather was

also calm and dry. The tide fluctuated between 1.5 m to 1.85 m during the morning and the time of the measurement. The peak tide of 1.88 m occurred at 1:30 pm and the low tide of 0.9 m at 11:30 pm according to the tide station at Institute of Oceanography. Sediment samples of the top layer at the berm at Section 1-8 and additional samples at four locations along the beach profile at Section 1, Section 4 and Section 8 were collected during the morning.

Figure 24 points out the locations of the sample stations along the south beach of Nha Trang bay and in Appendix 1 the specific coordinates for the stations with the type of sampling that were carried out can be found.

Figure 24. Locations of sampling stations during the field trips on the 7th of March and the 11th of April 2015 at the beach south of Cai river mouth in Nha Trang bay.

5.2 Shoreline and Beach Profiles

5.2.1 Experimental Setup and Procedure

The shoreline at the 7th of March 2015 was measured by walking along the shoreline in the swash zone with a GPS connected to a levelling instrument. Also, four beach profiles at Section 1, Section 2, Section 3 and Section 4,

mostly located in the northern part of the Nha Trang beach south of Cai river mouth, were measured with the levelling instrument. On these sites, data of historical measured beach profiles existed and fixed base marks with known coordinates and levels could be used as reference. A ProMark 2 system from Ashtech with two GPSes, see Figure 25, was used to establish the coordinates of the beach profiles. The accuracy for the system is 0.012 m+ 2.5 ppm m in the horizontal direction and 0.015 m + 2.5 ppm in the vertical direction (Thales Navigation, 2004). From the known point, new coordinates were taken with the GPS roughly around every 10 metres in the direction of the profile, using the stop-and-go function of ProMark 2. The final coordinate of each beach profile, i.e. closest to the mean sea level, was collected in the swash zone. The beach profiles at the four sections were later plotted with the software MapInfo.

Figure 25. The levelling instrument with a ProMark 2 system from Ashtech was utilized to compile the coordinates for the present time shoreline and beach profiles.

5.2.2 Data Collected and their Properties

5.2.2.1 Shoreline Evolution

To get an understanding of how Nha Trang beach has evolved during the recent years, the program Google Earth was used. The program uses satellite images, which allows the user to see the chosen location from a plan view. Satellite image between the years of 2003-2014 were available over the bay of Nha Trang. To see changes in the shoreline, selected years were digitalized using the software Grapher 10. Because of tidal and seasonal variations the position of the shoreline varies distinct, but during the digitalization the shoreline was

set to be at the end of the swash zone present at the time the satellite image was shot. The shorelines for several years were then plotted and visualized in a graph. By presenting shorelines from several years in the same graph, trends for the shoreline evolution could be seen. The selected years were fairly even distributed over the time span and the satellite images were photographed in different seasons of the year. Two graphs were digitalized; one graph for the whole south beach of Nha Trang with a distance of 7 km and another graph for only the northern part of the south beach. Due to observed erosion in the north part, a more close-up plan view for several shorelines both from Google Earth satellite images and GPS-measurements were drawn.

Shorelines digitalized from Google Earth satellites images from August 2003, May 2009 and March 2014 can be seen in Figure 26. In Figure 27 a more detailed visualization of the shoreline evolution of the northern part of the beach south of Cai river mouth is shown. The shoreline coordinates from the years 2007, 2008 and 2009, measured with a GPS by Tran Van Binh and Le Quang Thanh at the Department of Marine Geology, Institute of Oceanography in Nha Trang, are included in the analysis of the shoreline evolution and can be seen in Figure 27.

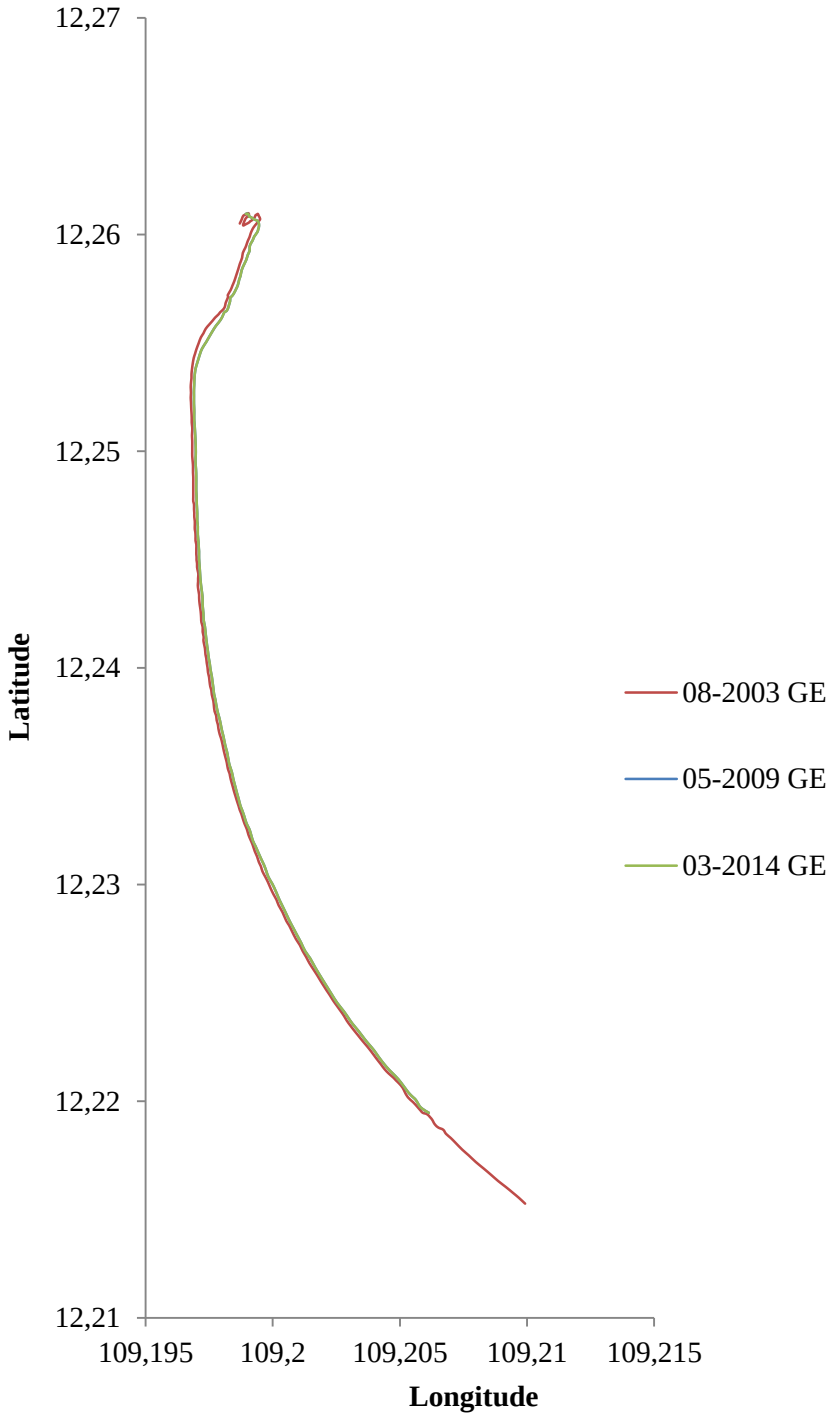

Figure 26. Shoreline positions at August 2003, May 2009 and March 2014 digitalised from Google Earth images (GE).

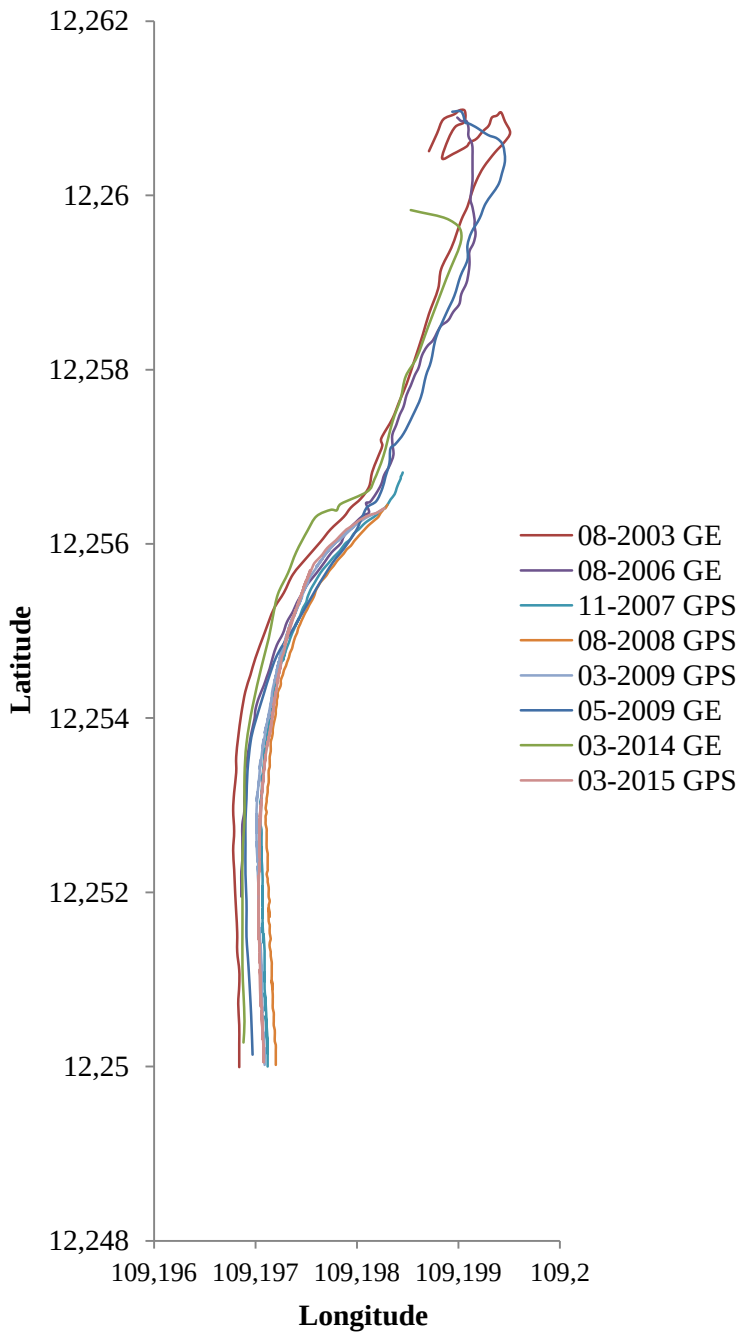

Figure 27. A close-up view of the shoreline positions at the northern part of the beach south of the river mouth with data measured with both GPS (GPS) and from Google Earth images (GE).

In Figure 27, the early years show a sand spit of approximately 190 metres long and 75 metres wide in the most northern part that has eroded over the more recent years. In March 2014, the shoreline from Google Earth shows the most narrow beach stretch south of the restaurant complex. The widest beach stretch is achieved in the measurements done by GPS in August 2008.

5.2.2.2 Beach Profile Evolution

Results of the measured beach profiles from the 7th of March 2015 for sample locations Section 1, Section 2, Section 3 and Section 4 can be found in Figure 28, Figure 29, Figure 31 and Figure 27, respectively. Previous measurements of the beach profiles at Section 2, Section 3 and Section 4 from November 2007, August 2008 and March 2009, were performed by Bui (2009). In the cases where data from several years exists for the same sample location, the data have been plotted in the same graph for clear visualisation and comparability of the beach profile evolution. The graphs present the elevation in metres compared with the lowest sea level on the y-axis and the distance in metres between the start and end point of the measured profile. The angle presented in the graphs inform about the sections' relation to true north.

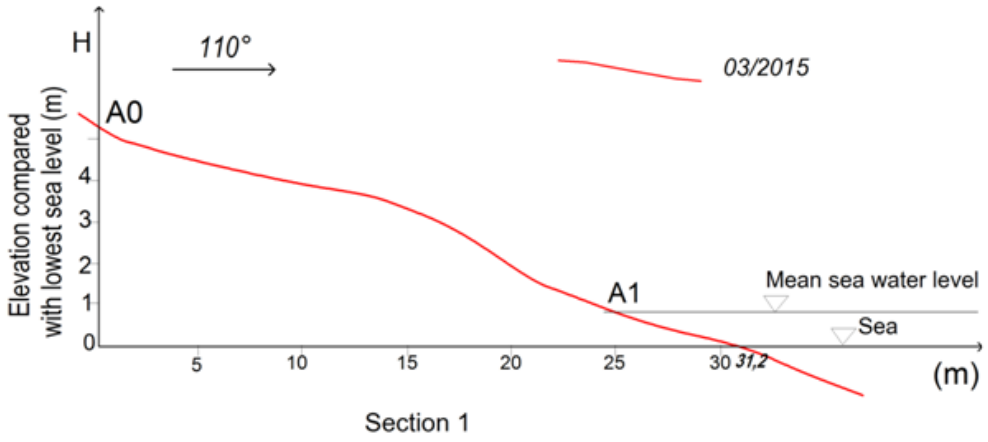

Figure 28. Beach profile at Section 1 in March 2015.

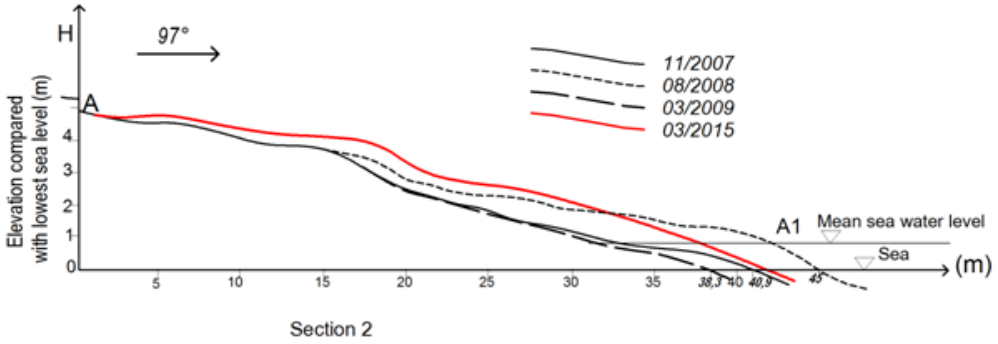

Figure 29. Beach profiles at Section 2 in November 2007, August 2008, March 2009 and March 2015.

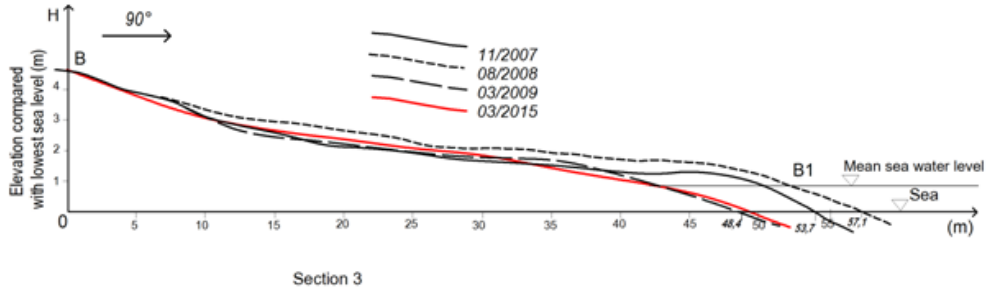

Figure 30. Beach profiles at Section 3 in November 2007, August 2008, March 2009 and March 2015.

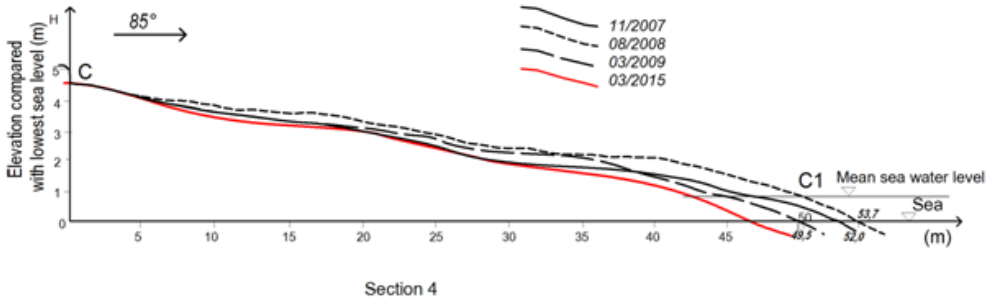

Figure 31. Beach profiles at Section 4 in November 2007, August 2008, March 2009 and March 2015.

The results the beach profiles clearly show the influence of the seasonal fluctuations. Figure 28 shows that the beach is most narrow at Section 1 with a width of 31.2 m, compared with the width at the other sections. In Figure 29, the measurements from March 2015 shows that the beach had a greater

elevation than previous years, but it was more narrow than in August 2008 when the beach had a width of 45.0 m. In Figure 31, the beach had the greatest elevation and was most wide, 57.1 m, in August 2008. The measurements from March in 2009 and 2015 coincide well and show when the beach had the lowest elevation and most narrow with a width between 48.4-50.0 m. Figure 31 shows that the beach was most narrow in March 2015 with a width of 49.5 m and it also had the lowest elevation. In August 2008 the beach was widest, 53.7 m, and had the greatest elevation.

5.3 Sediment Core Samples

5.3.1 Experimental Setup and Procedure

Sediment core samples were taken along the beach profile at Section 2 at the mean sea level and the upper berm. A 92 cm and a 115 cm long plastic pipes with a diameter of 0.09 m, for the sampling at the mean sea level and at the berm, respectively, were used to collect the core samples by hammering it down and pulling the core up, see Figure 32.

Figure 32. Sediment core samples were achieved by hammering down plastic pipes and pulling the cores up.

In the laboratory the core was visualized by cutting the plastic pipe with the sediment core into two pieces. The core was inspected visually and different layers were identified as grain size and colour of the sediment varied throughout the core. The different layers were numbered and samples were taken from the layers for analysis. The samples were washed with tap water to remove any organic material and salt from the seawater. After washing the

samples they were placed in beakers and put into an oven at 100 degrees Celsius until the samples were completely dry.

To determine the grain sizes of the sample, a sieve was used, see the configuration in Figure 33. The sieve consisted of several layers of mesh with different sizes, starting with the coarsest mesh at the top and the finest mesh at the bottom. The samples were poured over the coarsest mesh and the grains that were too small fell through the different mesh until it could not penetrate further. The used mesh size consisted of following sizes; 4.0 mm, 2.0 mm, 1.0 mm, 0.5 mm, 0.25 mm and 0.125 mm. The sieve was placed on a mechanical sieve shaker with a frequency of 40 Ampere. The samples were shaken for approximately 10 minutes, until all grains were sorted. The grains were thereafter weighed and noted in a protocol. To see the distribution of the different grain sizes in a sample, the weight percentage of the different sizes and the accumulative weight percentage were calculated and a grain size distribution graph was plotted.

Figure 33. The instrumental setup used for sieving.

To determine the parameter d50 for all samples, the software Gradistat Version 8 based on the Folk & Ward method and developed by Dr. Simon J Blott was used.

Previous sediment core measurements were carried out in the years 2007 and 2008 nearby Section 2 and Section 4 (Bui, 2009). Same procedure was obtained for plotting grain distribution graphs and running the software Gradistat for the previous measured sediment samples, for comparison with the results of the field trip data.

5.3.2 Data Collected and their Properties

The two sediment core samples collected at the upper berm (B-core) and the mean sea level (S-core) at Section 2 on the 7th of March 2015, were divided into 3 and 14 layers, for the B-core and the S-core respectively, according to visual layers with different grain size and sediment colour, see Figure 34

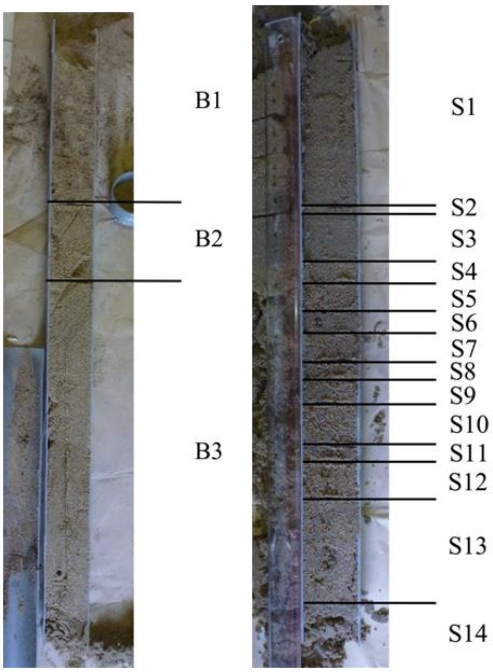

Figure 34. The sediment core samples, collected at the upper berm (left-hand side) and at the mean sea level (right-hand side), were divided into three and fourteen layers, respectively, by visual observations of grain size and colour shifting.

The grain size distributions of the 17 layers for the B-core and the S-core are presented in and Figure 36, respectively, with the accumulated percentage of the sediment samples on the y-axis and the grain size in the units millimetres and Φ on the x-axis. Table 1 and Table 3 present the d50 for the different layers and in Figure 37 the graph show the depth as a function of d50.

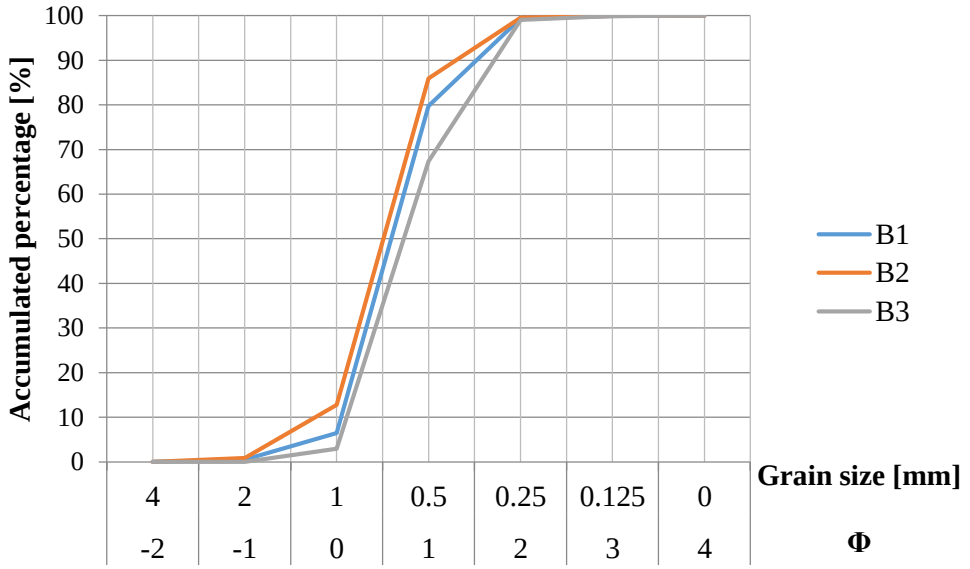

Figure 35. Grain size distributions for the three layers in the berm sediment core at Section 2.

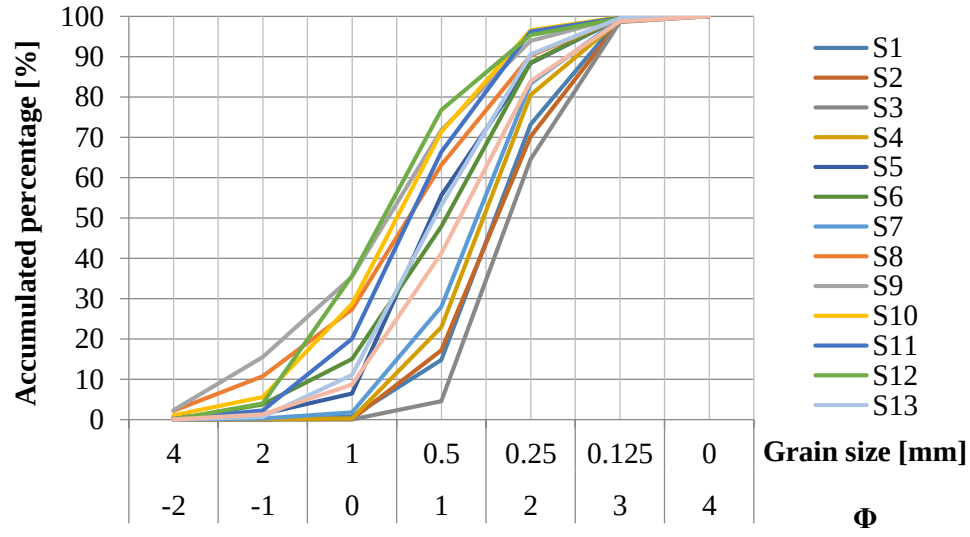

Figure 36. Grain size distributions for the 14 layers in the upper swash zone sediment core at Section 2.

Table 2. Values of d50 for the three layers in the berm sediment core at Section 2.

Berm core Sample	d50 [µm]	Φ
B1	662	0.594
B2	703	0.509
B3	603	0.730

Table 3. Values of d50 for the fourteen layers in the upper swash zone sediment core at Section 2.

Upper swash zone Sample	d50 [µm]	Φ
S1	170	2.56
S2	325	1.62
S3	296	1.76
S4	361	1.47
S5	541	0.887
S6	482	1.05
S7	379	1.40
S8	645	0.634
S9	757	0.401
S10	707	0.500
S11	639	0.647
S12	785	0.349
S13	526	0.926
S14	434	1.21

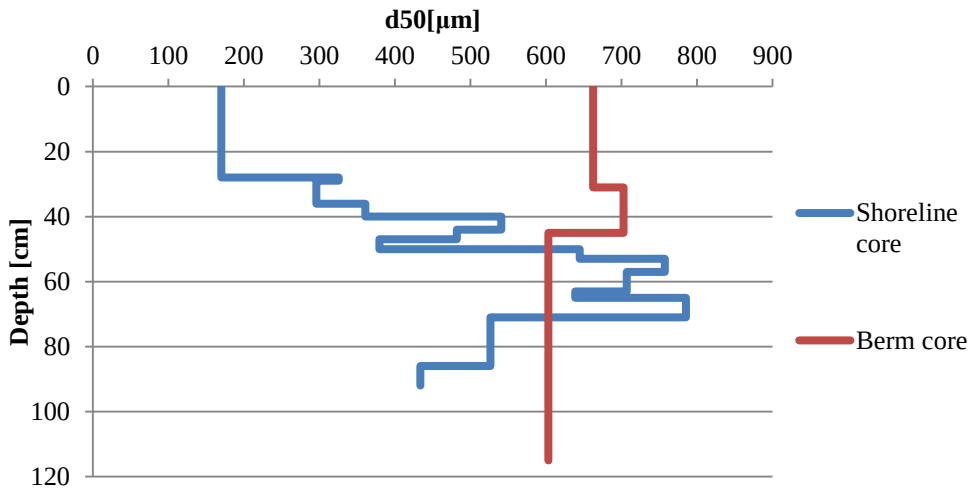

Figure 37. The value d50 as a function of depth for the upper swash zone and berm core.

Figure 35, Table 2 and Figure 37 show little variations in the grain size distribution among the three layers in the berm sediment core. The bottom layer of the core sampled at the berm at Section 2, consisted of the finest grain sizes of the complete core while the coarsest grain sizes were found in the middle of the core.

In Figure 36, Table 3 and Figure 37 it can be seen that the sediments of the layers in the upper swash zone core varies more among the layers than in the berm core, with the finer grain sizes in the top layers, i.e. samples S1-S4. The layer with the finest grain sizes is found in sample S3. The coarsest sediment is located in the middle of the core.

For Section 2, data from November 2007 and August 2008 collected by Bui (2009) were compared with the top layer from the field trip at 7th of March 2015, see Figure 38.

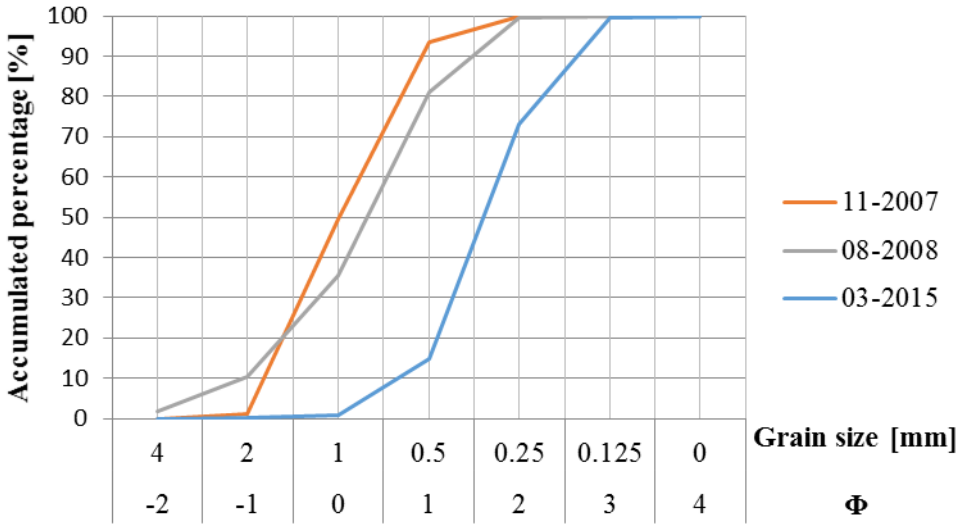

Figure 38. Grain size distributions for the three layers at the year of 2007, 2008 and 2015 collected at the top layer sediment at the upper swash zone at Section 2.

The grain size distribution graphs in Figure 38 and the d50 values presented in Table 4 show that the sediment was the finest in March 2015 while the samples from 2007 and 2008 were coarser and quite similar in grain size.

Table 4. Values of d50 for the top layers in the upper swash zone sediment core at Section 2 taken year 2007, 2008 and 2015.

Section 2	d50	
Date	[µm]	Φ
11-2007	497	1.01
08-2008	401	1.32
03-2015	170	2.56

5.4 Top Layer Sediment Samples

5.4.1 Experimental Setup and Procedure

On the 11th of April 2015, sediment samples of the top layer of the berm were collected at Section 1-8. Additional four samples for each of the beach profiles at Section 1, Section 4 and Section 8 were collected, i.e. a complete series of five samples for each profile were collected. The stretch of the samples were from the berm to as far out in the water as the sample could be collected by walking and the sampling locations are illustrated with a sketch in Figure 39.

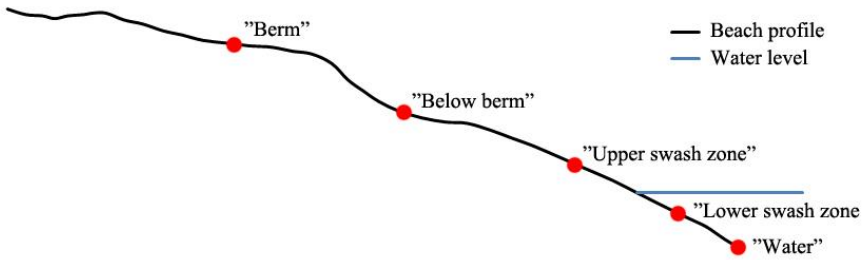

Figure 39. Sketch illustrating the locations of sediment sampling along the beach profiles. Observe that the sketch is not to scale.

The samples were stored in plastic bags for further analysis in laboratory, where the samples were cleaned from salt water and organic material with tap water and dried in oven before being sieved. The sieve consisted of several layers with the mesh sizes 4.0 mm, 2.0 mm, 1.0 mm, 0.5 mm, 0.25 mm and 0.125 mm and the sieve was placed on a mechanical sieve shaker with a frequency of 40 Ampere until all the grains were sorted. The grain size fractions of the samples were weighed, accumulated weight percentages were calculated and grain size distribution graphs could be drawn.

5.4.2 Data Collected and their Properties

In Figure 40, Figure 41 and Figure 42 the grain size distribution graphs, based on the sediment samples collected from the top layer on the 11th of April 2015, for the beach profiles at Section 1, 4 and 8 can be seen.

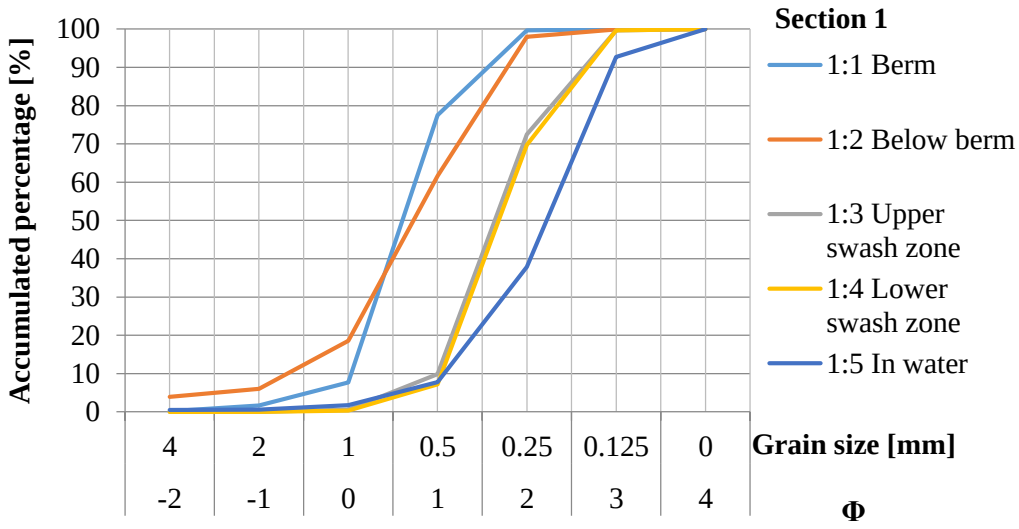

Figure 40. Grain size distributions for the top layers at Section 1.

In Figure 40 and Table 5 it is shown that the finest sediment at Section 1 was found in the water. The grain size in the lower and upper swash zone coincide very well to each other, while the coarsest sediment was found at the berm.

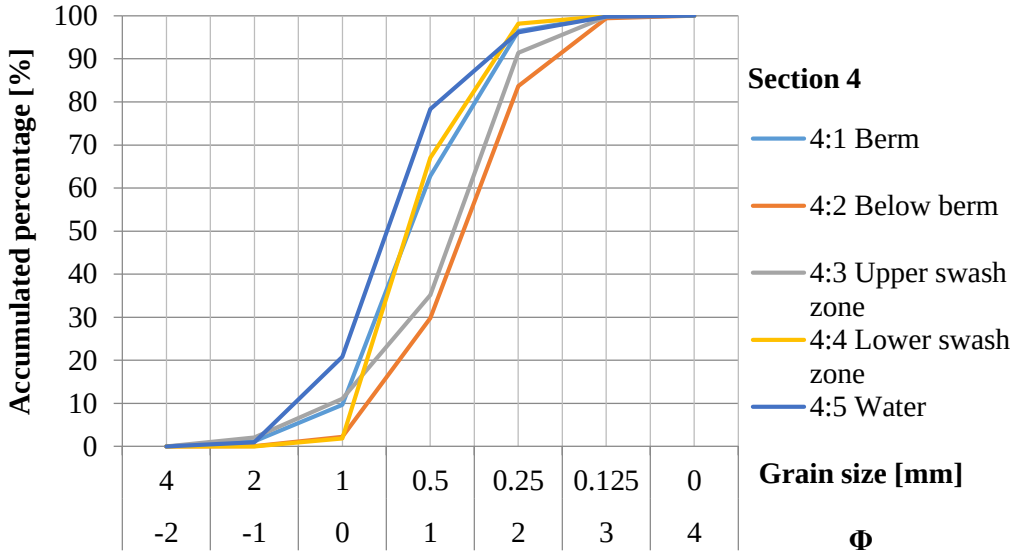

Figure 41. Grain size distributions for the top layers at Section 4.

In Figure 41 and Table 6 it can be seen that the coarsest sediment at Section 4 was found in the water while the finest sediment was located below the berm.

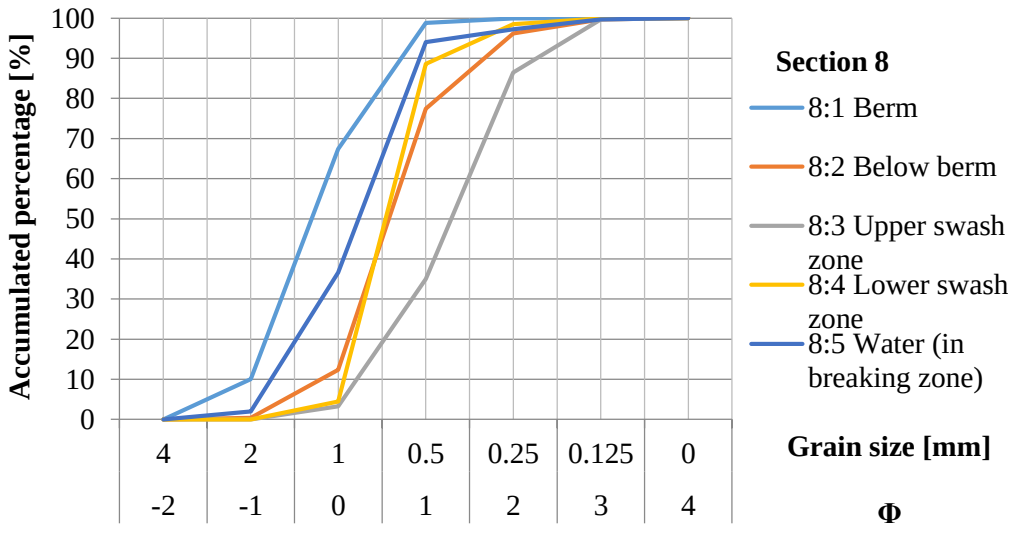

Figure 42. Grain size distributions for the top layers at Section 8.

In Figure 42 and Table 7 it is shown that the coarsest sediment at Section 8 was located at the berm while the finest sediment was found at the upper swash zone.

Table 5. Values of d50 for the five locations at Section 1.

Sample	Location	d50 [µm]	d50 Φ
1:1	Berm	657	0.606
1:2	Below berm	603	0.731
1:3	Upper swash	321	1.64
1:4	Low swash	311	1.69
1:5	Water	214	2.22

Table 6. Values of d50 for the five locations at Section 4.

Sample	Location	d50 [µm]	d50 Φ
4:1	Berm	591	0.759
4:2	Below berm	385	1.38
4:3	Upper swash	416	1.26
4:4	Lower swash	599	0.739
4:5	Water	704	0.507

Table 7. Values of d50 for the five locations at Section 8.

Sample	Location	d50 [µm]	d50 Φ
8:1	Berm	1230	-0.303
8:2	Below berm	670	0.578
8:3	Upper swash	409	1.290
8:4	Lower swash	687	0.542
8:5	Water	851	0.233

In Figure 43, a comparison of all the grain size distribution graphs for Sections 1-8 can be seen.

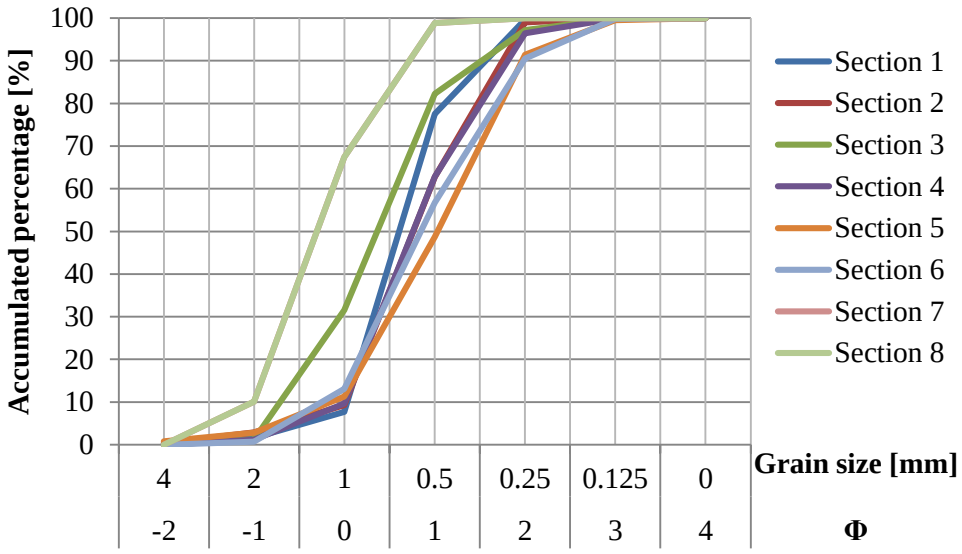

Figure 43. Grain size distributions at the berm for the top layers along Sections 1-8.

Figure 43 shows that the grain size varies slightly along the shorelines. Section 8 has the coarsest material, followed by Section 3 and Section 1. The other sections show little deviation in grain sizes from each other.

The d50 values of the samples gathered from the berm at all sections along the shoreline, presented in Figure 43, showed no clear pattern of neither increasing nor decreasing figure in the southward direction along the shoreline. At the berm of Section 1-8 along the shoreline, the d50 values vary from the lowest value of 0.490 mm at Section 5 to the highest value of 1.24 mm at Section 8. For Section 1, see Table 5, it can be seen that d50 increased from 0.214 to 0.657 mm in the onshore direction. For Section 4, see Table 6, the smallest d50 was 0.385 mm below the berm and the biggest was 0.704 mm in the water. For Section 8, see Table 7, the highest d50 of 1.24 mm was on the berm. The smallest d50, 0.409 mm, was located in the upper swash zone.

Table 8. Values of d50 for the eight berm sections along the shoreline.

	d50	
Sample	**[µm]**	**Φ**
1:1	657	0.606
2	590	0.762
3	777	0.363
4:1	591	0.759
5	490	1.03
6	596	0.747
7	556	0.846
8:1	1230	-0.303

5.5 Nagata Sediment Trap

5.5.1 Experimental Setup and Procedure

Sediment samples were also collected from the water column in the nearshore zone in all cardinal directions with a Nagata sediment trap, see Figure 44. The four sand traps with a diameter of 42 mm and a net mesh of 0.062 mm were located in one layer on a level of approximately 15 cm above the seabed in a water depth of approximately one meter. Free drifting sediment transported by waves and currents were collected by the Nagata sediment trap for five minutes at the three locations Section 2, Section 3 and Section 4. The sediment samples were then stored separately in plastic bags with seawater for further analysis in the laboratory.

Figure 44. A Nagata sediment trap, developed by Yutaka Nagata, catches sediment transported in all cardinal directions in the nearshore zone .

The samples from the Nagata sediment trap were washed with tap water, transferred into beakers and placed in an oven at 100 degrees and were kept in the oven until all water had evaporated from the sample. Since crystallized salt precipitated as the samples dried, the samples had to be washed with tap water and dried once more to remove the salt. The samples were thereafter weighed and noted in a protocol. With the known diameter of the trap, time of measurement and weight of trapped sediment, sediment transport rates in all cardinal directions for the three measurement stations could be calculated from the results. The grain sizes of the captured sediments were not analysed due to its fine sizes. The sediment transport rates were plotted and presented in separate graphs showing direction and amplitude of the transport.

5.5.2 Data Collected and their Properties

The amounts of sediments being transported in all cardinal directions at Section 2, Section 3 and Section 4 during the field trip on the 7th of March 2015 are presented in Table 9. At Section 2 the highest crosshore transport was in the onshore direction with 2.67 g/m^2/s compared to the offshore transport of 2.26 g/m^2/s. The sediment transport was highest in the northward direction with 0.30 g/m^2/s, whilst in the southward direction the transport was 0.17 g/m^2/s. Little transport was shown at Section 2 in all cardinal directions except the onshore direction, where the transport was 2.29 g/m^2/s. The transport offshore was 0.15 g/m^2/s and in the southward direction and northward direction the

transport was 0.10 g/m^2/s and 0.02 g/m^2/s, respectively. The offshore transport was 1.63 g/m^2/s at Section 3 and thus bigger than the onshore transport of 1.11 g/m^2/s. The longshore transport was small, 0.10 g/m^2/s in the southward direction and 0.05 g/m^2/s in the northward direction.

Table 9. The sediment transport [g/(s·m^2)] in all cardinal directions.

Direction	Upward	Downward	Onshore	Offshore
	↑	↓	←	→
Sampling location				
Section 2	0.298	0.171	2.67	2.26
Section 3	0.0217	0.135	2.29	0.149
Section 4	0.0457	0.0986	1.11	1.63

5.6 Measurements of Wave and Current Data

5.6.1 Experimental Setup and Procedure

Real-time data of wave height, wave direction, wave time period, water pressure, current speed and current direction were collected with Nortek AWAC (Acoustic Wave And Current Profiler) sensor, see Figure 45 and Figure 46, between the hours 9 am and 4 pm on the 7th of March 2015. The wave data, including height, time period, speed and direction of the wave, were registered once every hour while the current date, including speed and direction of the current, were registered every tenth minute. The AWAC sensor was placed 0.70 m above the seabed of a water depth of approximately 2 m at Section 2.

A rose diagram of the current speed and directions was plotted for greater understanding of the wave climate in the bay and for comparison with the result from Nagata sediment trap at Section 2, which was placed approximately 15 m from the location of AWAC.

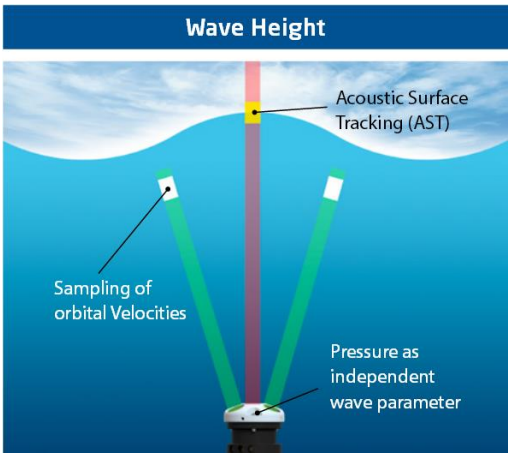

Figure 45. Graphic illustration of the principles of AWAC's sensors (Nortek AS, 2014).

Figure 46. The Nortek AWAC (Acoustic Wave And Current Profiler) sensor used during the fieldtrip for gathering wave and current data.

5.6.2 Data Collected and their Properties

The wave data, compiled between 9 am to 4 pm on the 7th of March 2015, registered data of significant wave height varying between 0.33 and 1.16 m, mean period varying between 1.99 and 5.02 s and waves with an incoming wave angle of mainly between 85 and 123 degrees to the true north. The results of the measured wave currents showed a current speed and current direction varying between 0.01 and 0.18 m/s and 60 and 264 degrees to true north, respectively. The registered angles of the currents is illustrated in a current rose presented in Figure 47, which indicates that the currents mainly go in a southwest direction, i.e. downwards the shoreline.

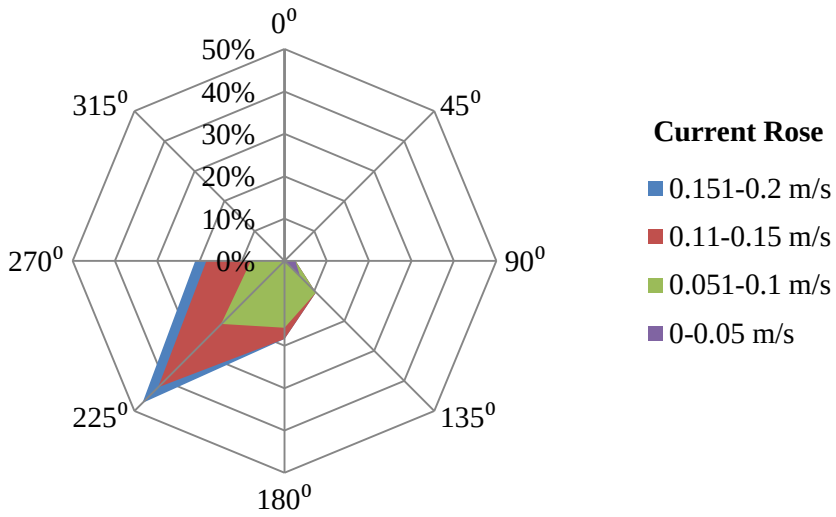

Figure 47. The current rose illustrates the distribution of the current directions registered every tenth minute during the hours 9 am to 6 pm on the 7th of March 2015.

6. Mathematical Modelling of Nearshore Waves

6.1 Background and Theoretical Formulation

A multi-directional random wave transformation model, EBED, based on the energy balance equation was formulated by Mase (2001) for transferring offshore wave data and simulating nearshore waves, currents and sediment transport. With the model inputs significant wave height, H_s, significant wave period, T_s, and mean wave direction, $\bar{\theta}$, for offshore waves the same parameters as output values can be obtained for a nearshore climate. The energy balance equation, stated as Equation 10, consists of energy diffraction and dissipation terms to the right-hand side as the first and second term respectively. The coefficient κ is used to regulate the effect of diffraction, while the parameter ε_b is the energy dissipation coefficient.

$$\frac{\partial(v_x S)}{\partial x} + \frac{\partial(v_y S)}{\partial y} + \frac{\partial(v_\theta S)}{\partial \theta} = \frac{\kappa}{2\omega}\left\{(CC_g cos^2\theta S_y)_y - \frac{1}{2}CC_g cos^2\theta S_{yy}\right\} - \varepsilon_b S \quad (10)$$

Where S is the angular-frequency spectrum density, θ is the angle measured counter clockwise from the x-axis, ω is the frequency, C is the phase speed and C_g is the group speed. The propagation velocities, v_x, v_y and v_θ, are calculated with Equation 11.

$$\left(v_x, v_y, v_\theta\right) = \left(C_g cos\theta, C_g sin\theta, \frac{C_g}{C}\left(sin\theta \frac{\partial C}{\partial x} - cos\theta \frac{\partial C}{\partial y}\right)\right) \quad (11)$$

It was shown that the original model overestimated the output wave parameters compared to measured values in the nearshore zone. To improve the result of the model the term for the energy dissipation caused by breaking waves was modified by Nam et al. (2009). The new energy dissipation term was instead based on a model performed by Dally et al. (1985) and the energy balance equation could instead be expressed Equation 12, which follows

$$\frac{\partial(v_x S)}{\partial x} + \frac{\partial(v_y S)}{\partial y} + \frac{\partial(v_\theta S)}{\partial \theta} = \frac{\kappa}{2\omega}\left\{(CC_g cos^2\theta S_y)_y - \frac{1}{2}CC_g cos^2\theta S_{yy}\right\} - \frac{K}{h}C_g(S - S_{stab}) \quad (12)$$

Where h is the still-water depth, K is a dimensionless decay coefficient and S_{stab} is the stable wave spectrum density. Since S_{stab} can be determined with the stable wave height, $H_{stab}(= \Gamma h)$ and with the assumption that S and S_{stab} are functions of ${H_s}^2$ and ${H_{stab}}^2$, respectively, the dissipation term in the

modified energy balance equation can be rewritten as follows (Equation 13) (Nam et al., 2009).

$$D_{diss} = \frac{K}{h} C_g S \left[1 - \left(\frac{\Gamma h}{H_s}\right)^2\right] \quad (13)$$

6.2 Input Data for Wave Modelling

Offshore wave data, including specific wave height, peak time period and wave direction in relation to true north in geographic coordinates, between the years 1990 to 2014 was extracted from the wave propagation model SWAN (Simulating WAves Nearshore), which is developed at Delft University of Technology (Courtesy of Duong Cong Dien, Institute of Mechanics, Hanoi). The wave data was hindcasted for the offshore location with coordinates 109.5E, 12.25 N at a water depth of 80 metres based on a predicted global wind field. The wind data origin from The National Centers for Environmental Prediction (NCEP) Climate Forecast System Reanalysis (CFSR) (Saha et al., 2010, Saha et al., 2011, updated monthly). The data was collected every third hour, 12 am, 3 am, 6 am, 9 am etcetera. A total collection of eight measurements every day for 25 years were available. A wave rose with the wave heights and directions at the offshore location for the years 1990-2014 can be seen in Figure 48. The detailed data of the bathymetry in Nha Trang Bay used for the wave modelling was developed from Vietnam Navy maps of the East sea and neighbouring seas with an accuracy of 0.1 m. The collected bathymetry data was combined with the nearshore bathymetry data measured with a sonar instrument in the project by Nguyen (2013).

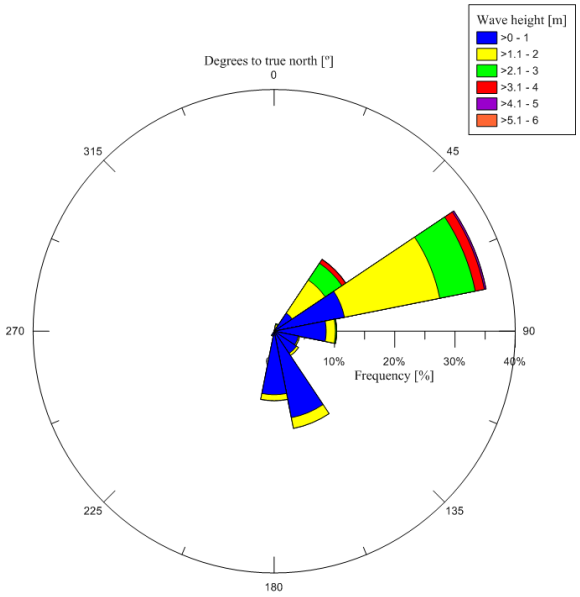

Figure 48. Wave heights and directions for offshore waves simulated by the model SWAN for the years 1990 to 2014.

6.3 Model Implementation

The bathymetry in Nha Trang Bay is complex due to the presence of islands in the area which causes fluctuations in water depth. Also the depth changes rapidly in the nearshore zone. The area chosen for the simulation needs to include the most significant features to give an accurate model. In Figure 49 the outer borders of the chosen area of interest can be seen. The grid placed in the study area needs to be fine enough to mirror the changes in bathymetry, but the downside of a fine grid is the long processing time for the software EBED as a small grid means more cells to process. Different grid sizes were tested; 50 m x 100 m, 100 m x 100 m and 200 m x 200 m. A grid with cell sizes of 100 m x 100 m gave a satisfying result in relation to the simulation time after running EBED for a test wave series and was decided to use for the simulation. The grid consisted of 209 columns and 275 rows, which covers an area in the bay of 20,900 m x 27,500 m. For a more detailed description and explanation for the used input parameters in the model see Appendix 2.

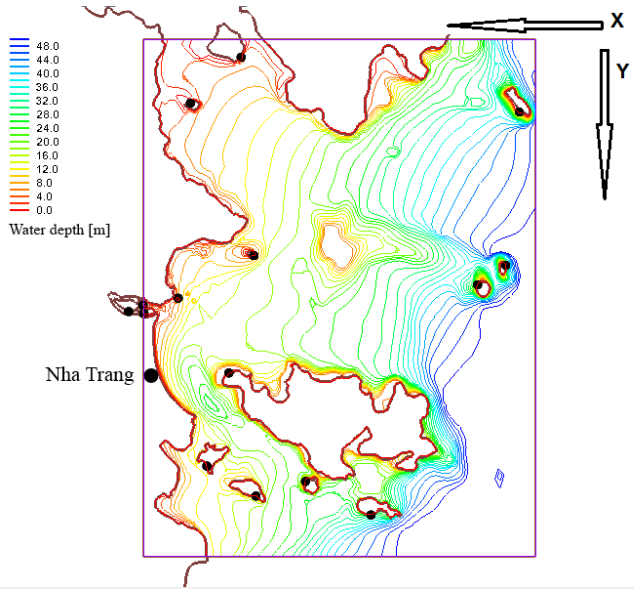

Figure 49. A map over the bathymetry contour lines for Nha Trang bay with the area studied in EBED marked (Courtesy of Duong Cong Dien, Institute of Mechanics, Hanoi). The grid consisted of 209 cells and 275 cells in the x- and y-direction, respectively.

The wave data simulated with SWAN, contained in total data for 73,048 different waves during 1990-2014, a period of 25 years.

The reference point of EBED's coordinate system is different from the received wave data, where the wave direction is measured against true north. Therefore the raw data needed to be processed before being used as an input file for the model. The incoming wave angles were rotated 90 degrees clockwise for the conversion. Since EBED only can include waves that enter the grid on the border parallel to the shoreline, i.e. waves with a direction of 90 degrees to -90 degrees, the waves with a direction beyond this span had to be removed from the input file. The numbers of waves in the series used as input were then reduced to 71,060.

The wave output data gained from the model EBED was the wave input data used in the shoreline evolution model GENESIS (GENEralized model for SImulating Shoreline change). Therefore, the grid used in EBED was studied to locate appropriate cells to extract the nearshore wave climate data. In total five cells at a water depth of 10 metres located along the shoreline were selected as output data cells, see Figure 50 and Appendix 2 for coordinates. The chosen water depth for the output data cells was based on the calculation

of 1.5 times the highest measured wave height, to certify that the output data were received from EBED before the propagating wave had broken.

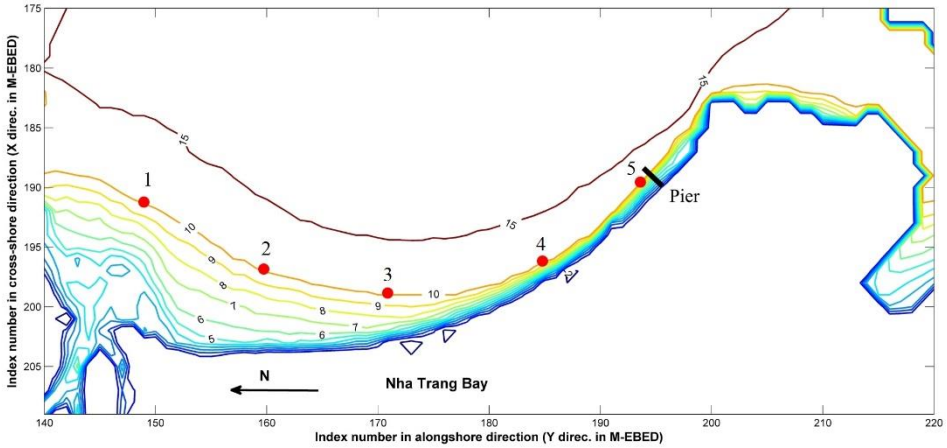

Figure 50. The red dots illustrate the location of the five cells where output data were gathered for further use in the model GENESIS.

When running the simulation model EBED the parameters significant wave height, H_s [m], significant wave period, T_s [s] and the mean wave direction, $\bar{\theta}$ [º], were obtained for the five selected locations along the Nha Trang bay. Wave roses, illustrating the range of wave heights and wave directions at the locations, were drawn, see Figure 51, Figure 52, Figure 53, Figure 54 and Figure 55. The results of the wave directions coincide well with theory, with dominating waves from northeast due to the isolating islands and the direction of the strong northeast monsoon. The waves coming from a southeast direction probably pass through the thin passage between the shoreline and the island Hon Tre and as area is sheltered and the water depth shallow the wave climate is calmer.

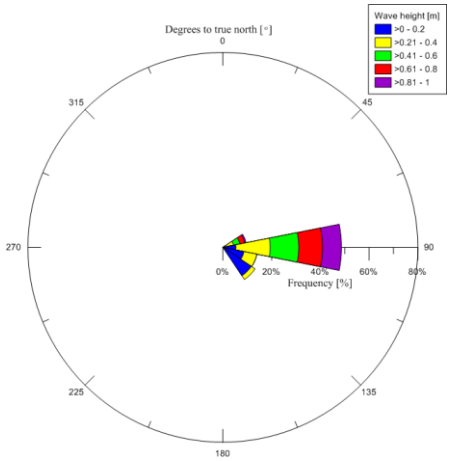

Figure 51. Wave height and wave direction at Location 1.

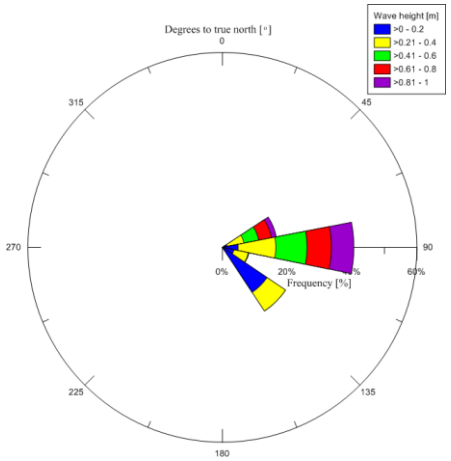

Figure 52. Wave height and wave direction at Location 2.

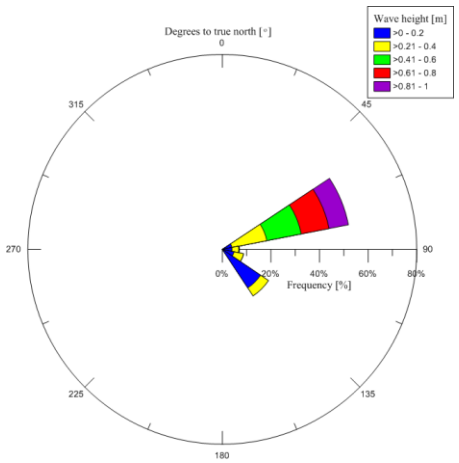

Figure 53. Wave height and wave direction at Location 3.

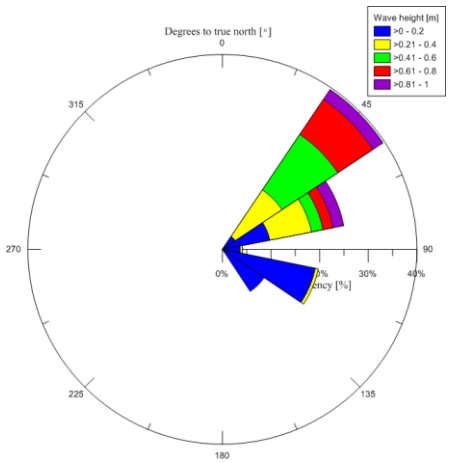

Figure 54. Wave height and wave direction at Location 4.

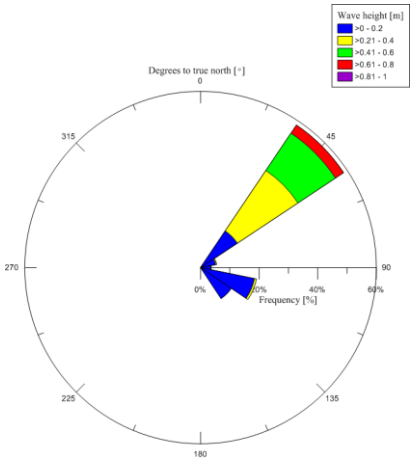

Figure 55. Wave height and wave direction at Location 5.

6.4 Model Validation

To validate the model, the simulated results of the nearshore significant wave heights were compared with measured data collected during a project performed by Nguyen (2013). In the project wave and current data for seven days in May and December 2013, respectively, was gathered at the location 12°15.112'N, 109°12.289'E. Simulated results of wave height from the grid cell representing the same location and from the same dates were compared with the measured data and visualized in Figure 56 and Figure 57. Waves with incoming wave angles not valid for the model EBED have been sorted out and hence the timeline of the x-axis in the figures are not to scale.

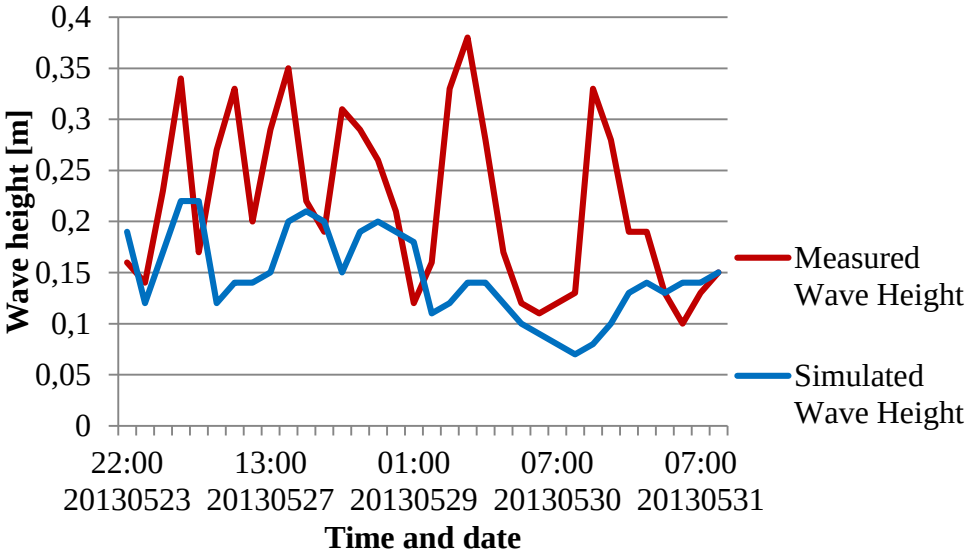

Figure 56. A validation of the model result performed by comparing wave heights achieved from the EBED model with measured data from May 2013.

In Figure 56 it can be seen that the simulated wave height from May 2013 lies lower than the measured wave heights and the wave heights are therefore underestimated by the model. The root mean square was calculated to be 0.109 for the time series.

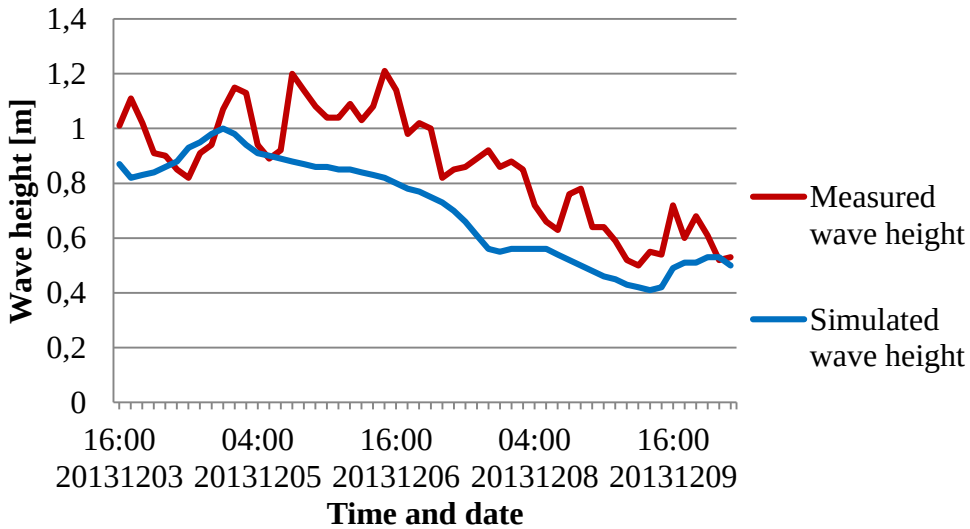

Figure 57. A validation of the model result performed by comparing wave heights achieved from the EBED model with measured data from December 2013.

The same goes for the validation of the simulated wave heights from December 2013, which also indicates that the model underestimates the real value of the nearshore wave heights and can be seen in Figure 57. Though, the trend of the simulated wave heights follows the measured wave heights well. The root mean square was calculated to be 0.196 for the time series.

One explanation for the underestimated results from the simulation is that the model does not include the effects of local wind. The force of winds blowing over the sea surface has a great impact on the propagating waves as they transfer their energy to the waves, which has been described in *2. Coastal Processes*, and hence the results will not coincide completely with reality. Especially during the summer, when the wave heights are lower, the energy of the wind has a greater impact. Thus, the validation curve for May has a less good fit compared to the validation curve for December. A cell circulation of the wind is created as the higher temperature during day time force winds offshore, while the lower temperature during night time force winds onshore. The distance from the offshore to the nearshore data station is approximately 32 km and hence the long fetch length will increase the wave height during the wave propagation.

Other factors contributing to the error sources of the validation are the used input wave data and grid size. The wave data used as input for the model EBED originate from the model SWAN and hence the risk of errors and uncertainties of the result are increased. The grid with a cell size of 100 m x 100 m might be too coarse and the simulation result can be too rough and imprecise estimated.

The data were never re-simulated with modified model parameters for a better validation result due to the restricted time schedule for the project. Also, the conclusion that there still would be uncertainties of the simulated data even if the parameters were modified, since the offshore wave data used as input data for EBED also origin from a simulation.

6.5 Analysis of Model Results

Because of the complexibility of the output data received from the model EBED, some visualizations of the output was done to get a general understanding of the nearshore wave data in the project area.

6.5.1 Wave Transformation

To get an overview of the results from the model EBED, three waves with different incoming wave angles were selected to be visualized and presented. The waves were carefully selected to cover the complete spectrum of the project area. A wave with incoming angle of -89.7, -0.1 degrees and 75.4 degrees can be seen in Figure 58, Figure 59 and Figure 60, respectively. Note that the presented incoming wave angles in this section refer to the coordinate system of EBED, i.e. a wave with an angle of 0 degrees approach from the east according to the geographic coordinate system.

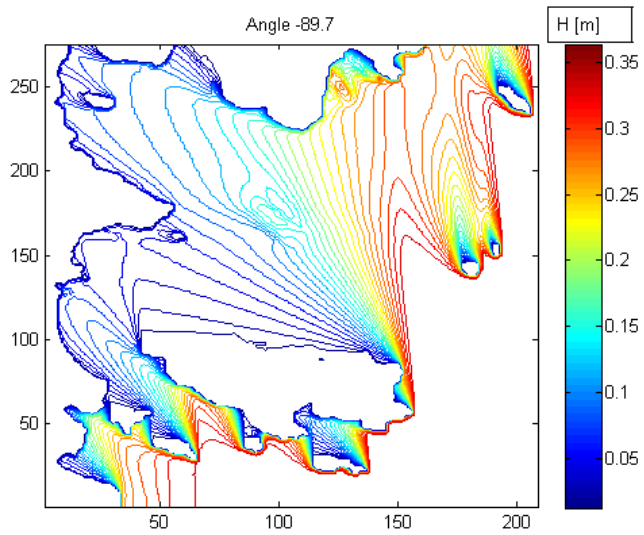

Figure 58. A wave with incoming angle of -89.7 degrees occurring on the 1st of August 1992 at 3 am.

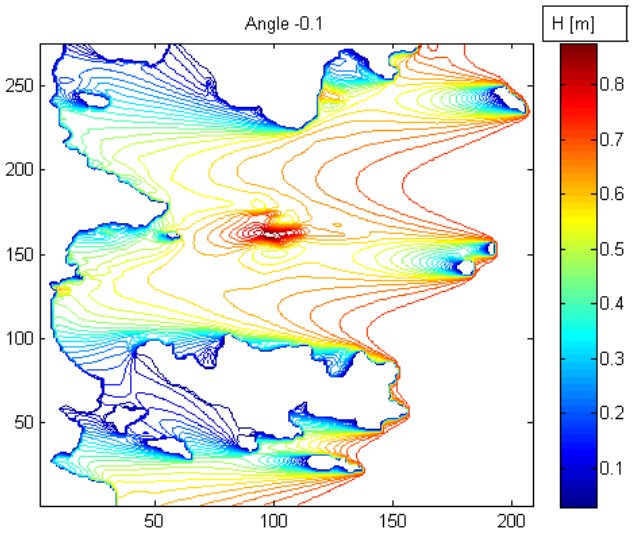

Figure 59. A wave with incoming wave angle of -0.1 degrees occurring at the 24th of March 1993 at 12 pm.

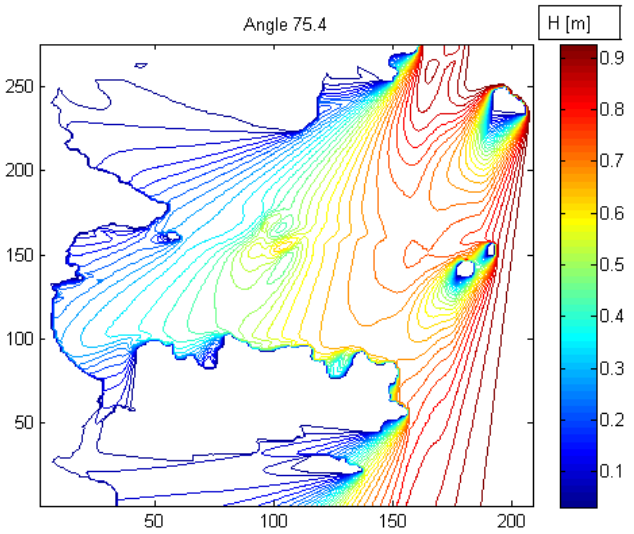

Figure 60. A wave with an incoming wave angle of 75.4 degrees occurring on the 19th of October 1998 at 12 am.

The result shows that the wave heights are highly affected by the direction of the incoming wave, due to the surrounding islands. The islands create shadow zones when the waves are diffracted around the islands (see *2.4.4 Wave Diffraction*), in which the wave height decreases. Waves with an incoming

angle of approximately 90 degrees will create a shadow zone, with lower wave heights, south of the island Hon Tre, while waves with an incoming of approximately -90 degrees will create a shadow zone north of the island. In the centre of the bay there is a shallow, which also affects propagating waves by creating an area with an increased wave height climate. This area is especially distinguished in Figure 59.

Worth noting is the model EBED do not include the effects of the wave transformation process reflection, so the real wave climate in the bay would most likely evolve a bit differently. Also the graphs lack a background with land contours, which might give a false illusion of for example size and shape of the island Hon Tre.

The wave transformation coefficient, K, was estimated for the five different output cells used in the model EBED, see Figure 50 in *6.3 Model Implementation* for exact positions, for the 25 year wave series. The coefficient K, which describes how much the wave height increase as it progresses, was retrieved by fraction of the nearshore wave height, H_2, and the deep water wave height, H_1, according to Equation 14.

$$K \cdot H_1 = H_2 \tag{14}$$

Graphs illustrating the correlation between K and the incoming wave angle for the five locations are presented in following figures, see Figure 61 - Figure 65.

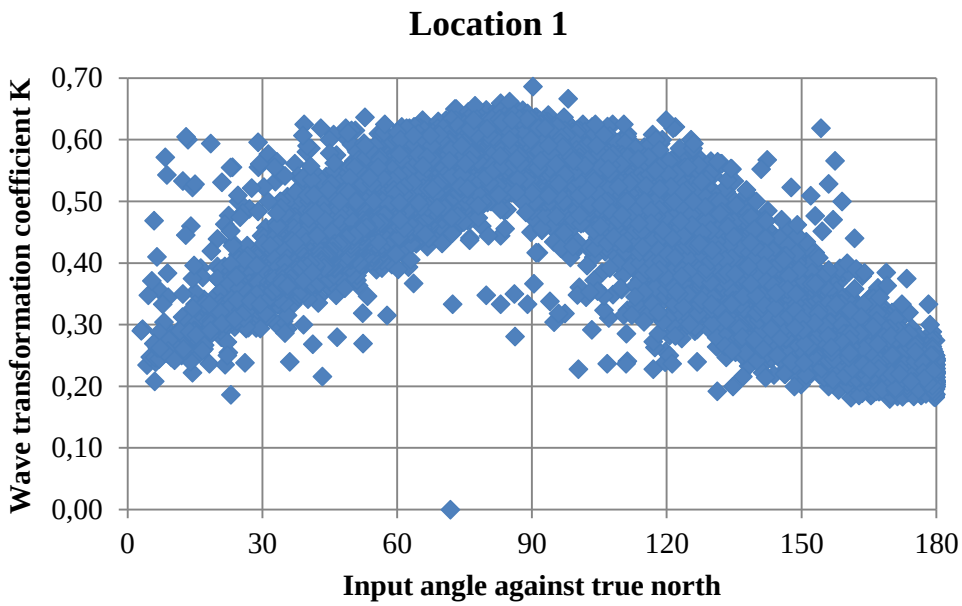

Figure 61. The wave transformation coefficient *K* as a function of the incoming wave angle against true north at Location 1.

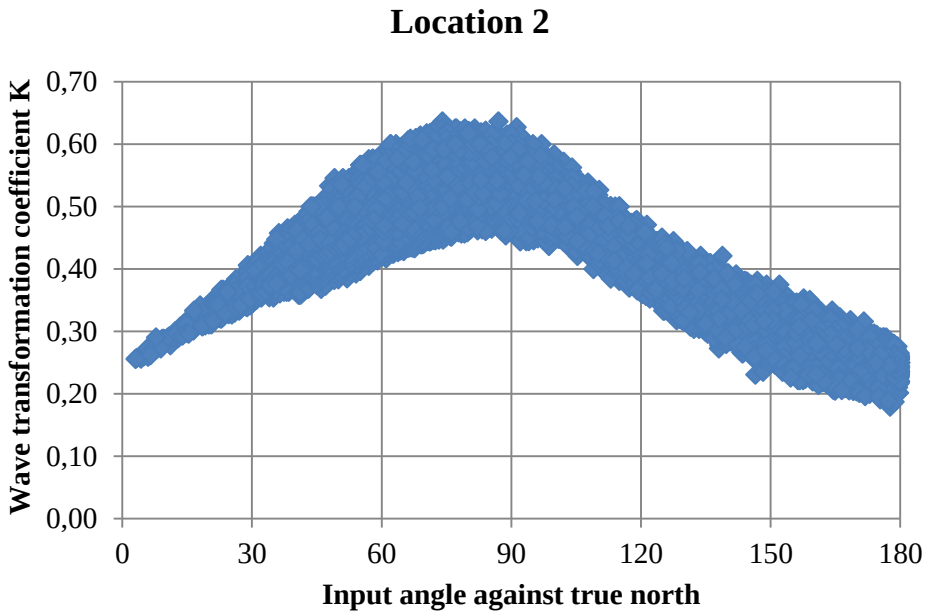

Figure 62. The wave transformation coefficient *K* as a function of the incoming wave angle against true north at Location 2.

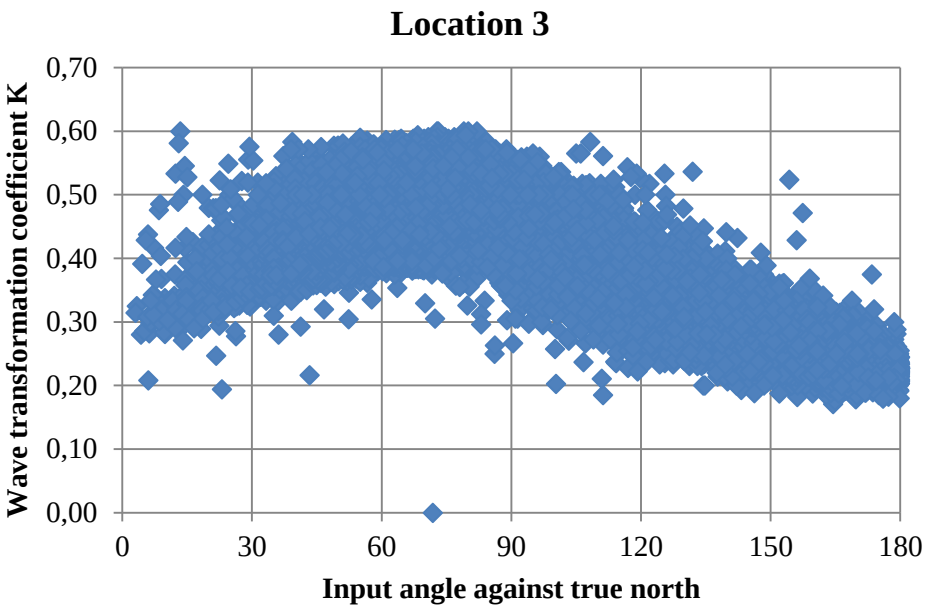

Figure 63. The wave transformation coefficient *K* as a function of the incoming wave angle against true north at Location 3.

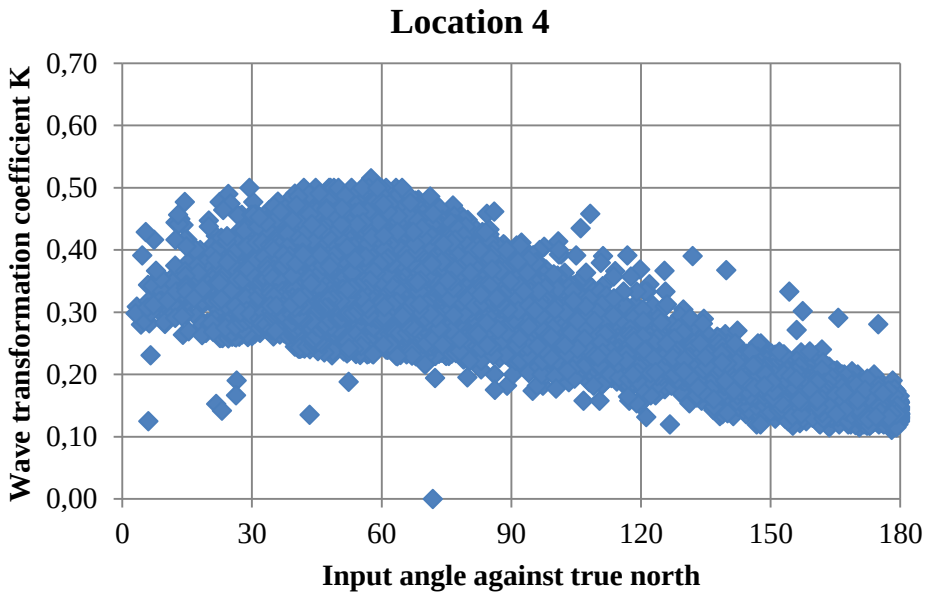

Figure 64. The wave transformation coefficient *K* as a function of the incoming wave angle against true north at Location 4.

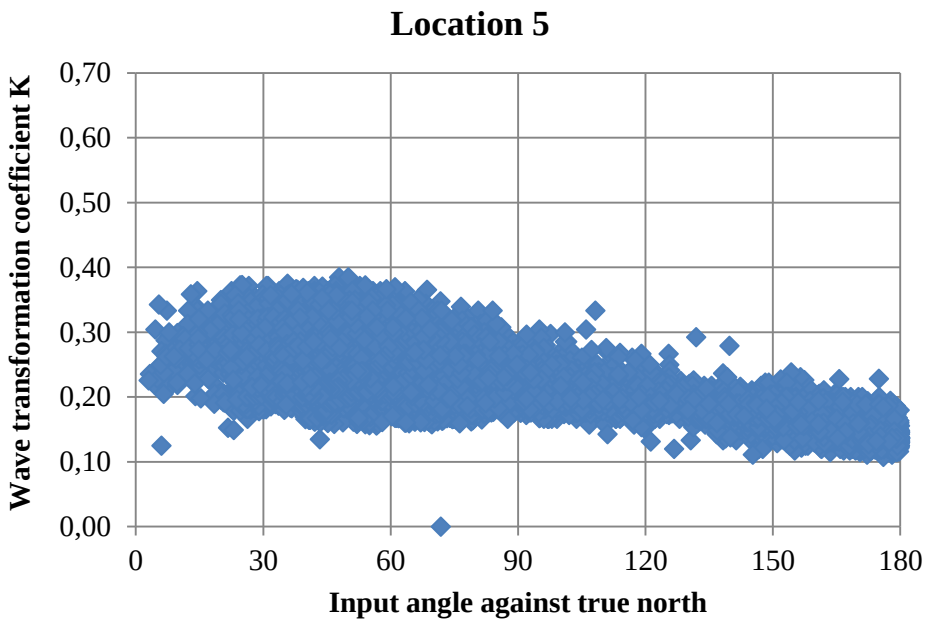

Figure 65. The wave transformation coefficient *K* as a function of the incoming wave angle against true north at Location 5.

When looking at Figure 61 - Figure 65 it can be seen that *K* is decreasing the further south along the shoreline the location is situated. The maximum *K* at location 1 is around 0.68 while it is around 0.38 at Location 5. A smaller *K* means a larger difference in the incoming wave height and the nearshore wave height and hence the area is more sheltered.

It can also be seen that the incoming wave angle plays a major role to *K* when looking further north along the shoreline. At Location 1, *K* fluctuates between 0.18-0.68 for different input angles, with the smallest value occurring for the minimum and maximum input angle. The largest value occurs when approaching the beach at an angle of 90 degrees in the geographic coordinate system. At Location 5, *K* only fluctuates between 0.1-0.38. At the locations situated more south, the islands in the bay may work as a hinder and thus refract the waves as they progress towards the shoreline. This may be why the wave heights are smaller at the southern locations and thus the wave heights of the deep water waves play a minor role for the wave climate near the islands.

7. Longshore Transport and Coastal Evolution Modelling

7.1 Background and Theoretical Formulation

The numerical model GENESIS, developed by Hans Hanson, Faculty of Engineering (LTH), Lund, is a well working model for computing long-term change of shoreline position. The model can be run for a time interval of months to years, for shoreline stretches from one up to tens of kilometres and manages to include effects of the wave transformation processes shoaling, refraction and diffraction, as described in *2.4 Wave Transformation.* It also includes sand transportation around constructions like groins, jetties, detached breakwaters and seawalls, and beach fills.

Based on the one-linear theory, the model assumes that the bottom profile will remain unchanged over the time of the simulation. Only the longshore sediment transport is taken into account in the model and the equilibrium of the profile is simply based on that the amounts of transported sand to and from the profile are equal to each other. Further, the assumption that the sand actively moves over the profile over a long time period until it reaches a limiting depth, referred to as the depth of closure, D_C, is made for the model.

The stated assumptions make it possible to calculate the continuity of sand for an infinitely small stretch, *dx*, of the shoreline according to Equation 15 and Figure 66.

$$\frac{\partial y}{\partial t} + \frac{\frac{\partial Q}{\partial x} + q}{D_B + D_C} = 0 \qquad (15)$$

where *y* is the shoreline position [m], *x* is the longshore coordinate [m], *t* is the time [s], D_B, is the average berm height above mean sea level [m], D_C, is the depth of closure [m], *Q* is the longshore sediment transport rate [m^3/s] and *q* stands for possible sources and/or sinks along the shoreline [m^3/s/m shoreline].

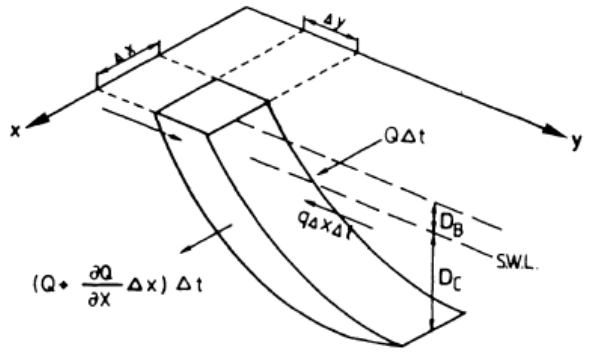

Figure 66. The continuity equation for sand transported through an infinitely small length, *dx*, of the shoreline (Hanson, 1989).

Solving Equation 15 demands the computation of depth of closure, D_C, longshore sediment transport, Q, and possible sources/sinks to the shoreline, q. GENESIS determines D_C by the simple relation presented in Equation 16 based on the formulation by Hallermeier (1983) that the annual depth of closure is twice of the extreme annual significant wave height (H_{mas} [m]) for the existing shore.

$$D_C = 2H_{mas} \tag{16}$$

The longshore sediment transport volume rate, Q, is calculated in GENESIS with Equation 17, which includes the longshore gradient of breaking wave heights for a realistic simulation of the shoreline evolution.

$$Q = \left(H^2 C_g\right)_b (a_1 \sin 2\alpha_{bs} - a_2 \cos\alpha_{bs} \frac{\partial H}{\partial x})_b \tag{17}$$

where C_g is the wave group velocity [*m/s*] calculated according to the linear wave theory (see *2. Coastal Processes)*, α_{bs} is the angle of the wave crests to the shoreline and the subscript b denotes the breaking condition. The parameters $a_1$and a_2 are non-dimensional and expressed as Equation 18 and Equation 19.

$$a_1 = \frac{K_1}{16\left(\frac{\rho_s}{\rho}-1\right)(1-p)1.416^{5/2}} \tag{18}$$

$$a_2 = \frac{K_2}{8\left(\frac{\rho_s}{\rho}-1\right)(1-p)tan\beta 1.416^{5/2}} \tag{19}$$

where ρ_s and ρ are densities of sediment and water [kg/m3], respectively, p is the porosity of the sediment, $tan\beta$ is the average bottom slope from the shoreline to the depth of the longshore transport and the factor 1.416 converts the significant wave height into RMS (root mean square) wave height. The figures K_1 and K_2 are calibration parameters, which determine the relative strength between the two terms of the longshore sediment transport volume rate formula and the time scale in the model.

The first term of the longshore sediment transport volume rate formula (Equation 17) is referred to as the CERC formula (see Equation 8 in *2.5.5 Longshore Sediment Transport*), while the second term include the effects on the transport caused by the longshore variation in breaking wave height.

The average berm height over the mean sea level, D_B, is either measured in field or achieved from an assumed beach profile (Hanson, 1989).

7.2 Model Implementation

The studied beach stretch used for the GENESIS simulation was 4,925 metres. The shoreline orientation used as an initial shoreline in the simulation was extracted from a Google Earth image photographed in July 2014 with the help of the software Grapher 10. It was divided into 197 cells of 25 metres width each. In Figure 67 the area used for the simulation can be seen as well as the locations of the cells.

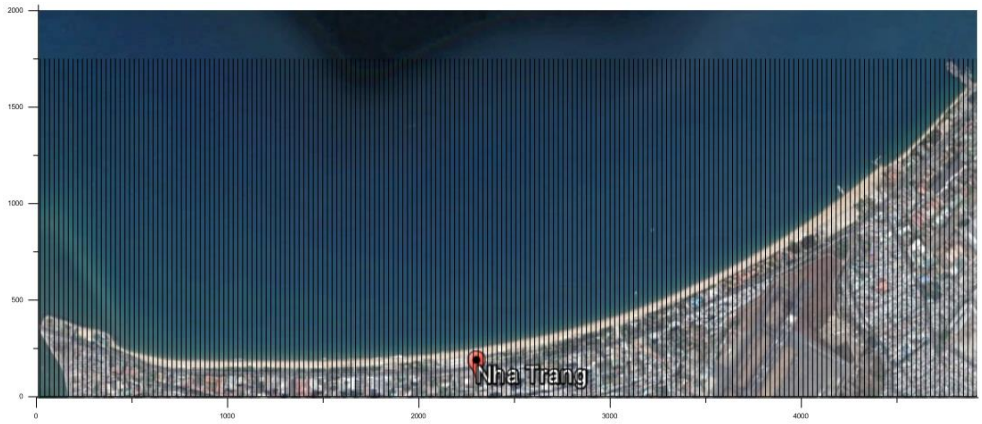

Figure 67. The area used in the GENESIS simulation and the cells it is divided into (background image achieved from Google Inc (2015)).

The wave climate used as input in GENESIS was the five locations that were the output from the EBED model. GENESIS interpolates the wave heights in the cells between the locations to get the wave climate in all the cells for the entire model.

The setup of the model and its parameters were done to imitate the historical evolution of the shoreline. As indication from the review of the GPS-measurement and Google Earth images, the beach is not changing to a great extent. The wanted result from the simulation was therefore a stable shoreline with not too much changes occurring. The wave series, going back 25 years, was used when simulating with GENESIS. Different parameters and boundary conditions were used to get satisfying results of the situation at Nha Trang beach, which a relative stable shoreline evolution. The left hand boundary was set to "gated", meaning that there is a structure prohibiting transport beneath its location. The boundary at the right hand side was set to "pinned", which allows transport possibilities past it. The tetrapods and the Vinpearl ferry terminal were neglected in the model due to the assumption of their low influence on the sediment transport. For the coding, parameters and conditions used in the model see Appendix 4. The shoreline evolution during the 25 years long simulation period can be seen in Figure 69.

7.3 Analysis of Model Results

The results of the shoreline change model GENESIS showed that the beach will retreat in the northern part and accrete in the southern part. Over the 25 years simulation the beach retreat up to approximately 45 metres in the north and accrete up to approximately 35 metres in the south, which can be seen in Figure 69. The retreat in the north transcend to accrete in the south near the end of the seawall around 2 kilometres from the northern tip. The mean net sedimentation transport for each cell is presented in Figure 70 and the mean value of the transport in each cell over the 25 years (black graph) shows that the shoreline is quite stable with some retreat at the beginning of the shoreline

and accretion further down the shoreline. In Figure 68 an illustrative sketch of the net transport along the shoreline is shown.

Figure 68. Sketch of the net sediment transport along shoreline with arrows illustrating the magnitude of the transport (background image achieved from Google Inc (2015)).

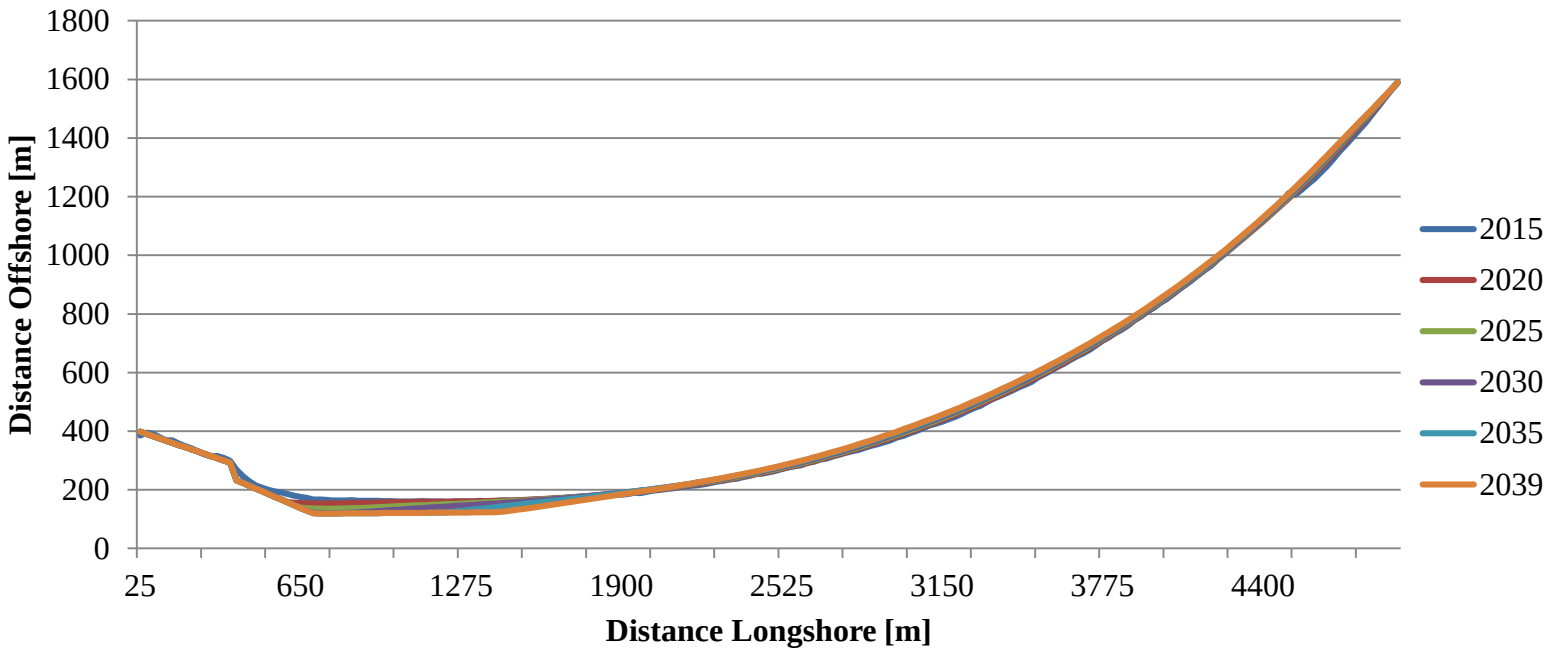

Figure 69. The future shoreline change for the 25 years-simulation period of Nha Trang beach.

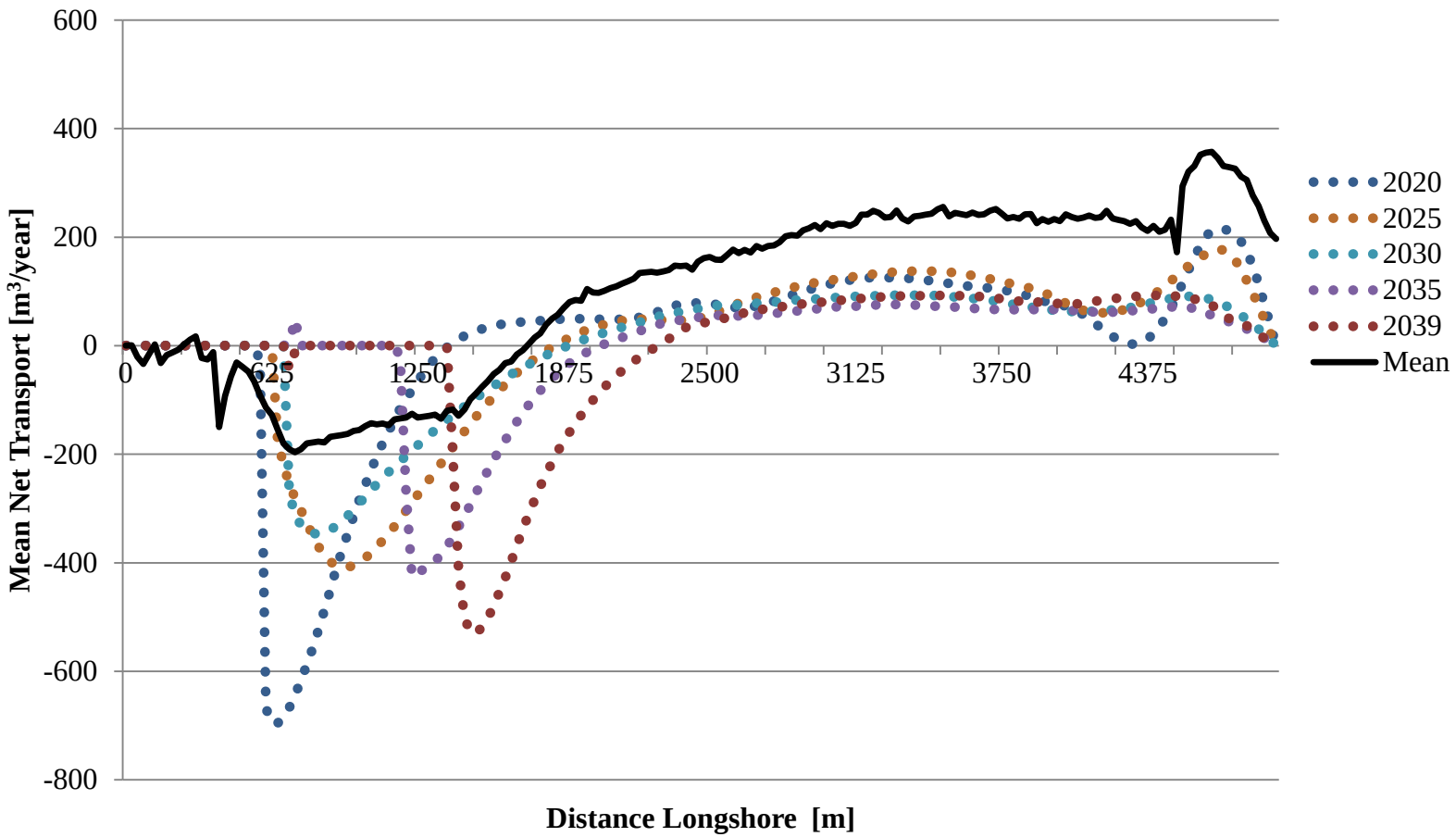

Figure 70. The resulting mean net sediment transport per cell along the shoreline for 25 years.

7.4 Model Validation

To get a general and simple overview of the longshore sediment transport volumes along the shore in Nha Trang Bay a version the CERC formula, see Equation 8 in *2.5.5 Longshore Sediment Transport*, presented by Soulsby (1997) was used. The calculations were performed for the five investigated locations along the shoreline at a depth of 10 metres. For clear description of used parameters for the CERC formula see Appendix 3. The values are used as a way to validate and compare the transport rates simulated by GENESIS.

As described in *2.5.3 Sediment Budget*, the net transport is interesting to study when looking at beach erosion. The annual sediment transport was calculated by the CERC formula for each year between 1990 until 2014 and the results of the net transport at the five different locations used in GENESIS are presented in Figure 71. The net transport for the 25 years long wave series simulated by GENESIS for the five locations were also plotted and can be seen in Figure 72.

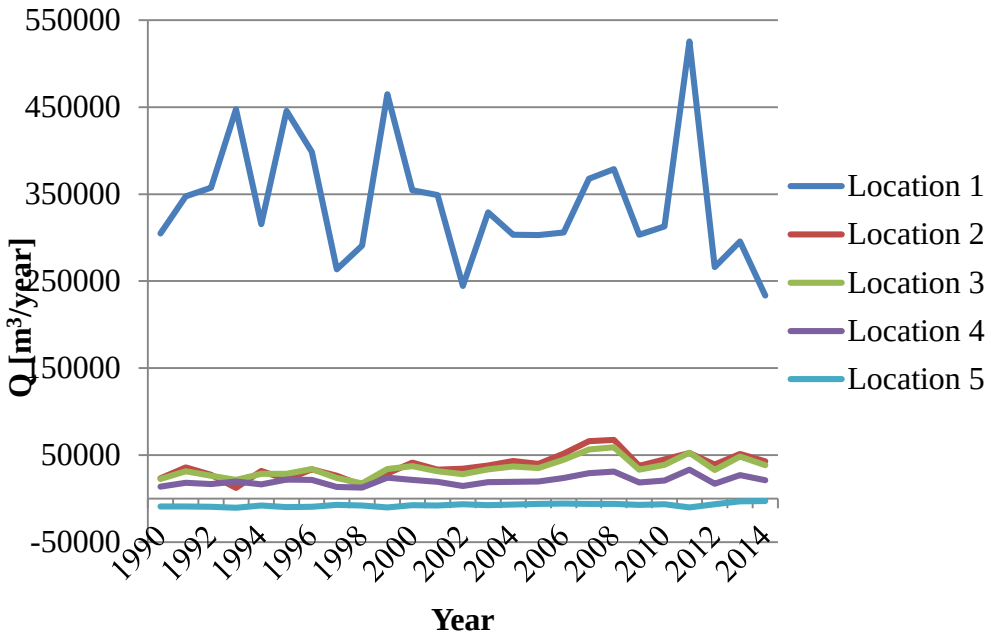

Figure 71. Net sediment transport per year at five locations in Nha Trang bay calculated by the CERC formula.

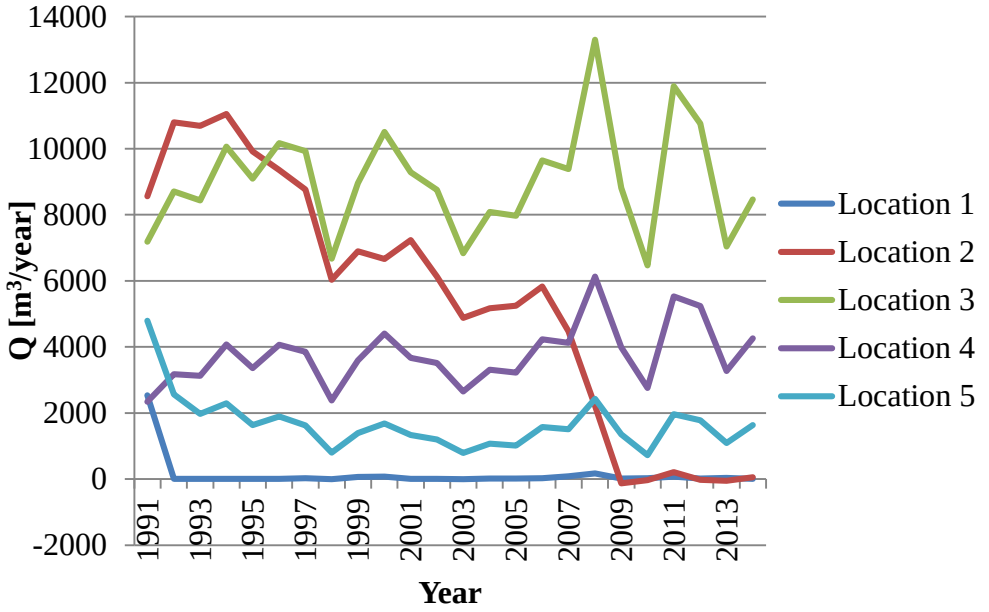

Figure 72. Net sediment transport per year at five locations in Nha Trang bay calculated by GENESIS.

In Figure 71 it is clearly visible that the longshore sediment transport is decreasing in the southbound direction. Location 1 shows a much higher net transportation then the rest of the locations, with the maximum transport value of 525,419 m^3/year occurring at year 2011. Location 5 is the only location where the sediment is transported from the south to north, i.e. the net transport is negative. In Figure 72 Location 1 is showing negative net transport and is deviating much from the high values seen in Figure 71. The net transport is not decreasing in the southbound direction in the simulated transport rates by GENESIS, the highest rate is found at location 3 where 13,295 m3/year of sediment is transported in the year of 2008.

In Table 10 the average for the net transport calculated by the CERC formula and simulation of GENESIS in the time period 1990-2014 are presented. The transport values calculated by GENESIS are somewhat smaller than the values from the CERC formula.

Table 10. Average net sediment transport for Location 1 to Location 5 calculated with the CERC formula and the model GENESIS.

Location	Average Net Transport CERC [m^3/year]	Average Net Transport GENESIS [m^3/year]
1	340,300	133.8
2	37,770	5,414
3	35,170	9,018
4	20,690	3,761
5	-7,340	1,672

7.5 Simulation of Future Evolution

One scenario of beach nourishment with 20 metres of additional added shoreline was placed in cell 16-25, i.e. along the 250 metres stretch right beneath the Nha Trang View restaurant, was simulated. The area was chosen because the beach showed sign of retreat backwards. The simulation was run to investigate possible benefits with beach nourishment and how the long time it would take for the shoreline to retreat to its initial condition. The initial shoreline orientation, to which the beach nourishment was performed at, was based on a satellite plan view image photographed in 2014 for the software Google Earth. Shorelines for the years following the beach nourishment were plotted until the shoreline had retreated past the initial shoreline and the result of the shoreline evolution is presented in Figure 73.

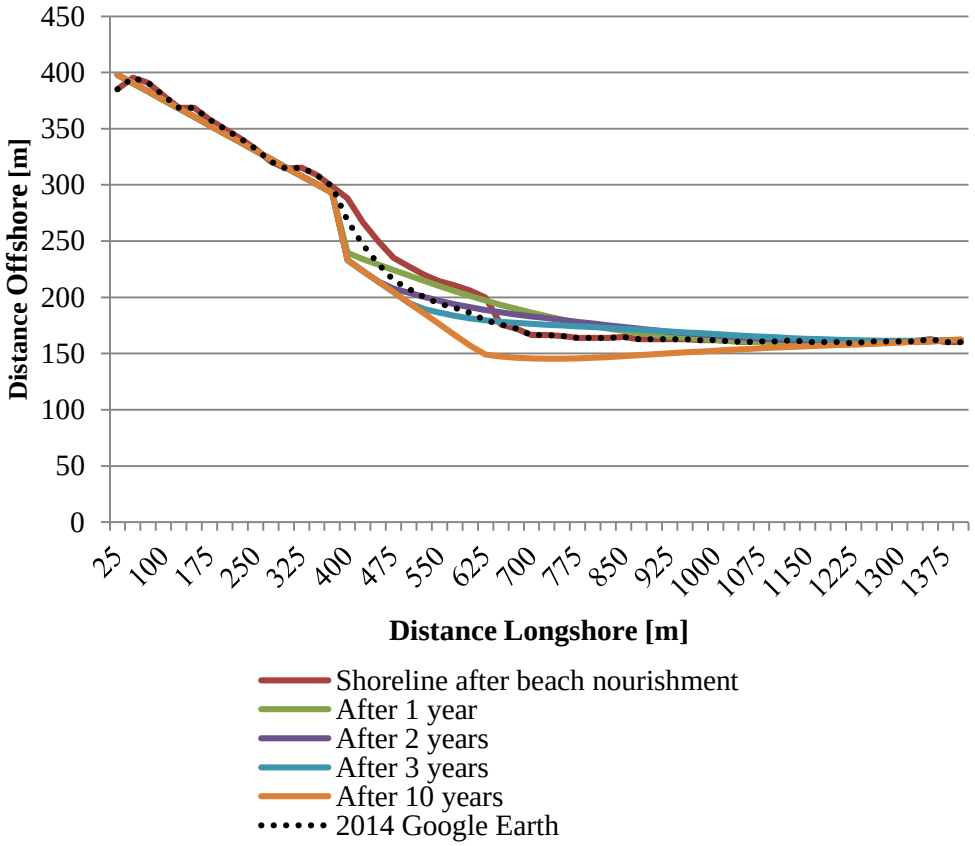

Figure 73. Shoreline evolution for selected years after a beach nourishment of 20 metres over a stretch of 250 metres.

The simulation results show that the shoreline will start to retreat past the initial shoreline in the most northern part of the beach already at the first year after the beach nourishment (green shoreline). After three years have passed, almost the complete beach nourishment volume will have been transported southward (blue shoreline). Ten years after the beach nourishment, the shoreline has retreated back to the seawall (orange shoreline).

Another simulation was run to investigate the shoreline evolution if another beach nourishment would be performed at the same stretch after two years and the results are shown in Figure 74.

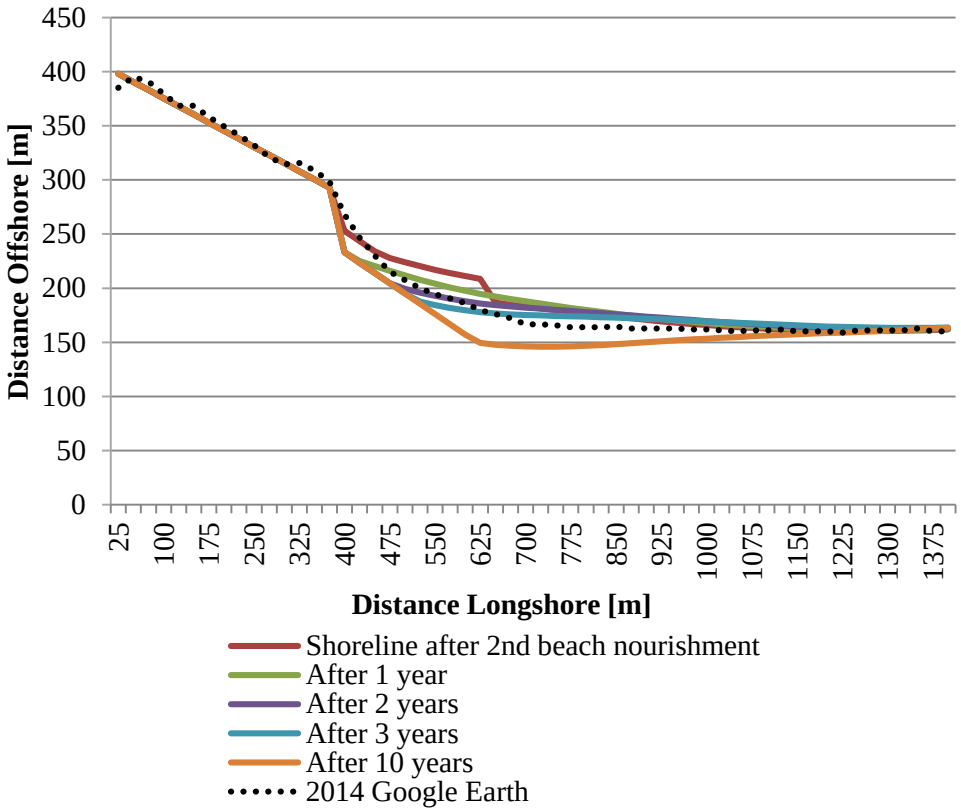

Figure 74. Shoreline evolution for selected years after a second beach nourishment of 20 metres over the same stretch as the previous simulation.

The results show similar results as the previous simulation of the first beach nourishment occasion. Already two years after the sand filling the shoreline has retreated passed almost the whole stretch of the initial shoreline (dotted shoreline). Hence, to benefit from the beach nourishment it would be necessary to redo it every second year.

7.5.1 Cost Estimation

Beach nourishment can be a good alternative when wanting to recover a beach, but such a measure is not for free. An estimation of the amount sand needed for a nourishment project is done with the estimation that GENESIS is using, the profile is not changing its slope along the shoreline and the beach profile remains the same after the filling. The volume fill needed per meter of shoreline is presented in Equation 20.

$$V = dy(D_B + D_C) \quad (20)$$

where *dy* is the shoreline position change [m], D_B is the average berm height above mean sea level [m] and D_C is the depth of closure [m], which equals 2.0 m and 2.74 m, respectively.

A 250 metres long stretch of the beach was renourished in the scenario simulated with a width of 20 metres. Using Equation 20, it gives a total volume of 23,700 cubic metres of sand. With the estimated price of 130,000 VND/cubic metres (Nam, 2015) the total cost would be 2,905,500,000 VND, i.e. around 134 000 USD, for one beach nourishment project at this site. Cost of the labour and mobilisation would also have to be included in the cost estimation if a future beach nourishment is planned.

8. Discussion

Nha Trang beach obtains an unique wave climate due to its location in a sheltering bay and surrounding environment. The many islands in the bay and the mountainous area around the city modify the outcome of the tropical monsoon climate and the bathymetry, which influence the wave climate to a great extent and thus also the evolution of the shoreline.

Strength and direction of winds have a great impact on how the wave climate in a bay will evolve. Hence, the characteristic tropical monsoon climate over Vietnam and the Southeast Asian waters not only has a great impact on the weather conditions but also on the wave climate. The affect of the monsoons at Nha Trang bay distinguishes from the rest of the Vietnamese coastline due to its surrounding environment. Surrounding islands and mountains force the winds of the southwest monsoon, with winds coming from the southwest along the Vietnamese boarder normally in June to September, to take another direction and actually blow in a southeast direction. Thereby, the wave climate in the bay is affected differently from the rest of the Vietnamese coastline.

The shape of the bay's bathymetry influences the wave height and the direction of the propagating waves as the water depth shifts. The many islands in the area, which make the sea bed alternate, and shallows in the bay may also reflect and diffract the onshore shoaling waves.

8.1 Discussion of Field Measurement Results

The shoreline at Nha Trang is quite stable, i.e. the net sediment transport flow along the beach is in balance, and little deviations between the years being mapped from Google Earth and GPS measurements were shown. One notable large change is however at the furthest north of the beach, were a sand spit was located in the beginning of the investigated years. As the sand spit started to erode, the construction around Yersin Park were built to protect the park. Along the sides of the park seawalls were erected and the withdrawal of the shoreline at the spit was hindered. Instead another location, the area south of Nha Trang View restaurant, began to indicate a shoreline change the following years. One hypothesis is that by building the seawall around Yersin Park the sediment flow have been hindered and since no sediment could be provided from the sand spit, sediment is taken from the area south of the restaurant instead. One might suspect and fear that the retreat of the northern part of the beach will continue in a southward direction.

Confirmed by previous years' Google Earth and GPS measurements, the shoreline investigations indicate that the beach is varying with season. If looking at the beach profiles along the shoreline, there are also a clear connection between season and the vertical and horizontal variations. In winter, when the wind blows hard and thus creates high and energy-rich waves, the shoreline retreat which is followed by a decrease in the horizontal and vertical beach profile. In summer, when the wind is calmer and the waves thus smaller and less energy-rich, the crosshore transportation has a positive gradient towards land and the beach accrete. Consequently, the shoreline becomes wider and also the beach profile increases in both the horizontal and vertical direction during the summer.

The beach profiles along the shoreline indicate that the beach is accreting in the northern part and are showing signs of erosion at the centre of the shoreline. This is not in line with the general indications that the beach is eroding in the north and no clear explanation of the results could be proved. Maybe a storm passing the area before the days of the measurement could create harsh weather conditions and strong currents transporting sediments offshore, making the beach erode temporary. In the long run the affect of a storm would not change the outcome of the beach evolution as it is part of seasonal changes. More frequently measurements would be preferable to validate the results.

The beach profiles and some of the shorelines are measured with a GPS. According to the manufacturer, there is a risk factor of an error slightly above 1% for the location measurements. This risk factor will introduce some errors into the measurements, which could be most pronounced in the shoreline measurements as it is compared with measurements from a different technique, i.e. aerial photographs from Google Earth. Another uncertainty is the definition of the shoreline, as it is hard to state an exact location of the shoreline the definition might differ between the people performing the measurements. Moreover, the Google Earth digitalization was done with no consideration to tidal level, as information of the tidal level was not available for the dates, which also affect the definition of the shoreline. The digitalization was done manually and the exact definition of the shoreline might differentiate from the location of the shoreline walked along with the GPS. Both the GPS and Google Earth measurements for the shorelines and beach profiles are from different seasons and thus making the results less comparable. Measurements from the same season or month for different years would give a more correct image of the evolution. With the arguments mentioned above, the shoreline measurements are regarded as unsure with many uncertainties. Hence, too many conclusions should not be drawn from these results as they are not seen

as a complete image of the truth but more as an indicator of the evolution of the shoreline at Nha Trang bay.

According to theory, finer material should be found furthest away from a river mouth and coarser material should settle closer to the river mouth. The explanation for this is that the turbulent river flow will transport the finer material offshore and the sediments will later be transported with the longshore current further down the shoreline. This theory does not accord with the results of the sediment samples collected along Nha Trang beach in April 2015. Instead the coarsest material was found at the most southward sampling station. Maybe this is because of the special wave climate in the bay in Nha Trang caused by the surrounding mountains and islands. Name worthy, is that the beach slope at this sampling station was very steep, which indicates that grain size of the sediment should be coarse and the results agree with theory in this matter. Also, the beach profile at the most northern sampling station, located south of concrete seawall around Yersin Park and Nha Trang View restaurant, had a steep slope with coarse grains. Steep slopes are normally a sign of erosion, which the results of the shoreline evolution investigation of the northern, and at the present eroding, part of the beach verify. Seasonal impact on the beach and its material could also be confirmed by the collected sediment core samples, which show a clear pattern of different layers consisting of grains with different grain sizes and tones. There is a large difference in the d50 for the top layer of the cores at the berm and the upper swash zone. The different layers indicate seasons with different weather conditions during which sediment of diverse characteristics could be transported onshore to the beach and settle. It is also indicates that there is little exchange of sediment between the berm zone and the upper swash zone in the beach profile direction, as otherwise d50 would be similar. Most likely, the swashing waves never reach the berm and thus sediment cannot be transported to the berm.

Data of the wave and current speed and direction as well as measurements of longshore sediment transport were collected at end of the northeast monsoon. The results of the sediment transport received from the Nagata sediment trap should agree with the theory that the sediment transport is the greatest in southward and offshore direction during the northeast monsoon climate. However, that was not the case as the sediment trap showed irregular results and change of dominant direction of the sediment transport along the shoreline. As the crosshore transport always had a greater value than the longshore transport, it might be the result from that the sediment trap was placed at a height that correlated with the movement of the particle orbits. Also the Nagata sediment trap was placed offshore the breaking zone, where the longshore

sediment transport occurs, and thereby only trapped free drifting finer material. The size of the collected sediments were so fine that the transport most likely do not have any great impact on the shoreline evolution as it is to fine to settle at the beach.

The currents in the bay during the day of the field measurement had a dominant direction to the southwest, which is in line with theory as the northeast monsoon creates waves mostly travelling southwest. But the results do not coincide with the results of the sediment transport. Both these measurement techniques would be preferred to do at additional sites, for a longer duration and with more tests with sediment traps at several layers, to get a vertical transport profile. There are no tests done that can be used to validate the measurements performed by the sediment trap. This, together with the other requests, make the data hard to rely on and thereby use for any conclusion.

8.2 Discussion of Simulation Results

The wave climate in Nha Trang bay was modelled from hindcasted deep water wave data. The effect of diffraction was evident as the wave heights in the shadow zones created by the islands in the bay were smaller than wave heights at locations less sheltered. The shadow effect also depends heavenly on which direction the waves come from. During the northeast monsoon, when the waves usually are higher and enter the bay from northeast direction, the bay is less sheltered than during the southwest monsoon. As the waves propagate from the southeast direction during the southwest monsoon, Hon Tre and smaller islands will diffract the waves and a larger portion of the bay will be in the shadow zones. The islands will also reflect the incoming waves, but this wave transformation process is not included in the model EBED and hence the reality will most likely differ a bit. A less or more sheltered bay and shoreline, shifting with the monsoon periods, also implies a seasonal change of the shoreline.

The net sediment transport rate simulated from GENESIS was low compared to the net transport rate calculated by the CERC formula. Especially the transportation value calculated with CERC formula for the most northern location stands out with a very high transport which seems unlikely. One possible explanation for the unreasonable result could be that the site is located further seaward, making the shoreline direction hard to confirm. A small change in the shoreline angle could have a great influence on the calculated net transport rate.

The net sediment transport simulated by GENESIS showed a positive value from north to south along the shoreline, meaning a longshore sediment transport take place in the same direction. As the wind and waves are most dominant in this direction, the result correlate well with the transport pattern. But the retreat and accrete of the shoreline, simulated by GENESIS is questionable. It is believed to show higher change of shoreline than what feels reasonable from looking at the historical evolution. As the model setup was quite simple, the beach complexibility was not able to be fully mapped and included in the model. For example, the sediment flow from the river is not included. The river flow transports sediments and contribute to the material of the beach and it would be interesting to investigate how the nowadays more regulated flow will affect the shoreline evolution.

The wave climate used for the future longshore sediment transport and shoreline evolution simulation with the model GENESIS was the simulated historical wave series achieved from the model EBED. Furthermore, the offshore wave data used as input to the model EBED was based on simulated historical global wind field data and thus uncertainties of the accuracy has been introduced already in the beginning of the modelling chain. Historical simulated wave data were used for the simulations of the future shoreline evolution, since it is the best guess of the forthcoming wave climate when there is no information of future situation to be obtained. But it is well worth to keep in mind that the wave climate might not be the same then. The many warnings about global warming points towards a more extreme climate, which could lead to a more pronounced wind condition in Nha Trang bay. The model should be used precisely as a model and not as a mirror of the reality. The model gives an indication of the evolution and is a tool used to be able to understand the processes acting in the bay.

The beach nourishment scenario showed that regular refilling of the northern part of the beach every second year would be necessary if wanting to achieve a lasting beach. One important thing to take into consideration when do a filling is where the material is coming from. The area from which the sand is removed should be able to withstand such a loss and the operation should be done without interfering with the sediment balance as well as the ecosystem. Even if the sand used for renourishment is a cost for the municipality, a more attractive beach could lead to greater income for the business in the area if more tourists come to Nha Trang. At the present, a beach nourishment is not an urgent measure since the beach is mainly influenced by the seasonal variations. If considering beach nourishment further investigations need to be performed.

9. Conclusion

Few previous studies have been done on the hydrodynamic processes in Nha Trang bay and this master thesis was performed as an attempt to understand and map the governing processes affecting the evolution of the south beach in Nha Trang. At the present the shoreline of the southern beach in Nha Trang is in a quite stable condition with mainly seasonal variations, which was confirmed by shoreline and beach profile measurements. The simulation program GENESIS predicted a quite rapid retreat of the shoreline for the next 25 years, leaving no beach left in front of the seawall structure at the northern part of the beach. The result was regarded as unsure as the simulation was done under simplifications and assumptions. However, the northern section of the beach has experienced erosion since the sand spit at the river mouth of Cai disappeared. With the knowledge of the severe erosion at the beach north of the river mouth one might suspect and fear that the retreat of the northern part of the southern beach will continue in the southward direction along the shoreline. Beach nourishment was suggested as a soft measure to improve the condition of the beach, but renourishment every second year would be necessary to maintain a continuous shoreline. This would imply investment for the municipality and would have to be weighed against the profits of having an extra stretch of beach.

From studying grain sizes of a beach, material source and transport patterns can be understood. But the grain sizes from the measurements during the fieldtrips in Spring 2015 showed no clear correlation between distance from the river mouth and the d50 value. Also the grain sizes along the beach profile had no clear pattern in the studied cross-sections. However, the collected sediment cores showed that the beach experiences seasonal changes as many different layers were observed.

The area of Nha Trang bay, sheltered by the many islands and mountains, experiences an unique wind climate which affects the wave climate of the bay. From the simulation of the nearshore wave climate it was evident that the islands in the bay create shadow zones, where the wave heights become significant lower than in places more exposed to open sea. The wave climate, and consequently also the shoreline evolution, is also highly influence by the seasons and the monsoons taking place in Vietnam. The weather conditions and tidal variations create a complex system for the governing processes of the shoreline evolution. For complete understanding of the ongoing processes in the bay and better predictions of the future evolution, further studies are needed. The area has to be studied for a longer time period, more collection of

samples would be preferable and the simulation models need to be modified and adapted for this specific case to achieve a greater understanding and more reliable results.

10. Future Work

Due to the time limitation for the master thesis not everything wanted to study could be included. As the shoreline evolution in Nha Trang bay is affected by the seasons, studies over the whole year is of interest for covering the complete development processes. More measurements of the shoreline positions and beach profiles would be of high interest to be able to achieve a better understanding of the beach evolution. Sediment samples taken at the same locations as in this study at more occasions could be compared to this study to relate the changes to the sediment transport pattern in the bay.

Measurements of wave data in the bay over longer time series and at different seasons would be highly useful to validate the model EBED. Also look into the possibility to include the tidal and wind effects into a wave transformation model to achieve more reliable results.

It could also be of interest to look at optimization of the model GENESIS to get better reassembly of the evolution and to simulate other beach nourishment scenarios to see what give the best effect and to the lowest cost. Also other measures for improving the condition of the beach could be looked upon in a further study of the area. What-if analysis of for example extended harbour area and building of piers etc. could be interesting to simulate.

References

ANONYMOUS. 2006. *Seeking for Fresh Water Source* [Online]. Nha Trang, Vietnam: Khanh Hoa News. Available: http://www.baokhanhhoa.com.vn/english/socio_politic/200604/seeking-for-fresh-water-source-1794258/ [Accessed 25 May 2015].

BUI, H. L. 2009. Impact Assessment of the Monsoonal Waves to South-Central Vietnam Coast from Phu Yen to Binh Thuan Provinces and Proposal the Measures to reduce the Damages for Sustainable Development. Nha Trang: Institute of Oceanography.

BUI, V. D., STATTEGGER, K. et al. 2014. Late Pleistocene - Holocene seismic Stratigraphy of Nha Trang Shelf, Central Vietnam. *Marine and Petroleum Geology,* 58**,** 789-800.

CAT, N. N., TIEN, P. H. et al. 2006. *Status of Coastal Erosion of Vietnam and Proposed Measures for Protection* [Online]. Food and Agriculture Organization of the United Nations. Available: http://www.fao.org/forestry/11286-08d0cd86bc02ef85da8f5b6249401b52f.pdf [Accessed 26 May 2015].

CENTER OF OCEANOGRAPHY 2015. Tidal Prediction Table 2015. Volume II ed. Vietnam.

DALLY, W. R., DEAN, R. G. et al. 1985. Wave Height Variation across Beaches of Arbitrary Profile. *Journal of Geophysical Research: Oceans,* 90**,** 11917-11927.

GOOGLE INC 2015. Google Earth.

HALLERMEIER, R. J. 1983. Sand Transport Limits in Coastal Structure Design. *In:* WEGGEL, R. J. (ed.) *Proceedings of Coastal Structures '83.* Arlington, Virginia: Amer Society of Civil Engineers.

HANSON, H. 1989. Genesis: Generalized Shoreline Change Numerical Model. *Journal of Coastal Research,* 5**,** 1-27.

HANSON, H. 2014a. *RE: Lecture 3. Wave transformation, Course Coastal Hydraulics.*

HANSON, H. 2014b. *RE: Lecture 5. Currents, Levels & Run-up, Course Coastal Hydraulics.*

HANSON, H. 2014c. *RE: Lecture 7. Sediment Transport Processes, Course Coastal Hydraulics.*

HANSON, H. & KRAUS, N. C. 1989. GENESIS: Generalized Model for Simulating Shoreline Change. Washington: US Army Corps of Engineers.

INMAN, D. 1966. Oceanographic and Engineering Report on Investigation of Sedimentation, Silting and Dredging Requirements. Saigon: Daniel Mann Johnson & Mendenhall.

KOMAR, P. D. 1998. *Beach Processes and Sedimentation,* Upper Saddle River, New Jersey, Prentice-Hall Inc.

LEFEBVRE, J.-P., ALMAR, R. et al. 2014. Contribution of Swash Processes Generated by Low Energy Wind Waves in the Recovery of a Beach Impacted by Extreme Events: Nha Trang, Vietnam. *Journal of Coastal Research***,** 663-668.

MASE, H. 2001. Multi-Directional Random Wave Transformation Model Based on Energy Balance Equation. *Coastal Engineering,* 43**,** 317-337.

MAU, L. D. 2014. Overview of Natural Geographical Conditions of Nha Trang Bay. Nha Trang: Institute of Oceanography.

MINISTRY OF NATURAL RESOURCES AND ENVIRONMENT 2003. Vietnam Initial National Communication. *In:* CHANGE, U. T. U. N. F. C. O. C. (ed.). Hanoi: Socialist Republic of Vietnam, Ministry of Natural Resources and Environment.

MÅRTENSSON, S. 2015. *Nha Trang* [Online]. Nationalencyklopedin AB, NE. Available: http://www.ne.se/uppslagsverk/encyklopedi/l%C3%A5ng/nha-trang [Accessed 26 May 2015].

MÅRTENSSON, S. & VON KONOW, J. 2015. *Vietnam* [Online]. Nationalencyklopedin AB, NE. Available: http://www.ne.se/uppslagsverk/encyklopedi/l%C3%A5ng/vietnam [Accessed 26 February 2015].

NAM, P. T. 2010. *Numerical Model of Beach Topography Evolution due to Waves and Currents, Special Emphasis on Coastal Structures.* Doctor PhD Thesis, Faculty of Engineering, Lund University.

NAM, P. T. 22 May 2015. Institute of Mechanics, Hanoi, Vietnam. *RE: Mail correspondence about cost of beach nourishment.* Type to BÖÖS, S. & DAHLSTRÖM, A.

NAM, P. T., LARSON, M. et al. 2009. A Numerical Model of Nearshore Waves, Currents, and Sediment Transport. *Coastal Engineering,* 56**,** 1084-1096.

NGUYEN, A. D., ZHAO, J. X. et al. 2013. Impact of Recent Coastal Development and Human Activities on Nha Trang Bay, Vietnam: Evidence from a Porites Lutea Geochemical Record. *Coral Reefs,* 32**,** 181-193.

NGUYEN, D. 9 April 2015. Institute of Oceanography, Nha Trang, Vietnam. *RE: Interview about river flow regulation.* Type to BÖÖS, S. & DAHLSTRÖM, A.

NGUYEN, M. H. & LARSON, M. 2014. Coastline and River mouth Evolution in the Central part of the Red River Delta. *In:* NGUYEN, D. T.,

TAKAGI, H. et al. (eds.) *Coastal Disasters and Climate Change in Vietnam.* First Edition ed. London: Elsevier.

NGUYEN, T. V. 2013. Study of Hydrodynamics and Sediment Transport in Estauries and Coastal Zone of Nha Trang Bay, Khanh Hoa Province. Hanoi: Water Resources University.

NORTEK AS. 2014. *AWAC Acoustic Wave and Current Profiler* [Online]. Nortek AS. Available: http://www.nortek-as.com/lib/brochures/datasheet-awac [Accessed 12 April 2015].

PADMALAL, D. & MAYA, K. 2014. *Sand Mining, Environmental Impacts and Selected Case Studies,* Thiruvananthapuram, Springer.

PERESYPKIN, V. I., SMUROV, A. V. et al. 2011. Composition of the Organic Matter of the Water, Suspended Matter and Bottom Sediments in Nha Trang Bay in Vietnam an the South China Sea. *Oceanology*, 51**,** 959-968.

PETHICK, J. 1984. *An Introduction to Coastal Geomorphology,* Newcastle upon Tyne, Hodder and Stoughton Limited.

PINET, P. R. 1998. *Invitation to Oceanography,* London, Jones and Bartlett Publichers International.

REEVE, D., CHADWICK, A. et al. 2012. *Coastal Engineering, Processes, Theory and Design Practise,* Abingdon, Oxon, Spon Press.

SAHA, S., MOORTHI, S. et al. 2010. NCEP Climate Forecast System Reanalysis (CFSR) Selected Hourly Time-Series Products, January 1979 to December 2010. NCEP National Centers for Environmental Prediction.

SAHA, S., MOORTHI, S. et al. 2011, updated monthly. NCEP Climate Forecast System Version 2 (CFSv2) Selected Hourly Time-Series Products. NCEP The National Centers for Environmental Prediction.

SOULSBY, R. 1997. *Dynamics of Marine Sands,* London, Thomas Telford Publications.

THALES NAVIGATION. 2004. *ProMark 2 System, User Guide* [Online]. Thales Navigation, Inc. Available: http://www.vtpup.cz/common/manual/PrF_geog_Ashtech_ProMark2_manual_EN.pdf [Accessed 10 March 2015].

U.S. ARMY CORPS OF ENGINEERS 1977. *Shore Protection Manual,* Washington, D.C., U.S. Corps of Engineers, Coastal Engineering Research Center.

U.S. ARMY CORPS OF ENGINEERS 1984. *Shore Protection Manual,* Washington, D.C., U.S. Corps of Engineers, Coastal Engineering Research Center.

U.S. ARMY CORPS OF ENGINEERS 2012. Coastal Engineering Manual. Washington, D.C.: U.S. Army Corps of Engineers.

VU, T. A. & NGUYEN, C. C. 19 March 2015. *RE: Interview concerning coastal constructions in Nha Trang.* Type to BÖÖS, S. & DAHLSTRÖM, A.

Appendix 1: Sampling locations

Table 1. Measured coordinates for the four beach profiles at Section 1, Section 2, Section 3 and Section 4 collected at the 7th of March 2015.

		Coordinates [decimal degrees, °]	
Section	Station	Longitude	Latitude
1	1:1	109.19707	12.25516
	1:2	109.1971	12.25515
	1:3	109.19715	12.25513
	1:4	109.19718	12.25512
	1:5	109.197193	12.255115
	1:6	109.19722	12.25511
	1:7	109.19725	12.255094
	1:8	109.19726	12.25509
	1:9	109.197339	12.255064
2	2:1	109.19682	12.2542
	2:2	109.19684	12.2542
	2:3	109.19685	12.2542
	2:4	109.19688	12.2542
	2:5	109.19691	12.25419
	2:6	109.19696	12.25418
	2:7	109.19699	12.25418
	2:8	109.19704	12.25417
	2:9	109.19706	12.25417
	2:10	109.1971	12.25416
	2:11	109.19712	12.25416
	2:12	109.19718	12.25415
3	3:1	109.19668	12.24712
	3:2	109.19674	12.24712
	3:3	109.19676	12.24712
	3:4	109.19685	12.24712
	3:5	109.19688	12.24712
	3:6	109.19693	12.24712
	3:7	109.19698	12.24712
	3:8	109.19702	12.24712
	3:9	109.19714	12.24712

4	4:1	109.19724	12.23961
	4:2	109.19726	12.2396
	4:3	109.19728	12.2396
	4:4	109.19734	12.23961
	4:5	109.19738	12.23962
	4:6	109.19742	12.23962
	4:7	109.19744	12.23962
	4:8	109.19746	12.23962
	4:9	109.19747	12.23962
	4:10	109.19752	12.23963
	4:11	109.19753	12.23963
	4:12	109.19768	12.23964

Table 2. Coordinates for the locations of the top layer sediment samples collected on the 11th of April 2015.

		Coordinates [decimal degrees, °]	
Section	Station	Longitude	Latitude
1	1:1	109.19717	12.25526
	1:2	109.19172	12.25525
	1:3	109.19726	12.25523
	1:4	109.1973	12.25522
	1:5	-	-
2		109.19698	12.25415
3		109.19668	12.24712
4	4:1	109.19737	12.23962
	4:2	109.19742	12.2396
	4:3	109.19745	12.23961
	4:4	109.19749	12.23961
	4:5	-	-
5		109.19855	12.23384
6		109.20060	12.22819
7		109.20371	12.22264
8	8:1	109.20619	12.21935
	8:2	109.20628	12.21943
	8:3	109.20630	12.21946
	8:4	109.20632	12.21946
	8:5	-	-

Table 3. Coordinates for the locations of the sediment cores collected on the 7th of March 2015.

		Coordinates [decimal degrees, °]	
Section	Station	Longitude	Latitude
2	S core	109.197007	12.254176
2	B core	109.196871	12.254194

Table 4. Coordinates for the locations of the Nagata sediment trap during the fieldwork on the 7th of March 2015.

		Coordinates [decimal degrees, °]	
Section	Station	Longitude	Latitude
3	Nagata 3	109.197243	12.247119
4	Nagata 4	109.197828	12.239647

Table 5. Coordinates for the locations of AWAC on the 7th of March 2015.

		Coordinates [decimal degrees, °]	
Section	Station	Longitude	Latitude
2	AWAC	109.197420	12.254117

Appendix 2: EBED

To run the multi-directional random wave transformation model EBED four files with input data are needed; information of parameters affecting the propagation of the waves and mesh size of the grid, bathymetry data of Nha Trang bay, a series of offshore wave data and x- and y-values of interesting grid cells with output data. To execute EBED, the four files need to be connected through the file "filenames", which states the filenames of the four input-files (see Table 1).

Table 1. Filenames of the input files needed for executing the model EBED.

NTrang_inp.dat
NTrang_inp_wave.dat
NTrang_dep_100.dat
NTrang_out.dat

The model only manages to transform waves with an incoming wave angle of 90 to -90 degrees to the horizontal offshore boarder of the grid. The wave parameters 25.0 and 8.0 are functions of the spreading and describes the two dimensional spectrum. The mesh size of the grid was investigated and the coarsest grid with the most accurate result was given by the mesh size 100 m times 100 m. Due to the complexity of including the variation of tidal level it was neglected in the model, hence it was given the value of zero. The components of frequency and direction were chosen to 20 and 36, respectively. Higher values of the components would give higher resolution of the frequency and direction of the waves but the execution time would be longer. The constants gamma, sigma A and sigma B with the values of 3.30, 0.07 and 0.09, respectively, are standard values used in the Jonswap model. The use of control parameters were neglected since the model is simplified. The grid of the studied area consisted of 209 cells in the x-direction and 275 cells in the y-direction. The dimensionless stable (Γ) and decay coefficient (K) and the roller dissipation coefficient are important parameters for the energy dissipation and were based on laboratory experiments performed by Nam (2010). The minimum water depth that distinguishes between land and sea was set as 0.1 m. All the explained input parameters and conditions for the run model can be found in Table 2.

Table 2. Input parameters and conditions for the model EBED.

```
CALCULATION OF WAVE TRANSFORMATION FOR NHA TRANG
1. WAVE PARAMETERS
  90.0 -90.0  25.0   8.0
2. MESH SIZE AND TIDE LEVE
  100   100    0.0
3. COMPONENT OF FREQUENCY AND DIRECTION
  20   36
4. GAMA, SIGMA A, SIGMA B IN JONSWAP MODEL
  3.30   0.07   0.09
5. CONTROL PARAMETER
   0    0    0    0
6. NUMBER OF GRID NODE IN THE MESH
  209  275
7. STABLE AND DECAY COEFF., ROLLER DISS. COEF.
 0.45    0.15    0.1
8. MINIMUM WATER DEPTH TO IDENTIFY SEA AND LAND
  0.1
```

The offshore wave data from the location 109.5E 12.25 N with a water depth of 80 metres simulated by the model SWAN by Duong Cong Dien, Institute of Mechanics in Hanoi, for the years 1990-2014 were presented in the format shown in Table 3. Number of run offshore waves was 2,699 and the input data include information about the date, time, specific wave height, specific time period, incoming wave angle and tidal effects of each wave scenario.

Table 3. Offshore wave data used running the model EBED.

```
9. NUMBER OF SENARIOS FOR RUNNING MODEL
  2699
++++++++++++++++++++++++++++++++++++++++++++++++++++++++
YYMMDD     HHMM     HS      TS       TETA     TIDAL
19920510   1200     0.470     3.600     -52.1       0.0
19920510   1500     0.410     3.560     -49.8       0.0
19920510   1800     0.360     3.550     -41.1       0.0
19920510   2100     0.310     3.570     -31.6       0.0
19920511      0     0.280     3.640     -25.1       0.0
19920511    300     0.250     3.680     -20.8       0.0
/.../
```

The bathymetry data of Nha Trang bay compiled by Duong Cong Dien, Institute of Mechanics in Hanoi, originate from the Vietnam Navy maps of the East sea and neighbouring seas with an accuracy of 0.1 m combined with nearshore bathymetry data collected with a sonar instrument by Nguyen (2013). The final bathymetry data was presented for each grid cell in a text file like shown in Table 4.

Table 4. Bathymetry data of Nha Trang bay used for running the model EBED.

46.5	46.6	46.6	46.7	46.8	46.9	46.9	47.0	47.1	47.2	47.4	47.5
47.6	47.7	47.8	48.0	48.0	48.0	48.1	48.2	48.3	48.2	48.2	48.2
48.1	48.0	47.8	47.7	47.4	47.2	46.8	46.1	45.5	45.0	44.3	43.7
42.7	41.1	40.5	41.7	43.9	45.0						
/.../											

The cell numbers in x- and y-directions of the five interesting locations with output data were stated in a file according to Table 5. In Table 6 the coordinates and water depths for the investigated locations can be found.

Table 5. Cells with desired output data.

CONTROL PARAMETER FOR OUTPUT FILE (0:whole domain 1:specific locations)
1
NUMBER OF INTERESTED LOCATIONS
5
SPECIFIC LOCATIONS IN THE DOMAIN (INDEX NUMBERS IN X AND Y DIRECTION)
191 148
197 159
199 171
196 186
189 194

Table 6. Coordinates for the cells with output data and the water depth at the locations.

			UTM Coordinates	
X	**Y**	**Water depth [m]**	**Longitude**	**Latitude**
191	148	10	305190	1355810
197	159	9.8	304590	1354710
199	171	10	304390	1353510
196	186	9.7	304690	1352010
189	194	11.1	305390	1351210

Appendix 3: Calculations of Longshore Sediment Transport with CERC formula

The annual longshore sediment transport at five locations along the shoreline in Nha Trang bay were calculated with Halcrow's version of the CERC formula for validation of the results simulated with the model GENESIS.

The density of sand and water were set to 2,650 kg/m^3 and 1,000 kg/m^3, respectively, and thus the relative sediment density became 2.65. The transport coefficient, *K*, used in Halcrow's version of the CERC formula was set to 0.13, which corresponds to a *K*-value of approximately 0.26 in the original CERC formula. The used porosity of sediment, *n*, was 0.4 and the used gravitational acceleration was 9.81 m/s^2. The longshore component of the energy flux, P_l, is dependent on the incoming wave and the angle at the breaking and thus obtains a different value for each time step.

The incoming wave angle used in the formula was calculated with respect to the normal for each one of the five shoreline stretches and presented in respective to the true north orientation, see Table 1. The southbound direction was set as the positive direction for the transport.

Table 1. The different incoming wave angles used in the CERC formula for the chosen locations.

Location	Normal orientation in respect to TN
1	108°
2	86°
3	77°
4	60°
5	43°

Appendix 4: GENESIS

The output files with nearshore wave climate data from five locations generated with the model EBED were used as input data for the simulation of the future longshore sediment transport and shoreline evolution with the model GENESIS. Conditions for the model were stated in the .gen-file, which can be read in Table 1 together with short explanations for the variables within the parenthesis. The left and right boundary conditions for the grid were set to gated boundary and pinned beach boundary, respectively. This assumes that the simulated area is delimitated by a groin in the north and the pinned beach boundary in the south allows free passing sediment. The sediment entering and leaving the cells at the gated boundary depends on the distance of the seaward tip of the groin to the shoreline, the beach slope and the permeability of the groin. The simulated area was divided into 197 vertical cells à 25 metres along the shoreline and output data were calculated for every quarter-hour but only printed in the output file once per year, which could be seen together with other detailed conditions stated under the heading "Model Setup".

Table 1. The Config-file stating the conditions for the model GENESIS.

GENCADE:

TITLE: NhaTrangBay
****** FILES ******
INIFILE: BeachCoordinates.shi (filename for file with shoreline coordinates)
NUMWAVES: 5 (number of wave series)
WAVEID: 5 10.00 71060 Location1.wave (Grid cell number at which the wave data
is located offshore, depth at which the wave data is taken, No. of lines in wave file, wave file name)
WAVEID: 49 9.80 71060 Location2.wave
WAVEID: 97 10.00 71060 Location3.wave
WAVEID: 158 9.70 71060 Location4.wave
WAVEID: 189 11.10 71060 Location5.wave
PRFILE: Console.prt (wanted filename for printout status of runned simulation)

***** MODEL SETUP *****
GENUNITS: (m) (Units of measure: m or ft)

```
X0:       0.0                 (X-grid origin)
Y0:       0.0                 (Y-grid origin)
AZIMUTH:  0                   (Angle between N and X-axis)
NX:       197                 (No. of cells alongshore)
DX:       25
     (Cell size)
SIMDATS:  19900101  (Start date YYYYMMDD)
SIMDATE:  20141231  (End date YYYYMMDD)
DT:       0.25                (Calculation time step in Hrs)
DTSAVE:   8760.00       (Time step in output file)
K1:       0.050000
 (Longshore transport coeff. K1)
K2:       0.250000
 (Longshore transport coeff. K2)
PRTOUT:   t                   (Output to PRFILE yes (t), no (f))
PRWARN:   f                   (Print warnings yes (t), no(f))
ISMOOTH:  11                  (Size of smoothing window)
IREG:     0                   (Use offshore contour yes (1), no(0))

***** WAVES *****
HAMP:     1.000000
(Height amplification factor H' = H*Hamp)
THETAAMP: 1.000000
(Angle  amplification factor Z' = Z*Thetaamp
THETADEL: 0.000000
(Angle offset Z' = Z+Thetadel)

***** BEACH *****
D50:      1.00000           (Grain size in mm)
BERMHT:   2.000000
(Berm height)
DCLOS:    2.74
   (Depth of closure)
LBCTYPE:  1    (LH boundary condition type: 0 = pinned beach, 1 = gated
(groin), 3 = moving)
LMOVY:    0       (shoreline displacement per "period" at LH bondary)
LMOVPER:  0     ("period" for LMOVY: entire simulation (0), day(1), time
step (2))
LGROINY:  0     (Length of groin on LH boundary from shoreline to seaward
tip)
```

RBCTYPE: 1 (RH boundary condition type: 0 = pinned beach, 1 = gated (groin), 3 = moving)
RMOVY: 0 (shoreline displacement per "period" at RH bondary)
RMOVPER: 0 ("period" for RMOVY: entire simulation (0), day(1), time step (2))
RGROINY: 0 (Length of groin on RH boundary from shoreline to seaward tip)

***** Gated (groin)/Yersin Park (LH boarder) *****
IXDG: 1 (X-coordinate groin)
YDG: 400 (distance from x-axis to tip of groin)
DDG: 10.00 (depth at tip of groin)
PDG: 0.0000 (groin permeability 0-1, 1 = 100%)

***** SEAWALL AROUND CITY VIEW RESTAURANT *****
ISWBEG: 1 (Start LH coord seawall)
ISWEND: 15 (End RH coord seawall)
SWY1: 398 (distance from x-axis to LH end of seawall)
SWY2: 293 (distance from x-axis to RH end of seawall)

***** SEAWALL CITY VIEW - LOTUS *****
ISWBEG: 16 (Start LH coord seawall)
ISWEND: 28 (End RH coord seawall)
SWY1: 233 (distance from x-axis to LH end of seawall)
SWY2: 119 (distance from x-axis to RH end of seawall)
ISWBEG: 29
ISWEND: 60
SWY1: 119
SWY2: 124
ISWBEG: 61
ISWEND: 75
SWY1: 124
SWY2: 156
ISWBEG: 76
ISWEND: 94
SWY1: 156
SWY2: 205

The grain size, berm height and depth of closure, which can be seen under the heading “Beach”, were all set to a fix value for the whole shoreline since the model assumes that the beach profile remains constant along the shoreline. The

grain size, or more correctly d50, was determined by comparing the mean beach profile of the four measured in April 2015 with the theoretical beach profile represented by Equation 1.

$$D = Ay^{2/3} \quad (1)$$

where D is the water depth [m] and A an empirical scale parameter [$m^{1/3}$], which is calculated as follows

$$A = 0.23d50^{0.32}, \quad 0.4 \leq d50 < 10.0$$
$$A = 0.23d50^{0.28}, \quad 10.0 \leq d50 < 40.0$$

The grain size distribution d50 is given in the unit millimetres. The mean beach profile had the greatest match with the theoretical beach profile (Hanson and Kraus, 1989) for the d50 value 1.0 mm, as can be seen in Figure 1.

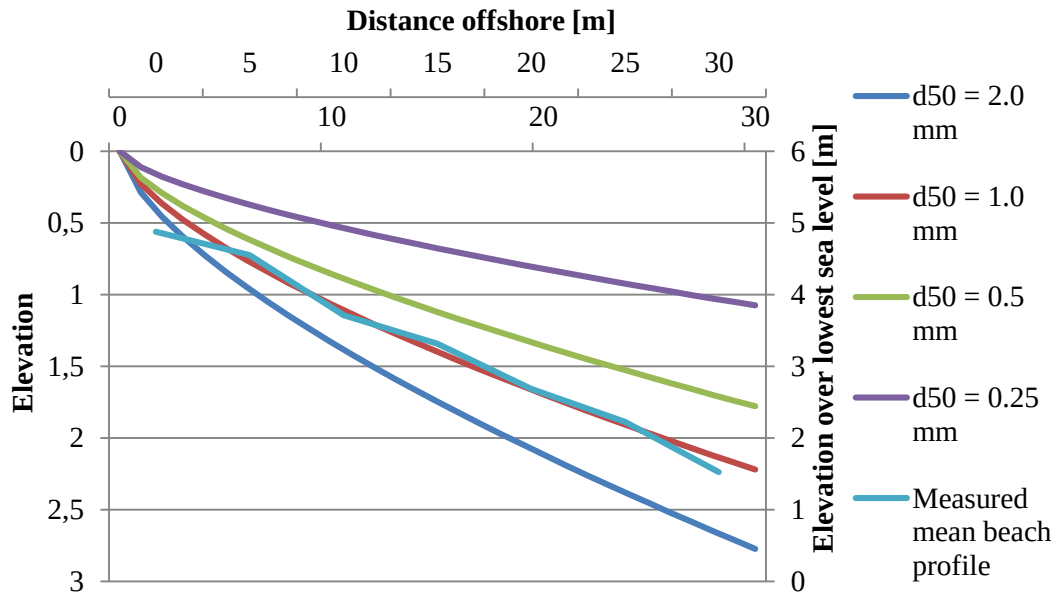

Figure 1. Selection of the value d50 for the model setup of GENESIS.

The berm height of 2.0 metres was estimated from the measured beach profiles from April 2015 as well. While depth of closure of 2.7 metres was calculated with Equation 16 in *7.1 Background and Theoretical Formulation* by determine the extreme annual significant wave height (H_{mas} [m]) from the offshore wave series used as input in the model EBED.

Finally in the .gen-file follow definitions of at which grid cells the different constructions, in this case seawalls and piers, are located.

The shoreline in July 2014 was digitalised from Google Earth with the program Grapher 10 and the coordinates were set as the present shoreline in the model GENESIS. Extractions from the input files with shoreline coordinates and wave data from a certain location can be seen in Table 2 and Table 3, respectively.

Table 2. Shoreline coordinates digitalised from a Google Earth satellite image photographed in July 2014.

```
*********************************
Nha Trang Bay Beach Coordinates
for GENESIS
*********************************
385.14707 395.32769 390.7732 379.52094 368.53658 368.53658 358.08805
349.78281 341.47756 332.10068
320.84841  314.41854  315.49019  308.79241  298.61179  268.06992
246.63704 229.75864 215.02353 207.52202
200.02051  194.39437  190.64362  186.08913  179.65926  175.90851
172.15775 166.53162 166.53162 165.72789
```

Table 3. An extraction from one of the input wave data series from one of the five locations received from the model EBED. From left to right the columns shows date [YYYYMMDD], hour [HHHH], wave height [m], wave period [s] and angle [°].

```
19900101  0      0.64   7.19   5.67
19900101  300    0.56   8.60   5.36
19900101  600    0.56   8.69   5.07
19900101  900    0.54   8.63   4.99
19900101  1200   0.53   8.55   4.96
19900101  1500   0.51   8.47   4.97
19900101  1800   0.50   8.40   5.05
19900101  2100   0.49   8.48   4.95
19900102  0      0.48   8.46   5.21
19900102  300    0.48   8.46   5.33
```